

The Pennsylvania State University

The Graduate School

Department of Materials Science and Engineering

**SYNTHESIS AND CHARACTERIZATION OF BLOCK COPOLYMER ANION
EXCHANGE MEMBRANES AND SUPERIMIDE PROTON EXCHANGE
MEMBRANES**

A Dissertation in

Materials Science and Engineering

by

Lizhu Wang

©2014 Lizhu Wang

Submitted in Partial Fulfillment
of the Requirements
for the Degree of

Doctor of Philosophy

May 2014

The dissertation of Lizhu Wang was reviewed and approved* by the following:

Michael A. Hickner
Associated Professor of Materials Science and Engineering
Dissertation Advisor
Chair of Committee

Ralph H. Colby
Professor of Materials Science and Engineering

Tze-Chiang Chung
Professor of Materials Science and Engineering

Enrique D. Gomez
Assistant Professor of Chemical Engineering

Suzanne Mohny
Chair of the Intercollege Graduate Studies
Professor of Materials Science and Engineering

*Signatures are on file in the Graduate School

ABSTRACT

Anion exchange membranes are of great interest due to their potential to enable low-cost solid polymer alkaline electrochemical technology. However, a significant problem for AEMs is long-lasting performance and robust materials stability under fuel cell and electrolyzer conditions. Block copolymers based on styrene having pendent trimethyl styrenylbutyl ammonium (containing 4 methylene groups between the ionic moieties and the aromatic rings) or benzyltrimethyl ammonium groups were synthesized by reversible addition-fragmentation radical (RAFT) polymerization. The stability under basic conditions of the block copolymers were evaluated under severe, accelerated conditions. The block copolymer with C4 side chain trimethyl styrenylbutyl ammonium motifs displayed improved stability compared to the benzyltrimethyl ammonium-based AEM at 80°C.

The AEMs obtained from polystyrene based block copolymers are brittle yet highly swollen in liquid water, thus hampering their study in fuel cell devices. However, crosslinked copolymer AEMs based on poly(vinylbenzyl chloride)-*b*-poly(butenylstyrene) copolymers using a low temperature olefin metathesis crosslinking route were self-supporting robust membranes. The covalent crosslinking afforded robust mechanical properties in dry materials and low water uptake and small dimensional changes for the hydrated membranes. The crosslinked membranes showed good ionic conductivity when in contact with liquid water, but had lower conductivity than samples of non-crosslinked AEMs at any given relative humidity hydration condition. The

morphologies of crosslinked AEMs as investigated by SAXS correlated with their conductivity values. The ionic conductivity of crosslinked samples decreased due to the disruption of ionic domains during the crosslinking process.

A detailed study regarding morphology, ion conductivity and water uptake with controllable hydrophobic block composition in AEMs was conducted. In this work I described how the properties of block copolymer anion exchange membranes (AEMs) vary with the hydrophobic block composition and ion content. Under the similar ion content ($\text{IEC} = \sim 2.0 \text{ meq g}^{-1}$), the block copolymers with methacrylate and styrenic hydrophobic blocks showed similar ionic conductivity. The water uptake of the materials slightly increased when the ion content of the samples was above 2.0 meq g^{-1} below which the hydration number almost remained constant (~ 7 water molecules per ionic moiety). The stearyl methacrylate containing sample was mechanically robust in liquid water due to the introduction of semicrystalline blocks. In particular, the factors conducive to the conductivity will be discussed in detail. The ionic polymers with long-range ordered microstructures and high ion content ($\text{IEC} = \sim 3.0 \text{ meq g}^{-1}$) had the highest conductivity.

Sulfonimide-containing random copolymers based on poly(arylene ether sulfone) (PAES), poly(2,6-dimethyl-1,4-phenylene oxide) (PPO) and poly(styrene) (PS) were synthesized by low cost post-polymerization modification under mild conditions. These synthetic routes provided universal scale-up approaches for industry production due to the absence of expensive monomers purification. The Radel samples in sulfonimide or

sulfonic acid form displayed higher proton conductivity than PPO analogues. These sulfonimide copolymers showed proton conductivity comparable to sulfonic analogs but lower water uptake. The thermal stability of sulfonimide copolymers was stable up to 250 °C under nitrogen atmosphere. The sulfonimide samples are applicable to high temperature PEMs due to its higher ionic moieties degradation temperature.

TABLE OF CONTENTS

LIST OF FIGURES	viii
LIST OF TABLES	xii
ACKNOWLEDGEMENTS	xiii
Chapter 1 Introduction to Anion Exchange Membranes.....	1
1.1. Introduction.....	1
1.2. Motivation for This Work.....	2
1.3. References.....	12
Chapter 2 Literature Review of Anion Exchange Membranes and Block Copolymers.....	14
2.1. Introduction.....	14
2.2. Chemical Degradation of Anion Exchange Membranes.....	16
2.2.1. Major Degradation Mechanism.....	16
2.2.2. AEM Degradation of Different Cations.....	18
2.3. Chemical Stability of AEM Polymer Backbone.....	20
2.3.1. Approaches to Improve Long-term Stability of AEMs.....	22
2.4. Methods to Improve Ionic Conductivity of AEMs.....	25
2.4.1. Ionic Conductivity for Ion-containing Polymers.....	25
2.4.2. Approaches to Obtain Highly Ionic Conductivity.....	27
2.5. Block Copolymers.....	29
2.5.1 Synthesis of Block Copolymers.....	29
2.5.2 HBr Bromination of Butenylbenzene Group.....	32
2.5.3 Block Copolymer Phase Behaviors.....	33
2.5.4 Kinetic Trapping of Block Copolymers.....	38
2.6. References.....	40
Chapter 3 Experimental Details of RAFT polymerization, Membrane Fabrication and Characterization.....	45
3.1. Introduction.....	45
3.2. Materials.....	45
3.3. Synthesis of Block Copolymers.....	46
3.3.1. Synthesis of Block Copolymers.....	46
3.4. Characterization of Block Copolymers.....	47
3.4.1. Gel Permeation Chromatography.....	48
3.4.2. Quaternization of Block Copolymers.....	48
3.4.3. Nuclear Magnetic Resonance Spectroscopy.....	48
3.5. Membrane Fabrication and Characterization.....	49
3.5.1 Membrane Fabrication.....	49
3.5.2 Water Uptake	50
3.5.3 Conductivity Measurements.....	51
3.5.4 Calculation of Ion Exchange Capacity.....	52
3.5.5 Small Angle X-Ray Scattering.....	52

3.5.6 Transmission Electron Spectroscopy.....	53
3.5.7 Thermogravimetric Analysis.....	53
3.5.8. Differential Scanning Calorimetry.....	54
Chapter 4 Highly Conductive Side Chain Anion Exchange Membranes.....	55
4.1. Introduction.....	55
4.2. Experimental Section.....	58
4.3. Results and Discussion.....	62
4.4. Conclusions.....	84
4.5. References.....	86
Chapter 5 Low-Temperature Crosslinked Anion Exchange Membranes.....	88
5.1. Introduction.....	88
5.2. Experimental.....	90
5.3. Results and Discussion.....	93
5.4. Conclusions.....	105
5.5. References.....	106
Chapter 6 Properties of Highly Ordered Block Copolymer Anion Exchange Membranes.....	108
6.1. Introduction.....	108
6.2. Experimental.....	110
6.3. Results and Discussion.....	113
6.4. Conclusions.....	134
6.5. References.....	135
Chapter 7 Synthesis and Characterization of Polymeric Sulfonimide Proton Exchange Membranes.....	137
7.1. Introduction.....	137
7.2. Experimental Section.....	139
7.3. Results and Discussion.....	140
7.3.1 Synthesis of Sulfonimide Containing Polymers.....	140
7.3.2 Water absorption and proton conductivity.....	145
7.3.3 Thermal stability.....	140
7.4. Conclusions.....	151
7.5. References.....	152
Chapter 8 Summary and Future Research Direction.....	154
8.1 Summary and Conclusions.....	154
8.2 Future Research Direction.....	156
Appendix A Synthesis of Side Chain Block Copolymers for Stable Anion Exchange Membranes.....	158
Appendix B Low-Temperature Crosslinked Anion Exchange Membranes...	162
Appendix C Properties of Highly Ordered Block Copolymer Anion Exchange Membranes.....	165

LIST OF FIGURES

Figure 1.1. Diagram of an anion exchange membranes based fuel cell.....	2
Figure 1.2. Preparation and thermal stability of anion exchange resins with alkylene spacers.....	6
Figure 2.1. The cations mainly studied in AEMs for fuel cells	18
Figure 2.2. Aryl-ether bond cleavage of quaternary ammonium functionalized PAEs under high alkaline environment.....	20
Figure 2.3. The hydrolysis of quaternary carbon and ether bonds in poly(sulfone) tethered with benzyltrimethylammonium cations.....	22
Figure 2.4. Phosphonium functionalized poly(ethylene) for anion conducting membranes.....	24
Figure 2.5. Improved durability with crosslinked ionomer	25
Figure 2.6. O ₂ effect on HBr addition to 3-bromo-1-propene.....	33
Figure 2.7. The diagram of diblock copolymer with increased volume fraction	34
Figure 2.8. Phase diagram of diblock copolymers. OOT = Order Order Transition; ODT = Order Disorder Transition	35
Figure 2.9. Ionic conductivity as a function of interdomain spacing and temperature.....	37
Figure 4.1. ¹ H NMR spectra (300 MHz) of macro-PS ₁₀₀ , brominated PS ₁₀₀ - <i>b</i> -PBBS ₁₆₀ and PS ₁₀₀ - <i>b</i> -PBeS ₁₆₀	65
Figure 4.2. Gel permeation chromatograms of a) fully brominated PS ₁₀₀ - <i>b</i> -PBBS ₄₅ from diblocks b) PS ₁₀₀ - <i>b</i> -PBeS ₅₄ by chain extension and c) Macro-PS ₁₀₀ initiator.	67
Figure 4.3. ¹ H NMR spectra (300 MHz) of PS ₁₀₀ - <i>b</i> -PVBC ₄₉ PS ₁₀₀ - <i>b</i> -P(VBC ₁₂ - <i>r</i> -BeS ₃₃) and brominated PS ₁₀₀ - <i>b</i> -P(VBC ₁₆ - <i>r</i> -BBS ₂₆)	69
Figure 4.4. ¹ H NMR spectra (300 MHz) of quaternized PS ₁₀₀ - <i>b</i> -PVBC ₁₀₄ in d ₇ -DMF/CD ₃ OD (trace) and PS ₁₀₀ - <i>b</i> -BBS ₁₆₀ in d ₇ -DMF.	72
Figure 4.5. SAXS patterns of copolymer AEMs from (A) 1 : PS ₁₀₀ - <i>b</i> -PVBC ₄₉ , 2 : PS ₁₀₀ - <i>b</i> -PVBC ₁₀₄ , 3 : PS ₁₀₀ - <i>b</i> -PVBC ₁₆₇ , (B) 4, 5, 6 corresponding to the side	

chain samples made from PS ₁₀₀ - <i>b</i> -P(VBC ₁₆ - <i>r</i> -PBBS ₂₆), PS ₁₀₀ - <i>b</i> -P(VBC ₃₂ - <i>r</i> -PBBS ₆₇) and PS ₁₀₀ - <i>b</i> -P(VBC ₁₂ - <i>r</i> -PBBS ₁₃₂).....	74
Figure 4.6. SAXS patterns of quaternary copolymer AEMs from PS ₁₀₀ - <i>b</i> -PBBS ₄₅ (7), PS ₁₀₀ - <i>b</i> -PBBS ₁₆₀ (8).....	76
Figure 4.7. Interdomain spacing comparison of PS- <i>b</i> -PBBS, PS- <i>b</i> -PVBC and PS- <i>b</i> -P(VBC- <i>r</i> -BBS) block copolymers at the same hydrophobic block length.....	77
Figure 4.8. Solvent and ion effects on conductivity of (■) PS ₁₀₀ - <i>b</i> -PVBC ₁₆₇ , (▲) PS ₁₀₀ - <i>b</i> -P(VBC ₁₂ - <i>r</i> -BBS ₁₃₂) and (●) PS ₁₀₀ - <i>b</i> -PBBS ₁₆₀ at 30 °C as a function of ion exchange capacity, a: cast from CHCl ₃ /1-propanol/methanol (v/v/v = 2:1:1), b: cast from DMF/1-propanol (v/v = 3:1), c: cast from toluene/1-propanol (v/v = 1:1).....	78
Figure 4.9. SAXS patterns of quaternary copolymer (A) PS ₁₀₀ - <i>b</i> -PVBC ₁₆₇ ; (B) PS ₁₀₀ - <i>b</i> -PBBS ₁₆₀ , 3 , 8 : cast from toluene/1-propanol (v/v = 1:1); 9 , 10 cast from DMF/1-propanol (v/v = 3:1).	81
Figure 4.10. (A) Stability of (●) Q-PS ₁₀₀ - <i>b</i> -PBBS ₄₅ and (■) Q-PS ₁₀₀ - <i>b</i> -PVBC ₄₉ ; (B) (▼) Q-PBBS and (▲) Q-PVBC in NaOD/D ₂ O at 80 °C.	84
Figure 5.1. ¹ H NMR spectra of a) macroinitiator PVBC ₁₀₀ and b) block copolymer PVBC ₁₀₀ - <i>b</i> -PBeS ₁₀₇	95
Figure 5.2. GPC profiles of macroinitiator PVBC ₁₀₀ and block copolymer PVBC ₁₀₀ - <i>b</i> -PBeS ₁₀₇ and PVBC ₁₀₀ - <i>b</i> -PBeS ₁₈₃	96
Figure 5.3. Conductivity versus water uptake for crosslinking AEMs.	99
Figure 5.4. Small-angle X-ray scattering (SAXS) patterns and TEM micrographs of non- crosslinked and crosslinked AEMs in the dry state under vacuum from the precursor PVBC ₁₀₀ - <i>b</i> -PBeS ₁₈₃	101
Figure 5.5. Humidity dependence of conductivity and water uptake in Cl ⁻ form crosslinked and non-crosslinked AEMs from PVBC ₁₀₀ - <i>b</i> -PBeS ₁₈₃ at 30 °C, Homo = homogeneous quaternization, Hetero = heterogeneous quaternization.	104
Figure 6.1. ¹ H NMR spectra (300 MHz) of 4-butylstyrene.	116
Figure 6.2. GPC chromatograms of a) PHMA ₆₀ macroinitiator and b) PHMA ₆₀ - <i>b</i> -PVBC ₃₄	119

Figure 6.3. Small angle X-ray scattering (SAXS) patterns of A) PHMA ₆₀ - <i>b</i> -PVBC ₃₄ ; B) PVBC ₄₄ - <i>b</i> -PBS ₈₄ ; C) PLMA ₆₈ - <i>b</i> -PVBC ₆₅ of quaternized samples.	121
Figure 6.4. TEM micrographs of A) PHMA ₆₀ - <i>b</i> -PVBC ₃₄ sample with lamellar morphology; B)PVBC ₄₄ - <i>b</i> -PBS ₈₄ sample with lamellar morphology; C)PLMA ₆₈ - <i>b</i> -PVBC ₆₅ sample with cylindrical morphology. All samples were unstained.	122
Figure 6.5. Hydration Number (λ) as a function of ion content at 30 °C under 95% relative humidity, PVBC- <i>b</i> -PBS (●) and PLMA- <i>b</i> -PVBC(■).	125
Figure 6.6. DSC thermograms of block copolymers with different side chains during the second heating scan. A: PSMA ₇₅ , B: PSMA ₇₅ - <i>b</i> -PVBC ₇₃ , C:quaternized PSMA ₇₅ - <i>b</i> -PVBC ₇₃ , D:quaternized PLMA ₆₈ - <i>b</i> -PVBC ₆₅ , E: quaternized PHMA ₆₀ - <i>b</i> -PVBC ₃₄ , F: quaternized PVBC ₄₄ - <i>b</i> -PBS ₈₄	127
Figure 6.7. Conductivity dependence of relative humidity of a)PHMA ₆₀ - <i>b</i> -PVBC ₃₄ ; b) PVBC ₄₄ - <i>b</i> -PBS ₈₄ ; c) PVBC ₄₄ - <i>b</i> -PBeS ₈₂ ; d) PLMA ₆₈ - <i>b</i> -PVBC ₆₅ at 30 °C from 20 to 95% relative humidity in chloride (Cl ⁻) form.	130
Figure 6.8. Conductivity dependence of ion contents, PVBC- <i>b</i> -PBS (▲), PLMA- <i>b</i> -PVBC (●) and PVBC- <i>b</i> -PBeS (■) in chloride (Cl ⁻) form.	132
Figure 7.1. ¹ H and ¹⁹ F NMR of sulfonated PPO, functionalized PPO sulfonimide and PPO sulfonimide..	142
Figure 7.2. Water uptake as a function of ion exchange capacity at room temperature. SI-PPO (▲), S-PPO (▼), S-Radel (●) and SI-Radel (■).....	145
Figure 7.3. Conductivity of sulfonated and sulfonimides polymers. SI-PPO (▲), S-PPO (▼), S-Radel (●) and SI-Radel (■).....	147
Figure 7.4. Proton Conductivity vs Temperature in liquid water. SI-PPO (★) (2.00 meq g ⁻¹), S-PPO (☆) (2.79 meq g ⁻¹), S-Radel (▲) (2.20 meq g ⁻¹) and (▼) (1.34 meq g ⁻¹), SI-Radel (●) (1.80 meq g ⁻¹) and (■) (1.10 meq g ⁻¹).....	148
Figure 7.5. TGA curves of PPO and PS samples.....	150
Figure 7.6. TGA curves of S-Radel and SI-Radel samples..	151
Figure A.1. GPC graphs of macroinitiator PS ₁₀₀ , PS- <i>b</i> -PVBC, PS- <i>b</i> -P(VBC- <i>r</i> -BeS), PS- <i>b</i> -P(VBC- <i>r</i> -BBS), PS- <i>b</i> -PBeS and PS- <i>b</i> -PBBS.....	158
Figure A.2. ¹ H NMR spectra of PS- <i>b</i> -PVBC, PS- <i>b</i> -P(VBC- <i>r</i> -BeS) and PS- <i>b</i> -P(VBC- <i>r</i> -BeS) block copolymers.....	159

Figure A.3. ^1H NMR spectra of PS- <i>b</i> -PBeS and PS- <i>b</i> -PBBS block copolymers in CDCl_3 at 25 °C.	160
Figure A.4. ^1H NMR spectra of (A) quaternized C4 side chain PS ₁₀₀ - <i>b</i> -PBBS ₄₅ and (B) benzyltrimethyl ammonium copolymers powder from PS ₁₀₀ - <i>b</i> -PVBC ₄₉ in 1M KOH at 80 °C for 30 days.-PhH denotes aromatic protons.	161
Figure B.1. ^1H NMR spectrum of 4-(3-butenyl)styrene.	162
Figure B.2. GPC graphs of macroinitiators and block and random copolymers.	163
Figure B.3. SAXS profiles of block AEMs formed under different conditions.	163
Figure B.4. Random PVBC ₄₉ - <i>r</i> -PBeS ₅₀ crosslinked AEM formed using heterogeneous amination.	164
Figure C.1. ^1H NMR spectra of block copolymers	165
Figure C.2. ^1H NMR spectrumquaternized PVBC ₄₄ - <i>b</i> -PBS ₈₄	165
Figure C.3. GPC chromatograms of A) PLMA- <i>b</i> -PVBC and B) PVBC- <i>b</i> -PBS	166
Figure C.4. TEM micrographs of A, B) PHMA ₆₀ - <i>b</i> -PVBC ₃₄ sample with defects; C) PSMA ₈₄ - <i>b</i> -PVBC ₈₄ sample with cylindrical morphology. All samples were unstained.	166
Figure C.5. SAXS profiles andTEM micrographs of PSMA ₇₃ - <i>b</i> -PVBC ₇₅ sample andPVBC ₄₄ - <i>b</i> -PBeS ₈₂ sample with lamellar morphologies. All samples were unstained	167
Figure C.6. SAXS profiles of PLMA- <i>b</i> -PVBC andPVBC- <i>b</i> -PBS samples. All samples were unstained	168
Figure C.7. TGA curves of block copolymers: A: PSMA ₇₅ - <i>b</i> -PVBC ₇₃ , B: quaternized PVBC ₄₄ - <i>b</i> -PBS ₈₄ ,C: quaternized PLMA ₆₈ - <i>b</i> -PVBC ₆₅ , D: quaternized PSMA ₇₅ - <i>b</i> -PVBC ₇₃ , E: quaternized PHMA ₆₀ - <i>b</i> -PVBC ₃₄	169

LIST OF TABLES

Table 4.1. Properties of the prepared side chain block copolymers.....	73
Table 5.1. Properties of crosslinked and un-crosslinked AEMs	98
Table 6.1. Parameters of block copolymers prepared by RAFT polymerization.....	117
Table 7.1. Properties of sulfonated and sulfonimide samples	145
Table A.1. Properties of Synthesized Block Copolymer Anion Exchange Membranes	160
Table B.1. Block Copolymer Molecular Weights and Polydispersity Indices.....	162
Table C.1. Water uptake and ionic conductivity of the prepared samples with IEC of $\sim 2.0 \text{ meq g}^{-1}$	168
Table C.2. Properties of samples with low and high ion contents	169

ACKNOWLEDGEMENTS

First, I would like to express my appreciation to my advisor, Dr. Michael Hickner, for offering me the research opportunity to pursue my PhD degree. Under his patient guidance over the years, I have switched to polymer scientist with organic chemistry background, more than what I expected. Without his revision, I could not accomplish the paper drafts. I really appreciated his time on my papers and dissertation. Dr. Hickner has taught me lessons that are beyond the research. I would also like to give my gratitude to my committee members, Dr. Ralph Colby, Dr. Mike Chung, and Dr. Enrique Gomez for serving on my committee and for their expertise that helped the dissertation completion.

I owe my thanks to the Hickner's research group for their support in research during the course of PhD study, particularly for the synthesis group: Li Nanwen, Chen Guang, Brian Chaloux and others. Thanks Pickle Dianna, Bradley Lokitz in Oak Ridge National Lab for teaching how to perform the controlling/living radical polymerization. I also recognized the help from Materials Characterization Lab in polymer characterization such as SAXS, TEM.

Last, I would like to thank my whole family for being with me. I cherish your supports and sacrifice.

Chapter 1

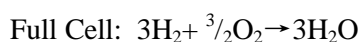
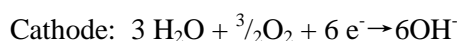
Introduction to Anion Exchange Membranes

1.1. Introduction

Fuel cells are of significant interest due to their use of energy-dense chemical fuels, and these devices can directly convert the fuels such as hydrogen, methanol to electrical energy in a clean and efficient manner. Fuel cells are a potential environmentally benign technology that uses hydrogen generated from renewable sources to make electricity while the only byproduct is water. The main difference of fuel cells from batteries is that fuel cells directly convert the fuels to energy without power storage and the production can be controlled by the fuel feeds. Another merit of fuel cells is their higher power density, 10 times that of lithium ion batteries. The most studied type of polymer membrane fuel cell is based on a proton exchange membrane (PEM), or solid polymeric proton conductor, in which hydrogen is oxidized to protons and electrons. The electrons travel along an electrical circuit while the protons are transported via the PEM (such as Nafion[®], a benchmark PEM), aided by the sulfonic acid groups and water. At the cathode, oxygen is reduced to water which is emitted from the cell. However, the presence of expensive noble metal catalyst used in the PEM fuel cell for hydrogen oxidation and oxygen reduction in the presence of an acidic polymer is one of the main factors hampering its widespread application in electric vehicles and as portable power sources. Currently, the community is seeking alternative options to amend the high cost in construction of commercial fuel cells. Anion exchange membrane (AEM) based fuels cells are the most efficient fuel cells at temperatures below 200 °C using non-noble metal

catalyst such as Ni or Ag under alkaline conditions.^{1,2} As shown in **Figure 1.1**, AEMs based fuel cells convert chemical fuels to electrical energy using high pH half reactions as outlined in the following equations:

For Hydrogen



For Methanol

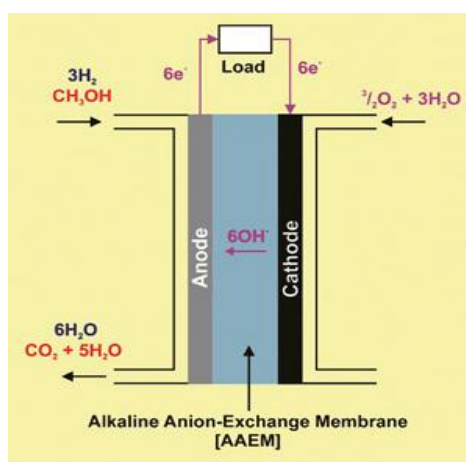
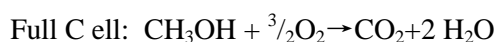
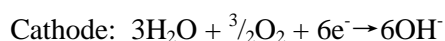


Figure 1.1. Diagram of an anion exchange membranes based fuel cell with hydrogen (black) and methanol (red) feed.³

1.2. Motivation for This Work

In alkaline energy conversion devices, the key component is the AEM, capable of transporting hydroxide ions while acting as a barrier for fuels while maintaining high performance, high conductivity, and low degradation. The performance of fuel cells and

other membrane electrochemical devices is closely associated with the properties of the polymer membrane. The development of an AEM based fuel cell or electrolyzer is concentrated on the improvement of the AEM properties in alkaline environment such as high conductivity, mechanical robustness, thermal, chemical and oxidative stability. In particular, the long-lasting stability under fuel cell operation conditions is one of the main issues in this field.

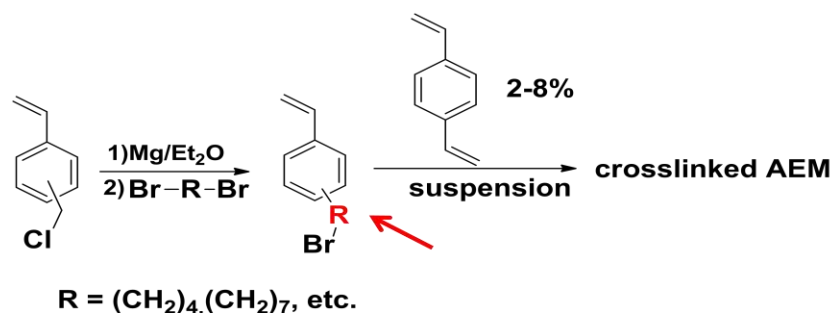
Fuel cells remain an important energy conversion technology due to their use of energy-dense chemical fuels such as methanol and compressed hydrogen. Methanol and other alcohol-fed fuel cells have the potential to be components in battery recharge and stationary power systems for primary and backup power¹ and hydrogen-fed fuel cells can provide driving ranges that current pure electrical vehicles (EVs) cannot.² However, wide-scale deployment of fuel cells has been hampered by their cost including expensive components such as perfluorinated membranes and precious metal-based catalysts. Solid polymer electrolyte membranes are key components in modern fuel cells for ion transfer between anode and cathode half reactions to maintain the cell current and to provide robust isolation of the fuel and oxidant. Proton exchange membranes (PEM) such as Nafion[®], a poly(perfluorosulfonic acid) derivative, have demonstrated excellent chemical and thermal stability and high proton conductivity as the standard membrane type in the fuel cell field. However, perfluorinated materials have some drawbacks such as high cost, high fuel and water crossover and poor mechanical stability at temperatures greater than 100°C. Moreover, acidic fuel cells can suffer from sluggish oxygen reduction and carbon-based fuel oxidation kinetics. High performance PEM fuel cells universally require

platinum-based and precious metal catalysts, which can be deactivated by carbon monoxide, and significantly raise the cost of fuel cell technology.³

In the pursuit of alternative PEMs, researchers have demonstrated that the nanophase separated morphology between hydrophobic polymer segments and the backbone-tethered acidic moieties leads to ion-conducting nanochannels responsible for water uptake and proton transport. Block copolymers with ion-containing blocks and hydrophobic blocks have been designed as one of the most predictable method to manipulate the ionic domain morphology of PEMs. Elabd, et al. showed the proton conductivity of sulfonated poly(styrene-*b*-isobutylene-*b*-styrene) (SIBS) (76 mS cm^{-1} , $\text{IEC} = 2.04 \text{ meq g}^{-1}$) was almost four times higher than that of sulfonated poly(styrene) (17 mS cm^{-1} , $\text{IEC} = 1.92 \text{ meq g}^{-1}$) at room temperature, likely due to ordered domain morphology.⁴ McGrath and coworkers demonstrated the conductivities of sulfonated multiblock poly(arylene ether) were greater than that of the random copolymer analogs at similar conditions due to well-connected hydrophilic domains as observed by atomic force microscopy.^{5,6} For these step-growth multiblock copolymers, conductivities from 80 to 320 mS cm^{-1} were measured with IECs from 0.95 to 2.29 meq g^{-1} and water uptakes from 49% to 470% . Recently, Park, et al. observed a range of ordered lamellar, gyroid and hexagonally packed cylinder microstructures from sulfonated poly(styrene-*b*-methylbutylene) (PS-*b*-PMB) despite the fact that the symmetric non-ionic block copolymers had volume fractions between 0.45 and 0.50 .⁷ The non-ionic block copolymers were anticipated to exhibit lamellar microstructures predicted by Flory-Huggins and self-consistent mean-field theories. Due to the strong segregation strength

between sulfonated blocks and non-ionic segments, sulfonated PS₁₄-*b*-PMB₂₀ showed the smallest domain spacing (5.2 nm) with gyroid structures as obtained from SAXS and TEM.

Recently, AEMs-based fuel cells have drawn great interest due to the use of non-noble catalyst such as Ni. However, perhaps the most significant challenge for AEMs is their chemical instability under alkaline conditions due to well-known degradation pathways of quaternary ammonium cations, particularly for benzyltrimethyl ammonium cations. However, AEMs with trimethylalkyl side chains have shown increased stability in a key early report. The AEMs with C4 side chains (having 4 carbons) in OH⁻ form retained 92% of the original ion exchange capacity (IEC) under hydrolytic condition at 100°C for 30 days (**Figure 1.2**).⁴



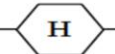
Spacer Chain ^a (R')	Strong Base Capacity ^b (mEq/L)		Remaining Ratio ^c (%)
	Initial	After Test ^d	
CH ₂ (DIAION [®] SA10A)	1.42	1.12	79
(CH ₂) ₄	0.84	0.78 (0.03) ^e	92
CH ₂ CH ₂ CH(CH ₃)CH ₂	0.77	0.71	92
	1.05	0.91	86
(CH ₂) ₃ CH(CH ₃)CH ₂ CH ₂	1.01	0.97	96
(CH ₂) ₇	1.13	1.03	92
CH ₂ CH ₂ -  -CH ₂	0.93	0.86	93

Figure 1.2. Preparation and thermal stability of anion exchange resins with alkylene spacers.⁴

In this study there were no directly observed benzyl and methyl substitution to the alkylene spacers in the anion exchange resins as the authors investigated degradation by FT-IR. However, minor Hofmann elimination occurred in the propyleneoxymethylene spacer based resin. The introduction of alkylene spacers between the benzene ring and quaternary nitrogen is thought to improve the stability of the material in the strongly basic conditions due to the steric hindrance from bulky alkane groups, which prevents benzyl substitution or Hofmann elimination on the pendant chain.

Separating the ion-conducting phase and the hydrophobic phase in an AEM-based block copolymer format enables independent tuning the ion conductive properties, water

swelling, and mechanical properties of the membrane. For example, quaternary ammonium-functionalized styrene-ethylene/butylene-styrene (SEBS) block copolymers had excellent dimensional stability during hydration. Continuous hydrophobic microdomains were observed by atomic force microscopy (AFM), which promoted hydroxide (OH^-) conductivity of 9.6 mS cm^{-1} (liquid water, room temperature) at IEC 1.54 meq g^{-1} but a high water uptake of 265 wt%.⁵ The presence of soft segments facilitates the membrane formation, but in some cases may lead to excessive swelling.

Many examples of AEMs have high water uptake due to the need for significant hydration to promote anion conductivity. Crosslinked AEMs have shown lower water swelling, better mechanical properties, higher conductivities and better chemical stability against the alkaline operational conditions in alkaline membrane fuel cells (AMFCs) compared to uncrosslinked samples. Chloromethylated poly(sulfone) crosslinked with hexane diamine showed high stability over 240 h in 2 M NaOH at 40 °C, although temperatures lower than 80 °C have proven to be ineffective for revealing true AEM stability.¹ Diamine crosslinked poly(vinylbenzyl chloride) (PVBC) AEMs displayed moderate fuel cell performance at 50 °C under methanol/ O_2 conditions where the loss of the ion exchange capacity was less than 5% after 233 h of operation with a peak power density of 1.1 mW.cm^{-2} .² The Friedel-Crafts type reaction between chloromethyl and dimethoxyphenyl groups was applied to chloromethylated and quaternary phosphonium poly(2,6-dimethyl-1,4-phenyleneoxide) (PPO) blends in which the chloromethyl groups and high electron density phenyl rings acted as crosslinking moieties.³ The self-crosslinked PPO AEM had 5-10 fold lower swelling ratio compared to non-crosslinked

PPO samples and also showed high hydroxide conductivity in liquid water (38 mS cm^{-1}) with $\text{IEC} = 1.23 \text{ meq g}^{-1}$) at 20°C . Ring-opening metathesis polymerizations of derivatives of cyclooctenes and norbornenes were employed to make crosslinked polyolefin quaternary ammonium and ruthenium based AEMs with tunable properties that have comparable conductivity (68.7 mS/cm , OH^- form, liquid water, 22°C) and mechanical strength to traditional quaternary ammonium-based AEMs.⁴ Crosslinking mitigated water swelling in these materials and provided mechanical integrity for high conductivity AEMs that originally suffered from significant liquid water swelling and very poor mechanical properties. The goal in this report was to extend the strategies for producing crosslinked AEMs using a low temperature crosslinking method. The post-polymerization olefin metathesis route reported herein enables design of block copolymer AEMs with well-established purification procedures and solvent processing of the materials before crosslinking is induced during final sample fabrication.

As a bifunctional monomer 4-(3-butenyl)styrene (BeS) containing a styrene polymerizable group and a terminal butene double bond has enabled the preparation of BeS copolymers with pendant alkene groups. It has been demonstrated that BeS can be used to synthesize amphiphilic block copolymers by living anionic polymerization of styrene and BeS sequentially followed by hydroxylation of the terminal olefinic groups.⁵ BeS and propylene were copolymerized to produce crosslinkable functionalized poly(propylene) with flexible styrene pendent moieties using a metallocene catalyst and methylaluminoxane (MAO) followed by high temperature crosslinking via the Diels-Alder [2+4] cycloaddition of two styrene moieties.⁶ In another example, bifunctional

BeS monomers were incorporated into bottlebrush copolymers through RAFT polymerization to fabricate amphiphilic organic nanotubes with tunable surfaces that had high selection and efficiency for nanomaterials and biomacromolecules. Crosslinkable shell layers were formed by metathesis of the butane double bonds using Grubbs 2nd generation catalyst and the inner cores of poly(lactide) (PLA) were etched away by NaOH at room temperature.⁷

Previous results showed block copolymer crosslinking was a promising approach to fabricate high performance AEMs. Quaternized block copolymers with high ion content can show high water swelling or even be soluble in water but this disadvantage can be solved by crosslinking. In my work, poly(vinylbenzyl chloride)-*b*-poly(4-butenylstyrene) ($-\text{PhCH}_2\text{CH}_2\text{CH}=\text{CH}_2$) with pendant crosslinkable olefinic double bonds was synthesized and studied in detail. Compared to non-crosslinked block copolymers, the crosslinked copolymers by second generation Grubbs catalyst have been used to fabricate robust anionic membranes while the conductivity was only slightly reduced due to the crosslinking. The relationship of water uptake, conductivity and morphology was researched to provide guidance for reverse engineering improved AEMs. This approach provides an opportunity to construct robust membranes in liquid water using low temperature crosslinking.

Most proton conducting membranes based on the materials with pendant sulfonic groups have been studied extensively in the fuel cell community. The effects of sulfonated block copolymers on the proton exchange membrane (PEM) performance have been demonstrated, resulting in increased proton conductivity relative to the

sulfonated random copolymers due to the formation of unique phase separation nanostructures.⁵ For example, hydrophilic blocks containing tethered sulfonic groups formed ionic microdomains of poly(styrene-*b*-isobutylene-*b*-styrene) (SIBS) and facilitated ion transport compared to randomly sulfonated poly(styrene)⁵. Park, et al. showed that the proton electrolyte membranes with less than 5 nm hydrophilic phases had enhanced proton conductivity and higher water uptake at temperatures up to 90 °C due to the capillary condensation. The addition of sulfonic groups to block copolymers to morphology changes that depend on the sulfonation degree.^{6a} Particularly, the block copolymer poly(ethylene)-*b*-poly(styrenesulfonic acid) containing crystalline blocks showed lower water uptake (6.5 wt%, hydration number, $\lambda = 1.1$) and comparable ionic conductivity (86 mS cm⁻¹) compared to Nafion[®] conductivity of 96 mS cm⁻¹ (water uptake = 34.5 wt%, hydration number, $\lambda = \sim 15$) under the similar conditions. The highly crystalline state of the hydrophobic phase maintained structural stability and less water swelling by surrounding the bicontinuous cylinders of hydrated PSS.^{6b} The fundamental understanding of how the phase separated morphology affects the transport properties and morphologies has been researched in PEMs. However, there is no consensus on the morphological evolution of the sulfonated copolymers due to the complicated phase behaviors. Block copolymers are a potential route to higher proton conductivity membranes but this has not been demonstrated much in anion exchange membranes (AEM) due to their intrinsically low ion mobility and the synthetic challenges in preparing the materials.

The properties of AEMs are highly related to the morphology of as-cast membranes. There have been a few reports on AEMs based on hydroxide conducting block copolymers. In their studies, block copolymer based membranes had greater conductivity than the random copolymer counterparts at the similar IEC. The conductivity of block copolymers depended on the morphology of membranes and the formation of continuous conductive nanochannels which facilitated ion transport. The quaternized block copolymers have improved mechanical strength compared to non crosslinked samples and reduced swelling compared to randomly functionalized copolymers.^{6,7,8} However, there is no detailed study in depth in regard to morphology, ion conductivity and water uptake with controllable hydrophobic block composition in AEMs.

The properties of block copolymer anion exchange membranes (AEMs) vary with the hydrophobic block composition and ion content have been elucidated in this work. The morphology was investigated through transmission electron microscopy (TEM) and small-angle x-ray scattering (SAXS), ion conductivity and water uptake relationships of various block copolymers at the different ion contents. The optimal AEMs performance was manipulated by the character of the hydrophobic blocks. The introduction of long-chain alkyl methacrylate hydrophobic blocks in AEMs afforded the robust membranes and limited swelling in liquid water.

1.3 Outline of the Thesis

In this thesis, Chapter 4 focuses on the synthesis and characterization of C4 side chain block copolymers via RAFT polymerization and post-polymerization modification. The side chain effect on the conductivity, interdomain spacing and chemical stability of AEMs was described in the chapter. In Chapter 5, construction of robust membranes against swelling in liquid water was examined. The crosslinking effect on the intrinsic properties of AEMs was studied through corresponding techniques exposed to liquid water and relative humidity conditions. Chapter 6 analyzed the hydrophobic effect, including semicrystalline blocks, on the properties of AEMs. As demonstrated in this section, the incorporation of semicrystalline block in AEMs rendered membranes with good mechanical integrity in liquid water. In Chapter 7, sulfonamide-containing polymers were synthesized to increase the acidity relative to traditionally sulfonic tethered polymers. Finally, Chapter 8 summarizes the dissertation and identifies directions for future research.

1.4 References

1. Hickner, M.A. *Mater. Today* **2010**, *13*, 34-41.
2. a) Elabd, Y.A.; Hickner, M.A. *Fuel Cells* **2011**, *44*, 1-11. b) Pan, J.; Chen, C.; Zhuang, L.; Lu, J. *Acc. Chem. Res.* **2012**, *45*, 473-481.
3. Varcoe, J.R. *Phys. Chem. Chem. Phys.*, **2007**, *9*, 1479–1486.
4. Tomoi, M.; Yamaguchi, K.; Ando, R.; Kantake, Y.; Aosaki, Y.; Kubota, H. *J. Appl. Polym. Sci.* **1997**, *64*, 1161-1167.

5. L. Sun, J.S. Guo, J. Zhou, Q.M. Xu, D. Chu and R.R. Chen, *J. of Power Sources*, 2012, **202**, 70-77.
6. Tanaka, M.; Fukasawa, K.; Nishino, E.; Yamaguchi, S.; Yamada, K.; Tanaka, H.; Bae, B.; Miyatake, K.; Watanabe, M. *J. Am. Chem. Soc.* **2011**, *133*, 10646-10654.
7. Zhao, Z.; Wang, J.H.; Li, S.H.; Zhang, S.B. *J. Power Sources* **2011**, *196*, 4445-4450.
8. Tsai, T.H.; Versek, C.; Thorn, M.; Tuominen, M.; Coughlin, E.B. Chpt 15, In *Polymers for Energy Storage and Delivery: Polyelectrolytes for Batteries and Fuel Cells*, ACS Symposium Series; Washington, DC, 2012.

Chapter 2

Literature Review of Anion Exchange Membranes and Ion-Conducting Block Copolymers

2.1 Introduction

Traditionally, anion exchange polymers are used for ion exchange membranes and resins in electrodialysis, and as conductive separators, sensors and solid polymer electrolytes. The alkaline fuel cell with liquid electrolyte was first discovered in the 1930s and was one of the oldest working fuel cells. Initially liquid alkaline fuel cells were used for the primary power source of the critical systems and drinking water supply of astronauts for the Apollo space program in the 1960s.¹ To date, due to the increase in the need for the next generation green energy, AEM fuel cells are of important interest for their high efficiency and environmentally benign power generation technology. This new generation of alkaline fuel cells uses a solid polymer membrane, instead of a separator filled with liquid electrolyte, as in previous alkaline fuel cell technology. In AEM fuel cells, the central component is the solid polymer membrane, serving as an ion conductor between cathode and anode, a fuel barrier and an electrical insulator. Compared to AEM-based fuel cells, proton exchange membrane (PEMs) fuel cells have very high ion conductivity and thermal and chemical stability imparted by perfluorosulfonic acid-based polymeric proton conductors. PEM fuel cells rely on well-established membrane technology, but depend on the use of expensive platinum and precious metal-based catalysts which greatly increases their cost. Because of low metal corrosion at high pH,

the use of non-noble catalyst allows AEM fuel cells to be an alternative candidate for the production of clean energy.^{2,3}

AEM fuel cells are operated under basic conditions facilitated by the hydroxide-conducting AEM. Exposed to working temperatures greater than 80 °C, AEM fuel cells showed poor performance due to long-term stability issues in which the polymer based membranes would be rapidly degraded, including the cationic ion transport moieties and polymer backbone.^{4,5} The chemical degradation of the AEM at high temperature will substantially reduce the lifetime of AEM fuel cells, and has thus far prevented the commercial development of AEM fuel cells in practical applications. Meanwhile, AEMs have an intrinsically lower ionic conductivity than those of PEM counterparts at similar IECs due to the lower mobility of hydroxide ions compared to protons. In addition, the formation of bicarbonate ions from the reaction of atmospheric carbon dioxide and hydroxide anions also will remarkably decrease the ionic conductivity of the material due to the low mobility of bicarbonate ions. Many of these issues also exist in electrolyzers and other polymer membrane electrochemical technology that rely on anion exchange membrane fuel cells. For AEM development for fuel cells and other devices, the AEM must be chemically, mechanically and electrochemically stable under operational conditions while maintaining reasonable conductivity to achieve good device performance.

The organic cations commonly used in AEMs are susceptible to degradation from hydroxide nucleophilic attack in the presence of alkaline conditions, which would

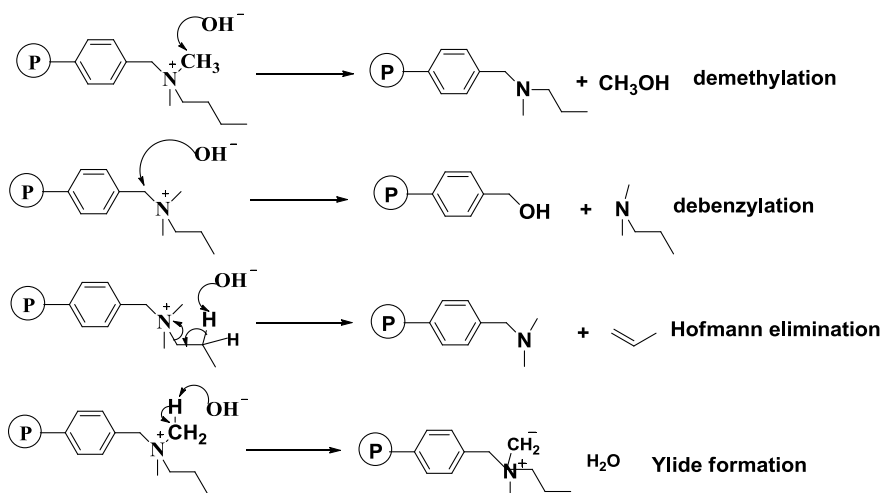
neutralize the bound cationic groups.⁶This degradation will gradually cause the conductivity loss. Recently, alternative cations such as imidazolium, phosphonium, sulfonium, and bis(terpyridine)ruthenium(II) were synthesized and held new promise as a new class of anion conducting membranes.⁷

Aside from the cation stability under high pH conditions, the chemical stability of the polymer backbone will affect the mechanical properties of the AEM, leading to catastrophic failure of the membrane electrolyte assembly in AEM fuel cells. The cationic group and polymer backbone stability will be elaborated in the following sections.

2.2 Chemical Degradation of Anion Exchange Membranes

2.2.1 Major Degradation Mechanism

The majority of AEM stability research has dealt with benzyltrimethylammonium cations. The recognized degradation pathways under high pH environments are S_N2 nucleophilic substitution, E2 Hofmann elimination and ylide formation, **Scheme 2.1**.^{8,9,10} Nucleophilic substitution takes place via hydroxide attack on the α -carbon of the cation, which can either abstract the methyl group from the cation moiety to form a tertiary amine or detach the cation by attack at the benzyl position to produce benzyl alcohol and trimethyl amine from the benzyltrimethylammonium cation. S_N2 substitution can be decreased by steric hindrance of the benzyl position as demonstrated by Tomoi, et al.¹¹



Scheme 2.1. Degradation pathways of ammonium cationic groups

Hofmann elimination occurs by hydrogen abstraction from a β -carbon by hydroxide anion attack, resulting in the formation of olefin and tertiary amine elimination from the neighboring carbon. At temperatures below 60°C , Hofmann elimination proceeds more slowly than at temperatures above 100°C as reported by Merle, et al.¹¹ In the absence of β -hydrogens, Hofmann elimination is unfavorable while nucleophilic substitution is the main decomposition in the AEMs. Preliminary reports show that there are significant contributions by both benzyl and methyl elimination with the ratio of the two mechanisms being dependent on the exact sterics and electronics of the cation. Hydroxide attack on the methyl group of the cation leads to the formation of ylide product along with water.

Moreover, the degradation of AEMs is influenced by the degree of hydration of the ammonium cations (the number of waters associated with each ionic moiety). Pivovar, et al.¹² found that the tetramethylammonium cation was relatively stable in

aqueous alkaline solution. However, when the number of water molecules coordinated to the ammonium cations was less than 3, the dehydration will accelerate the degradation in such conditions due to increased nucleophilicity and reactivity of the hydroxide.¹³

2.2.2 AEM Degradation of Different Cations

Different ammonium-based cations were measured for their chemical stability under alkaline conditions. It was reported that the phenyltrimethylammonium (PTMA) cation was less stable than the benzyltrimethylammonium (BTMA) cation in 2 M KOH aqueous solutions at 80°C during which the remaining ratio of PTMA was 30% compared to 90% remaining of BTMA. The methylene linker between the aromatic ring and N-centered cation enhanced the stability.¹⁴

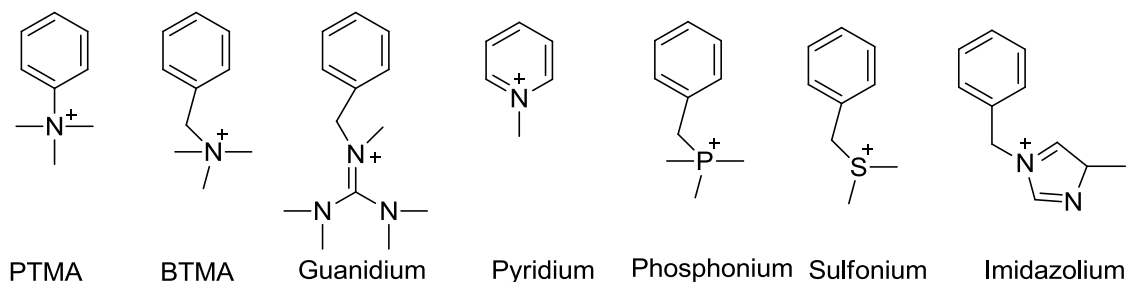


Figure 2.1. The cations mainly studied in AEMs for fuel cells.

It was believed that the higher pKa of 13.8 for pentamethylguanidine increased the alkaline stability of this cation compared to the 10.8 pKa of the benzyltrimethylammonium cation. Wang, et al. reported that benzyl guanidium based AEMs showed excellent ionic conductivity when exposed to 1M NaOH at 60 °C after 2 days.⁴ Meanwhile, Kim, et al. reported that phenyl guanidium based AEMs maintained decreased ionic conductivity in 0.5M NaOH at 80 °C. Both guanidium-containing AEMs

showed better conductivity and chemical stability than trimethylammonium based counterparts.¹⁵ Qu, et al. fabricated bi-guanidium-containing polysesquioxane AEMs which showed the highest power density of 321 mW cm^{-2} at 700 mA cm^{-2} at 40°C with borohydride fuel. The guanidium-based fuel cell lasted for 50 h with the voltage maintained at 0.76 V.¹⁶ But there was no detailed study regarding the degradation.

Bauer, et al. reported that pyridinium based AEMs had the lowest stability among the cations in the study, which was also confirmed by the research of Sata, et al. in the presence of alkaline solutions at higher temperatures. Pyridinium based AEM showed accelerated IEC and ionic conductivity loss under alkaline conditions.^{8,14}

Qiu, et al.¹⁷ studied the properties of imidazolium functionalized AEMs synthesized by in situ crosslinking of styrene, acrylonitrile and imidazolium vinylbenzyl chloride in the presence of a divinylbenzene crosslinker. The imidazolium based membrane showed reasonable hydroxide conductivity ($\sim 16 \text{ mS cm}^{-1}$, $\text{IEC} = \sim 1.50 \text{ meq g}^{-1}$) and chemical stability of up to 1000 h without apparent loss of ionic conductivity while the quaternary-ammonium-containing membrane degraded in 1M KOH media, leading to IEC loss from 1.62 to 0.93 meq g^{-1} . The greater chemical stability of the imidazolium moiety was probably due to steric hindrance and the resonance effect of the conjugated imidazole ring, weakening the attack of hydroxide ions to the cation.

Traditionally, phosphonium cations have lower stability than ammonium cations and phosphorous is a more expensive reagent than nitrogen.^{18a} Gu, et al. reported the synthesis of 2,4,6-trimethoxyphenyl (TMOP) phosphonium AEMs. The phosphonium AEMs were crosslinked with chloromethylated poly(sulfone) via Friedel-Craft like

intermolecular reactions. The crosslinked samples showed higher degradation temperature (183 °C) as characterized by TGA.^{18b} In addition, Stokes, et al. reported even higher thermal degradation temperatures (above 340°C) of trimethylphosphonium based poly(styrene) AEMs, but these samples were in the Cl form.¹⁹

Cyclic cations including quaternized 1,4-diazabicyclo(2,2,2)octane (DABCO), and piperidinium-based AEMs maintained high alkaline stability at 80 °C in 1.8 M aqueous NaOH conditions, with more than 90% of the cationic moieties remaining after 240 h. The reduction of Hofmann elimination and nucleophilic displacement was due to the unique structure of DABCO which provides internal steric hindrance between carbon and nitrogen and the decreased acidity from the presence of the second nitrogen in the para position. More interestingly, mono-DABCO based copolymer was more stable than bi-DABCO quaternized cations.²⁰⁻²⁴

2.3 Chemical Stability of the AEM Polymer Backbone

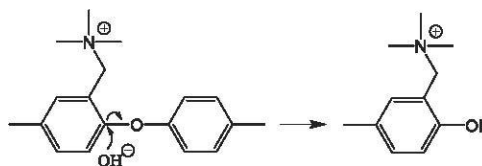


Figure 2.2. Aryl-ether bond cleavage of quaternary ammonium functionalized PAEs under high alkaline environment.

Compared to the extensive studies of the cationic groups, the degradation of the polymer backbone has received less attention. There have been some reports of basic

degradation of polymers, such as poly(vinylidene fluoride), poly(imide), etc. However, most of these studies were performed on hydrophobic polymers. The degradation of hydrophilic polymers can be highly accelerated due to the intimate contact between the polymer molecules and degrading moiety such as reactive oxygen, peroxide, or hydroxide. Generally, the backbone of AEMs was assumed to be much more stable than the cationic moieties. Backbone instability may be due to attack from the hydroxide anion or oxygen. For example, Slade, et al. observed the degradation of the poly(vinylidene fluoride) (PVDF) and poly(vinyl chloride) (PVC) backbone from the attack of OH^- , leading to E2 elimination through dehydrofluorination.^{9,25} In the presence of oxidants such as oxygen or peroxide, it is very likely that the styrenic backbone is oxidized to generate carboxylic acids and CO_2 , ultimately causing chain scission. Recently, Fujimoto, et al. observed that poly(arylene ether) (PAE) underwent aryl-ether linkage cleavage under high pH environments as confirmed by FTIR.²⁶ The degradation of the polymer backbone will influence the mechanical integrity of AEMs, thus reducing the performance of fuel cells by the increased high frequency resistance and catastrophic failure of membrane electrolyte assembly. PAE ionomers displayed good initial fuel cell performance after only 55 h while poly(phenylene) MEA had stable performance without intensive high frequency resistance increase for 300 h.

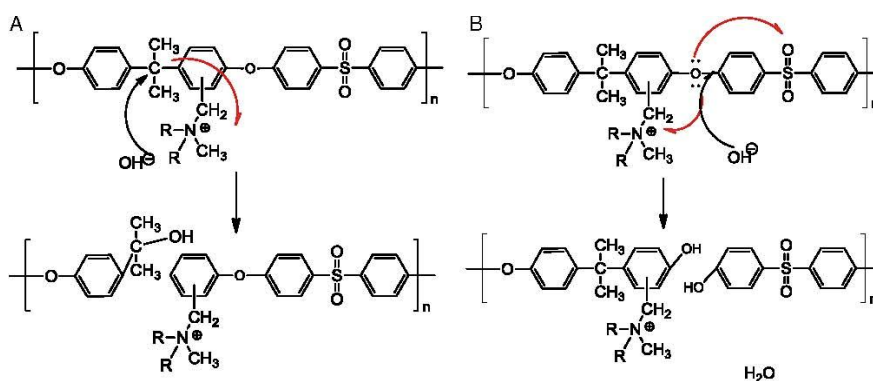


Figure 2.3. The hydrolysis of quaternary carbon and ether bonds in poly(sulfone) tethered with benzyltrimethylammonium cations.

In addition to the ether hydrolysis, the quaternary ammonium cations triggered the poly(sulfone) backbone degradation via quaternary carbon hydrolysis in Arge's degradation analysis.²⁷ The AEM degradation mechanism was elucidated by 2D NMR spectroscopy. Their analysis refuted that the cationic stability mainly dictated the whole AEM stability. They proposed that the longer alkyl side chain between the ring and ionic group, separating the cations from the quaternary carbon and ether bonds may stabilize the poly(sulfone) backbone.

2.3.1 Approaches to Improve Long-term Stability of AEMs

Most AEMs containing benzyltrimethyl ammonium cations suffer from hydroxide degradation, leading to decreases in ion exchange capacity and ion conductivity. However, AEMs with trimethylalkyl side chains have shown increased stability in Tomoi's report.¹⁴ The AEMs with side chains in OH⁻ form were prepared from bromoalkystyrenes with divinylbenzene (DVB) as the crosslinker by suspension polymerization, followed by trimethylamine quaternization and ion exchange with

NaOH. The sample with C4 side chain retained 92% of the original ion exchange capacity (IEC) under hydrolytic condition at 100°C for 30 days. There were no directly observed benzyl and methyl substitution to the alkylene spacers in the anion exchange resins. However, Hofmann elimination occurred in the propyleneoxymethylene spacer based resin as indicated by IR spectra. The degraded resin showed two absorption bands at 1640 and 990 cm^{-1} due to $-\text{CH}=\text{CH}_2$ double bonds. The introduction of alkylene spacers between the benzene ring and quaternary nitrogen is thought to improve the stability of the material in strongly basic conditions due to steric shielding.²⁸

Yan and coworkers reported the synthesis of the incorporation of C6 side chain between ring-ionic group to the poly(fluorene) ionomers using the concept in Tomoi's research. Imidazolium functionalized poly(fluorene)C6 side chain AEMs were synthesized by polycondensation polymerization, producing flexible yet mechanically tough. The hydroxide conductivity of the poly(fluorene) AEMs is up to 23.5 mS cm^{-1} at 30°C (IEC = 0.98, water uptake = 17.3%). Moreover, the synthesized membranes showed excellent alkaline stability in 1 M KOH at 60 °C for 400 h, enabling the C6 side chain poly(fluorene) a suitable candidate.²⁹

Crosslinking of the AEM precursors with diamine is a good synthetic strategy to fabricate mechanically robust AEMs while improving the alkaline stability and long-term fuel cell performance. N,N,N',N'-tetramethylhexane-1,6-diamine was used as the amination/cross-linker to crosslink non-ionic precursor due to high base stability of this diamine crosslinking approach. The crosslinked AEM showed 233 h lifetime and the IEC of the membranes declined by less than 5%, indicating the successful crosslinking. This

aliphatic chain length diamine crosslinker effect on the base stability was reported by Komkova, et al. and corroborated by Park, et al.³⁰ They reported that the AEMs stability increased with the increasing crosslinker chain length when exposed in 2 M NaOH at 40 °C.

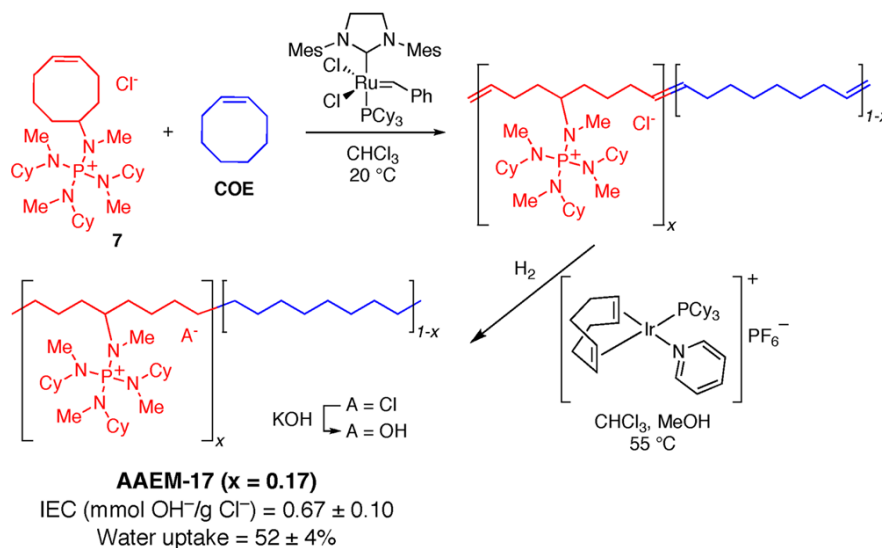


Figure 2.4. Phosphonium functionalized poly(ethylene) for anion conducting membranes.

Noonan, et al. synthesized a new base stable tetrakis(dialkylamino) phosphonium cation with bulky side chains appended to poly(ethylene) by the lab-made monomers via ring-opening metathesis polymerization. These materials showed only a small loss of hydroxide conductivity (from 22 to 18 mS cm⁻¹) in 1M KOH aqueous solution at 80 °C for 22 days. They ascribed the high stability to the phosphonium cations in alkoxide conditions due to the significant energy stabilization of delocalization of the amino phosphonium.³¹

In Holdcroft and coworkers' investigation, they introduced bulky groups adjacent to a benzimidazolium (methylated benzimidazole on nitrogen atoms) to improve the

alkaline stability of the polymer as proven by NMR analysis. The membrane stability was measured by immersing in 2M KOH aqueous solution for 13 days and showed good alkaline stability by measuring the membrane IEC. This realization of enhanced stability of benzimidazole unit provided a novel approach to construct chemically resistant membranes.³²

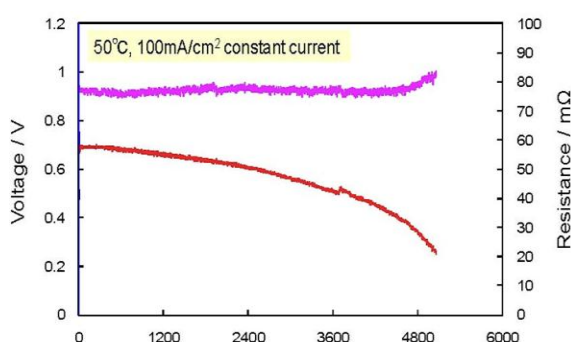


Figure 2.5. Improved durability with crosslinked ionomer.

A remarkable breakthrough was reported by Tokuyama in 2011 using crosslinked ionomer under high ion exchange capacity as tested in the Electrochemical Engineering Center at Penn State. The durability of this cell under 100 mA cm^{-2} at 50°C exceeds 4000 h and dropped to $\sim 80\%$ of the initial voltage. However, there was no detailed polymer structure information released on the material.³³

2.4. Methods to Improve Ionic Conductivity of AEMs

2.4.1. Ionic Conductivity for Ion-containing Polymers

Ion-containing polymers that conduct ions fall into two categories: segmental motion in non-aqueous conditions and water dynamics in hydrated membranes. Polymers

leveraged in anhydrous conditions such as those used in Li-ion batteries transport ions by polymer segmental motion. The segmental motion is dominated by glass transition temperature T_g , and dielectric constant of the system, driving ion pair dissociation. The temperature dependent conductivity of the Li-ion solid-state electrolyte follows a Vogel-Fulcher-Tamman (VFT) dependence indicating the conductivity is governed by long-range polymer segmental motion.³⁴

$$\sigma = \sigma_0 \exp\left(\frac{-B}{T - T_0}\right)$$

where σ is conductivity; σ_0 is the conductivity at infinite temperature; B is a constant; T is temperature; and T_0 is the Vogel temperature. Typically, the segmental motion conductivity ranges from 10^{-8} mS cm⁻¹ to 10^0 mS cm⁻¹.

Hydrated or ionic liquid swollen polymer systems mainly rely on water dynamics for ionic conductivity instead of polymer segmental dynamics and follow Arrhenius dependence because they are far above the T_g of water.^{35,36}

$$\sigma = \sigma_0 \exp\left(\frac{-E_a}{RT}\right)$$

where σ is conductivity; σ_0 is the conductivity at infinite temperature; E_a is the activation energy, R is the universal gas constant; and T is the absolute temperature. In the case of polymer electrolytes, activation energy of E_a is influenced by water absorption, ion content and the interaction of water and ions in the polymer electrolytes.

The thermally activated motion of water in the hydrated polymer facilitates the ionic conduction, allowing the higher conductivity compared to non-aqueous systems. The conductivity in hydrated systems varies from 10^{-1} mS cm⁻¹ to 10^3 mS cm⁻¹.

However, the detailed mechanism of ion transport in ion exchange membranes is still not fully elucidated though hopping and vehicle mechanisms were proposed to shed light on ion transport in pure water.³⁷⁻⁴⁰

2.4.2. Approaches to Obtain High Ionic Conductivity

In contrast to intrinsically high proton conductivity of PEMs, AMEs have poor hydroxide conductivity, resulting in moderate power density and energy density. The hydroxide conductivity is of concern for quaternary ammonium based AEMs. The highly conductive phosphonium-containing AEMs were devised by Gu, et al. The tris(2,4,6-trimethoxyphenyl)polysulfone-methylene quaternary phosphonium hydroxide showed enhanced conductivity (27 mS cm^{-1} , $\text{IEC} = 1.09 \text{ meq g}^{-1}$) at room temperature compared to quaternary ammonium AS-4[®] (13 mS cm^{-1} , $\text{IEC} = 1.30 \text{ meq g}^{-1}$) due to its higher basicity.¹⁸ The phosphonium AEMs exhibited moderate stability in 10M KOH for 48 h at room temperature and high flexibility. Because the 2,4,6-trimethoxyphenyl groups are strong electron donors through conjugation and the high steric bulky group of tris(2,4,6-trimethoxyphenyl)phosphine both of which prevent the central phosphorus atom and the α -carbon atom from hydroxide attack.

In the development of highly conductive PEMs, multiblock copolymers containing sulfonic acid groups in the hydrophilic blocks showed unique phase-separated morphology with well interconnected proton transporting channels. The proton conductivity of the sulfonated multiblock copolymers was high comparable to that of Nafion[®] under severe conditions of low relative humidity and high temperature. The

strategy of using hydrophilic/hydrophobic microstructures with ionic groups in the hydrophilic domains was expanded to synthesize highly conductive aromatic AEMs by Tanaka, et al.⁴¹ The multiblock copolymers were prepared by block copolycondensation of linear hydrophobic and hydrophilic oligomers, followed by post-polymerization. The AEMs showed hydroxide ion conductivities of 144 mS cm^{-1} at 80°C , in which the microphase separation plays a vital role in the high conductivity.

The AEM maintained high conductivity at 80°C for 5000 h under severe, accelerated-aging conditions. The maximum power density of 297 mW cm^{-2} was obtained using hydrazine as fed fuel. Poly(arylene ether sulfone) block copolymers were prepared by polycondensation by Zhao, et al. The block membrane displayed higher conductivity of 29 mS cm^{-1} than the random counterparts (10 mS cm^{-1}) at the similar ion contents.⁴²

Coates, et al. developed tetraalkylammonium-functionalized crosslinked poly(ethylene)-based AEMs using ring opening metathesis copolymerization of functionalized cyclooctenes catalyzed by second generation Grubbs catalyst. These materials showed high hydroxide conductivity of 68.7 mS cm^{-1} at 22°C and 111 mS cm^{-1} at 50°C with IEC 2.30 meq g^{-1} . The high conductivity is from the hydrophobic nature of these materials at high water content, which will promote ionic conductivity and reduce hydroxide ion reactivity within the membranes.²³ Ultimately, high ionic conductivity will help fuel cell operation at relatively low temperature, generating slow degradation.

Yan and coworkers studied quaternization order effects on the ionic conductivity of chloromethylated poly(sulfone): (1) direct quaternization with trimethylamine; (2)

quaternization with diamine crosslinker, followed by treating with trimethylamine; (3) quaternization with diamine crosslinker, followed by alkyl halide. They found the appropriate quaternization would exponentially increase the ionic conductivity of AEMs from 4.7 to 31 mS cm⁻¹ at the same polymer substrates.⁴³ However, they did not offer an explanation about the conductivity improvement. Probably, the post-process generated different morphologies of AEMs.

In summary, the ionic conductivity of AEMs can be increased by the introduction of bulky phosphonium ionic moieties; the corporation of hydrophilic units in the AEMs; the formation of ionic transporting pathways through block copolymer phase separation; the appropriate quaternization approaches. As demonstrated in my work, the ionic conductivity can be tuned by solvent induced long-range ordered microstructures and the soft segmental side chain introduction of aromatic ring and ionic cations.

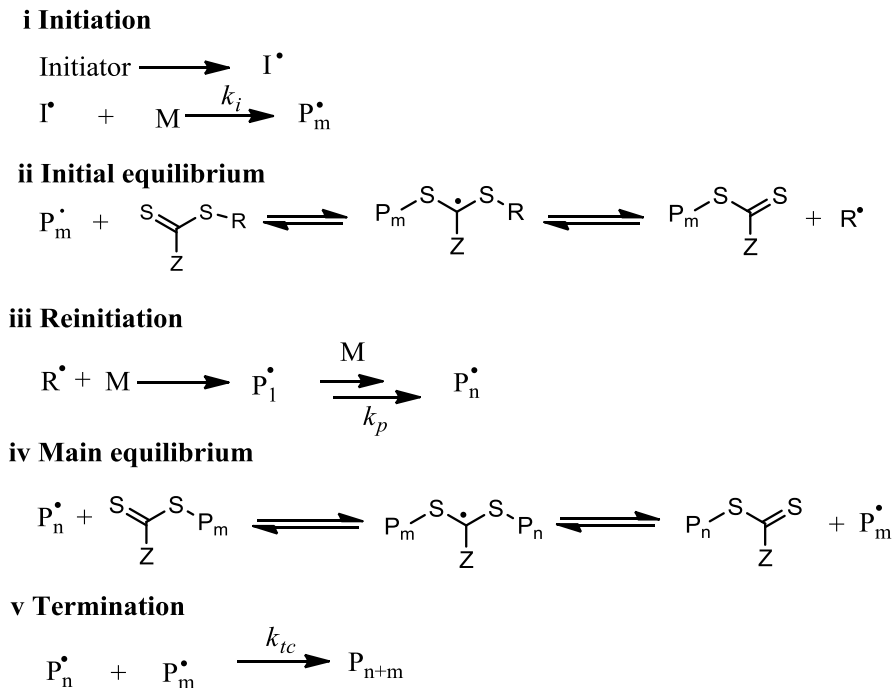
2.5. Block Copolymers

2.5.1. Synthesis of Block Copolymers

The synthesis of narrow polydispersity charged block copolymers with tunable hydrophobic and hydrophilic blocks can be accomplished by living polymerization including ionic polymerization (involving anionic and cationic active sites), condensation, catalyst transfer polymerization or controlled/living radical polymerization. To date, anionic polymerization, nitroxide mediated polymerization (NMP), atomic transfer radical polymerization (ATRP) and reversible addition-fragmentation chain transfer polymerization (RAFT) are the most popular techniques for block copolymer synthesis in controlled/living radical polymerizations. Anionic polymerization requires high purity monomers in anhydrous

condition using air sensitive initiators.⁴⁴⁻⁴⁵ Moreover, it is extremely difficult to obtain reproducible kinetic polymer products and functional monomers leading to ionic groups remain problematic. It should be noted that anionic polymerization maintains the active sites that, in theory, never self-terminate to yield a perfect living polymerization system. Thus this scheme is suitable to prepare multiple block copolymers with consecutive addition of different monomers. Anionic polymerization offers maximum control in polymer composition, low polydispersity and backbone topology. Catalyst transfer polymerization, such metallocene olefin polymerization, initiates and propagates by a catalyst and monomer, having living character. The typical covalent polymerization using organometallic initiator is ring-opening metathesis polymerization (ROMP) to catalyze strained rings.⁴⁶⁻⁴⁸ However, the monomer must be functionalized via multiple-step organic synthesis to generate solid state polymer electrolytes. The monomer synthesis in high purity would increase the expense and time involved in ROMP polymerization.

NMP polymerization necessitates higher polymerization temperature ($> 120\text{ }^{\circ}\text{C}$), long reaction time ($> 24\text{ h}$) and incompatibility with acrylates and methacrylates. ATRP polymerization is used to prepare the copolymers with halide initiators, impeding the feasibility of ATRP polymerization in halide-containing monomers, especially for the preparation of well-defined halide-containing block copolymers.⁴⁹⁻⁵⁴



Scheme 2.2. Generally accepted mechanism for RAFT polymerization.

RAFT polymerization is similar to an otherwise conventional free radical polymerization but uses the sulfur-containing chain transfer agent to mediate the polymerization.⁵³⁻⁵⁶ The commonly accepted mechanism of RAFT polymerization is given in Scheme 2.2. Initiation and propagation occurs in the same manner as conventional radical polymerization. The controlled nature of RAFT polymerization roots from reversible chain equilibration with RAFT chain transfer agent. Initiator and intermediate radical derived chains rapidly equilibrate and have the same probability of monomer addition, thus producing macroinitiator polymers with narrow molecular weight distribution ($\text{PDI} < 1.30$). The macroinitiator retains radical activity and continues to polymerize sequential monomer in presence of new initiator. Given a monomer, the control of RAFT polymerization mainly relies on Z and R groups on the RAFT agent, reaction conditions (concentration, temperature,

etc.) and the ratio of monomer to the RAFT agent. The macro-CTA must remain active to perform the second monomer addition due to the susceptibility of thiocarbonylthio functionality to oxidation, reduction, hydrolysis and aminolysis. Number-average molecular weight corresponds to the following Equation.

$$M_n = \frac{M_0}{[CTA]_0} \times m_M \times con\%$$

where $[M]_0$ and $[CTA]_0$ is the initial monomer and RAFT agent concentration, is the initial concentration of RAFT agent, m_M and $con\%$ are the molecular weight of the monomer and the conversion from monomer to polymers, respectively.

The advantage of RAFT polymerization over otherwise controlled/living radical polymerization is tolerant of functionalized radical active monomers. RAFT technique is able to place the ionic moiety on the desired location and tailor polymer's microstructure and backbone topology. In my research, RAFT polymerization is reliably leveraged to synthesize AB type block copolymers tethered with chloromethyl moieties, which is able to be further quaternized with trimethylamine. These affect the block copolymer self-assembly through solvent casting.

2.5.2. HBr Bromination of Butenylbenzene Group

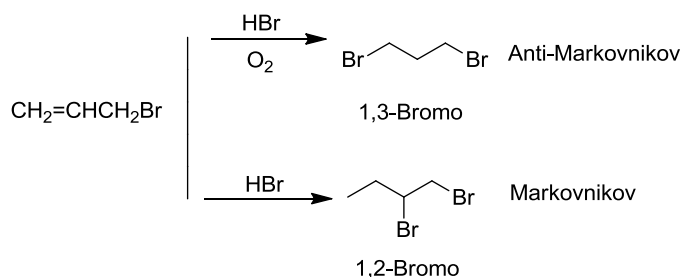


Figure 2.6. O₂ effect on HBr addition to 3-bromo-1-propene.

In the presence of trace oxygen, the principal product of the reaction of allyl bromide with HBr is 1,3-dibromopropane while under oxygen-free conditions, the major product is 1,2-dibromopropane. The terminal addition HBr to the allyl group was attributed to the peroxide effect due to atmospheric oxygen. Allyl bromide is sensitive to oxygen oxidation even in the dark at room temperature as confirmed by peroxide test. At inert atmosphere, the formation of 1,2-addition products was exclusive. Moreover, higher temperature is favorable to 1,3-addition. The addition of acetic acid to the reaction system would accelerate HBr terminal adducts. Based on these findings, the olefinic double bonds attached to butenyl group was brominated with HBr acetic acid exposed to atmospheric environment at room temperature to generate exclusive end addition product.^{55,56}

2.5.3. Block Copolymer Phase Behaviors

Most ion exchange membranes are based on random copolymers due to less synthetic challenge in obtaining these materials. Block copolymers are composed of two or more immiscible blocks of polymerized monomers that are covalently tethered. The thermodynamically immiscible blocks result in phase separation to form tunable and unique morphologies on the nanometer scale due to the incompatibility between unlike blocks.

Flory-Huggins theory can be applied to the thermodynamics of copolymer phase separation using free energy of mixing model.⁵⁷⁻⁵⁸

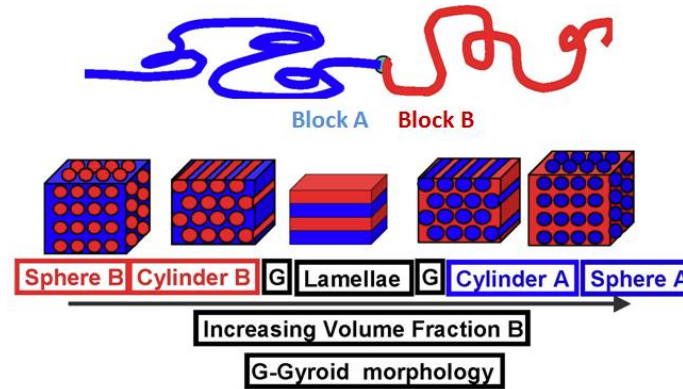


Figure 2.7. The diagram of diblock copolymer with increased volume fraction.⁵⁹

The theory incorporates the enthalpic effect into the interaction parameter, χ . The segregation strength, χN is defined as the interaction parameter, χ , multiplied by the average degree of polymerization, N . Given above a certain χN value and volume fraction, the polymer is in an ordered state above which the polymer phase separates into well-defined, predictable morphologies. The interaction parameter, χ , is calculated from Hildebrand solubility parameters for each component according to the following equation:

$$\chi = \frac{V_r (\delta_A - \delta_B)^2}{RT}$$

where V_r is the reference volume, δ_A and δ_B are the solubility parameters of A and B component, respectively, R is the ideal gas constant, and T is the absolute temperature.^{60,61}

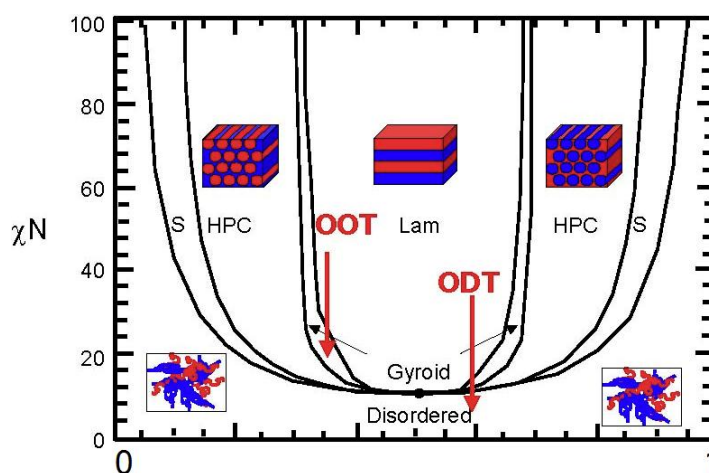


Figure 2.8. Phase diagram of diblock copolymers. OOT = Order Order Transition; ODT = Order Disorder Transition.

Block copolymers are capable of forming a myriad of self-assembled morphologies including spheres arranged on a cubic lattice, hexagonally packed cylinders, interpenetrating gyroids, and alternating lamellae depending upon the intrinsic parameters: volume fraction and segregation strength. In addition to the intrinsic parameters, the molecular weight also determines the stabilization of various morphologies in the case of ionic-neutral diblock copolymers as reported.⁶²

Block copolymer phase separation is principally treated with Flory-Huggins theory which is based on the free energy of mixing of the polymer segments and self-consistent mean field theory. The free energy of mixing, G , can be described by variables, H is enthalpy, T is the absolute temperature, and S is entropy. The system is favorable to minimize the free energy of mixing. The enthalpic part of the equation includes the interaction between monomers while the entropic part incorporates polymer configurations and the covalent bond between monomers.

$$\Delta G = \Delta H - T\Delta S$$

The ionic conductivity and mechanical properties of ion exchange membranes are linked to the morphology of the membranes. The properties of the membranes such as ionic conductivity and mechanical properties could be tuned by altering the morphology and the block materials' chemical compositions. The ease of the tunability of block copolymers would lead to improved membrane performance.

For fuel cell applications the membranes must be mechanically robust, highly conductive, and chemically stable under long-term alkaline conditions. Mechanically brittle membranes can in some cases be converted to robust membranes in liquid water by introducing soft segments such as poly(methacrylates) or a crystallizable block as described in my work.⁶³ The phase separation of ionic block copolymers has been demonstrated to increase the ionic conductivity through formation of ionic channels. But the degree of polymerization will influence the hydrophilic domain size as there is a greater energy barrier to the ordered morphology when the molecular weight of block copolymer increases. Moreover, the solvent used for casting the membranes can induce long-range ordered microstructures by selecting benign solvents to the ionic block copolymers, thus leading to greater ionic conductivity.^{64,65} The methods to enhance the chemical stability have been thoroughly discussed in previous section.

Functionalization of block copolymers with ionic moieties (sulfonic acid and quaternary ammonium groups) in the hydrophilic blocks greatly increases the interaction parameter compared to un-functionalized copolymers. This segregation strength increase can lead to an increase in the interdomain size through polymer chain stretching by introduction of ionic motifs. The ionic groups complicate the phase behavior, hindering theoretical and simulation advancement. Segalman and coworkers observed that the interdomain size

increases with the addition of trifluoroacetic acid due to the formation of charged side groups, leading to chain stretching as well as the increase in hydrophilic volume fraction.⁶⁶ In addition to the interdomain size increase, the ionic conductivity increases with the interdomain size by reducing the number of block copolymer interfaces and the interfacial width. The increase in interfaces number and interfacial width would hinder the ion mobility, thus reducing the ionic conductivity. The ion transport mainly relies on the polymer segmental motion but was consistent with Arrhenius behavior as indicated in **Figure 2.9**.

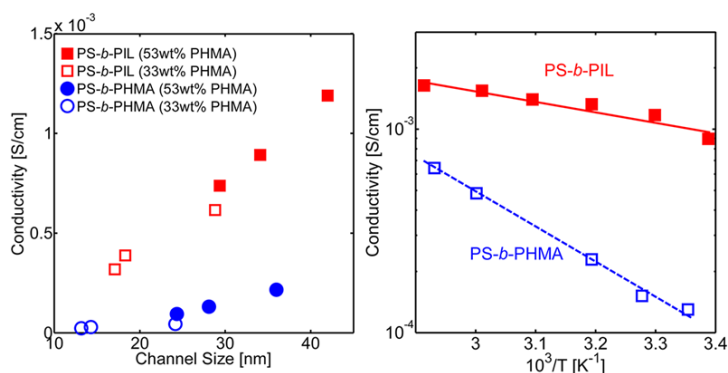


Figure 2.9. Ionic conductivity as a function of interdomain spacing and temperature.

In contrast to the conductivity dependence on chain motion, the changes in the domain size do not affect the ion transport for the ion conducting polymer in hydrated or swollen polymer systems. As described above, the ionic conductivity is dependent on the thermally activated dynamics of water. The incorporation of ionic motifs in block copolymers has concentrated on Nafion[®]-like fluorinated or aromatic backbones with sulfonic acid pendant groups. Elabd, et al. and found that poly(styrene-*b*-isobutylene-*b*-styrene) (SIBS) with lamellar morphologies showed enhanced proton conductivity compared to randomly sulfonated poly(styrene) under the same conditions.⁶² Park, et al. and Ye, et al.

in different groups have studied the relative humidity effect on the morphology changes of poly(styrene sulfonate)-*block*-poly(methylbutylene) (PSS-*b*-PMB) and poly(methylmethacrylate-*b*-1-[(2-methacryloyloxy)ethyl]-3-butyylimidazolium) (PMMA-*b*-PMEBIm).^{67,68} They found that long-range ordered microstructures were disrupted by increasing humidity and these block samples showed higher conductivity than random copolymers. Balsara, et al. has observed various microstructures for PSS-*b*-PMB in the location of lamellar morphology as predicted by Flory-Huggins and self-consistent mean field theories, but the ion introduction in the hydrophilic blocks led to perforate lamellar, cylindrical, and gyroid microstructures.

2.5.4. Kinetic Trapping of Block Copolymers

The term kinetic trapping is used to describe the polymer morphology in a non-equilibrium state, moving towards the lowest Gibbs free energy. Kinetic trapping would generate defect structures as observed in atomic force or transmission electronic microscopy images, interrupting long-range ordered microstructure formation. So, it is necessary to eliminate the defects in the block copolymer films to approach an equilibrium state in the lowest energy. Generally, thermal and solvent annealing is employed to annihilate and disperse defects in block copolymer membranes. However, high glass transition temperature, T_g , ion-containing polymers make thermal annealing fruitless but solvent annealing is a good choice due to swelling and plasticization of the ionic domains. Benign solvent casting at low evaporation rate during solid membrane formation allows sufficient time for the phase formation to obtain a near-equilibrium microstructure. The benign solvent for the polymers will solvate the polymers to some

extent to allow for segmental motion, favorable to the phase separation of the polymers. In essence, the solvent reduces the polymer's glass transition temperature. In this fashion, solvent casting behaves like thermal annealing to facilitate the polymer movement. Slow solvent casting is particularly useful in the case of ion-containing block copolymers as demonstrated in my research.

Block copolymer AEMs, particularly well-defined block copolymers have not been investigated in detail compared to their well-documented proton exchange membrane analogues due to the synthetic challenges involved with AEMs and less development of the chemistry in this field. In previous studies, quaternized poly(hexyl methacrylate)-*block*-poly(vinylbenzyl chloride) (PHMA-*b*-PVBC) block copolymers were synthesized by post-polymerization modification under relatively mild conditions to minimize side reactions and crosslinking, which will partially hydrolyze the ester moieties to acetic acid.⁷¹ This synthetic route suffers from low degree of functionalization and difficult repeatability. The small fraction of acid motifs on the hydrophobic block could prevent from the formation of long-range ordered morphology due to the electrostatic interaction with hydrophilic block as shown in small-angle X-ray scattering. The non-ionic block in quaternized block copolymers increased mechanical strength in comparison with randomly-functionalized copolymers by controlling the swelling. Miyatake, et al. confirmed that the selectively quaternized multiblock copoly(arylene ether) fluorene-*block* copolymers showed higher conductivity than random copolymer counterparts.⁴¹ It would be interesting to perform additional work on how to achieve high ionic conductivity and improve the mechanical robustness in liquid water based on block copolymers. Although considerable insights into phase behavior of sulfonated block copolymer have been accomplished, more efforts are necessitated to delineate the

universal picture of structure-morphology-property relationship of anionic block copolymers. The synthesis of well-defined ionic placement anionic block copolymers guides the direction for the purpose of designing and developing new ionic materials in water and gas separation applications and battery and fuel cells.

2.6 References

1. McLean, G. F.; Niet, T.; Prince-Richard, S.; Djilali, N. *Int. J. Hydrogen Energy* **2002**, *27*, 507-526.
2. Varcoe, J. R.; Slade, R. C. T. *Fuel Cells* **2005**, *5*, 187-200.
3. Mauritz, K. A.; Moore, R. B. *Chemical Reviews* **2004**, *104*, 4535-4585.
4. Wang, J. H.; Li, S. H.; Zhang, S. B. *Macromolecules* **2010**, *43*, 3890-3896.
5. Matsui, K.; Tobita, E.; Sugimoto, K.; Kondo, K.; Seita, T.; Akimoto, A. *J. Appl. Polym. Sci.* **1986**, *32*, 4137-4143.
6. Chempath, S.; Einsla, B. R.; Pratt, L. R.; Macomber, C. S.; Boncella, J. M.; Rau, J.; Pivovar, B. S. *J. Phys. Chem. C* **2008**, *112*, 3179-3182.
7. Zha, Y.; Hickner, M.A.; Tew, G.N. *J. Am. Chem. Soc.* **2012**, *134*, 4493-4496.
8. Bauer, B.; Strathmann, H.; Effenberger, F. *Desalination* **1990**, *79*, 125-144.
9. Merle, G.; Wessling, M.; Nijmeijer, K. *J. Membr. Sci.* **2011**, *377*, 1-35.
10. Ye, Y.; Elabd, Y.A. Chemical Stability of Anion Exchange Membranes for Alkaline Fuel Cells; In *Polymers for Energy Storage and Delivery: Polyelectrolytes for Batteries and Fuel Cells*. Page, K.A.; Soles, C.L.; Runt, J., Eds.; Oxford University Press, **2012**; ACS Symposium Series *1096*, 234-251.
11. Ghigo, G.; Cagnina, S.; Maranzana, A.; Tonachini, G. *J. Org. Chem.* **2010**, *75*, 3608-3617.
12. Einsla, B. R.; Chempath, S.; Pratt, L.; Boncella, J.; Rau, J.; Macomber, C.; Pivovar, B. *ECS Transactions* **2007**, *11*, 1173-1180.

13. Chempath, S.; Boncella, J. M.; Pratt, L. R.; Henson, N.; Pivovar, B. S. *J. Phys. Chem. C* **2010**, *114*, 11977-11983.
14. Sata, T.; Tsujimoto, M.; Yamaguchi, T.; Matsusaki, K. *J. Membr. Sci.* **1996**, *112*, 161-170.
15. Kim, D. S.; Labouriau, A.; Guiver, M. D.; Kim, Y. S. *Chemistry of Materials* **2011**, *23*, 3795-3797.
16. Qu, C.; Zhang, H.; Zhang, F.; Liu, B. *J. Mater. Chem.* **2012**, *22*, 8203-8207.
17. Qiu, B.; Lin, B.; Qiu, L.; Yan, F. *J. Mater. Chem.*, **2012**, *22*, 1040-1045.
18. a) Greso, A. J.; Moore, R. B.; Cable, K. M.; Jarrett, W. L.; Mauritz, K. A. *Polymer* **1997**, *38*, 1345-1356. b) Gu, S.; Cai, R.; Luo, T.; Chen, Z.; Sun, M.; Liu, Y.; He, G.; Yan, Y. *Angew. Chem. Int. Ed.* **2009**, *48*, 6499-6502.
19. Stokes, K. K.; Orlicki, J. A.; Beyer, F. L. *Polymer Chemistry* **2011**, *2*, 80-82.
20. Pandey, A. K.; Goswami, A.; Sen, D.; Mazumder, S.; Childs, R. F. *J. Membr. Sci.* **2003**, *217*, 117-130.
22. Komkova, E. N.; Stamatialis, D. F.; Strathmann, H.; Wessling, M. *J. Membr. Sci.* **2004**, *244*, 25-34.
23. Robertson, N. J.; Kostalik, H. A.; Clark, T. J.; Mutolo, P. F.; Abruna, H. D.; Coates, G. W. *J. Am. Chem. Soc.* **2010**, *132*, 3400-3404.
24. Scindia, Y. M.; Pandey, A. K.; Reddy, A. V. R. *J. Membr. Sci.* **2005**, *249*, 143-152.
25. Danks, T.N.; Slade, R.C.T.; Varcoe, C.R. *J. Mater. Chem.*, **2003**, *13*, 712-721.
26. Fujimoto, C.; Kim, D.S.; Hibbs, M.; Wroblewski, D.; Kim, Y.S. *J. Membr. Sci.* **2012**, *423-424*, 438-449.
27. Arges, C.G.; Ramani, V. *PNAS*, **2013**, *110*(7), 2490-2495.
28. a) Tomoi, M.; Yamaguchi, K.; Ando, R.; Kantake, Y.; Aozaki, Y.; Kubota, H. *J. Appl. Polym. Sci.* **1997**, *64*, 1161-1167. b) Hibbs, M.R.; *J. Polym. Sci.; B: Polym. Phys.* **2012**, in press
29. Lin, B.C.; Qiu, L.H.; Qiu, B.; Peng, Y.; Yan, F.; *Macromolecules* **2011**, *44*, 9642-9649.

30. a) Varcoe, J.R.; Slade, R.C.T.; Yee, E.L.H. *Chem. Commun.*, **2006**, 1428-1429. B) Pan, J.; Li, Y.; Zhuang, L.; Lu, J. *Chem. Commun.*, **2010**, 46, 8597-8599.
31. Noonan, K. J. T.; Hugar, K. M.; Kostalik, H. A.; Lobkovsky, E. B.; Abruña, H. D.; Coates, G. W. *J. Am. Chem. Soc.* **2012**, *134*, 18161–18164.
32. Thomas, O.D.; Soo, K.; Peckham, T.J.; Kulkarni, M.P.; Holdcroft, S. *J. Am. Chem. Soc.*, **2012**, *134*, 10753–10756.
33. Fukuta, K. 2011 AMFC Workshop, Tokuyama Ltd.
34. Klein, R. J.; Welna, D. T.; Weikel, A. L.; Allcock, H. R.; Runt, J. *Macromolecules* **2007**, *40*, 3990–3995.
35. Schuster, M. F. H.; Meyer, W. H.; Schuster, M.; Kreuer, K. D. *Chem. Mater.* **2004**, *16*, 329–337.
36. Hickner, M. A. *J. Polym. Sci. Part B Polym. Phys.* **2012**, *50*, 9–20.
37. Kreuer, K.-D. *Chem. Mater.* **1996**, *8*, 610–641.
38. Kreuer, K.-D.; Paddison, S. J.; Spohr, E.; Schuster, M. *Chem. Rev.* **2004**, *104*, 4637–4678.
39. Zawodzinski, T. A.; Neeman, M.; Sillerud, L. O.; Gottesfeld, S. *J. Phys. Chem.* **1991**, *95*, 6040–6044.
40. Marx, D.; Chandra, A.; Tuckerman, M. E. *Chem. Rev.* **2010**, *110*, 2174–216.
41. Tanaka, M.; Fukasawa, K.; Nishino, E.; Yamaguchi, S.; Yamada, K.; Tanaka, H.; Bae, B.; Miyatake, K.; Watanabe, M. *J. Am. Chem. Soc.* **2011**, *133*, 10646–54.
42. Zhao, Z.; Wang, J.H.; Li, S.H.; Zhang, S.B. *J. Power Sources* **2011**, *196*, 4445-4450.
43. Wang, G.; Weng, Y.; Chu, D.; Chen, R.; Xie, D. *J. Membr. Sci.* **2009**, *332*, 63–68.
44. Hawker, C.J.; Wooley, K.L. *Science*. **2005**, *309*, 1200-1205.
45. a) Szwarc, M. *Nature*. **1956**, *178*, 1168-1170. b) Sawamoto, M. *Prog. Polym. Sci.* **1991**, *16*, 111-172.
46. Webster, O.W. *Science*. **1991**, *256*, 887-893.
47. Bielawski, C.W.; Grubbs, R.H. *Prog. Polym. Sci.* **2007**, *32*, 1-29.

48. Gilliom, L.R.; Grubbs, R.H. *J. Am. Chem. Soc.* **1986**, *108*, 733-742.
49. Hawker, C.J.; Bosman, A.W.; Harth, E. *Chem. Rev.* **2001**, *101*, 3661-3688.
50. Moad, G.; Rizzardo, E.; Solomon, D.H. *Macromolecules*. **1982**, *15*, 909-914.
51. Otsu, T.; Yoshida, M, *Makromol. Chem. Rapid Commun.***1982**, *3*, 127-132.
52. Otsu, T. *J. Polym. Sci., Polym. Chem.* **2000**, *38*, 2121-2136.
53. Wang, J.S.; Matyjaszewski, K. *J. Am. Chem. Soc.* **1995**, *117*, 5614-5615.
54. Wang, J.S.; Matyjaszewski, K. *Macromolecules*. **1995**, *28*, 7901-7910.
55. Kharasch, M.S.; Mayo, F.R. *J. Am. Chem. Soc.*, **1933**, *55*, 2468-2496.
56. Farmer E.H. *Trans. Farady Soc.*, **1946**, *42*, 228-236.
57. Knychala, P.; Banaszak, M.; Park, M. J.; Balsara, N. P. *Macromolecules* **2009**, *42*, 8925–8932.
58. Lu, X.; Weiss, R. A. *Macromolecules* **1996**, *29*, 1216–1221.
59. The slides from MatSE 542: Polymer Materials in Penn State
60. Matsen, M. W.; Schick, M. *Phys. Rev. Lett.* **1994**, *72*, 2660–2663.
61. Bates, F. S.; Fredrickson, G. H. *Phys. Today* **1999**, *52*, 32–38.
62. Elabd, Y.A.; Napadensky, E.; Walker, C.W.; Winey, K.I. *Macromolecules***2006**, *39*, 399-407.
63. Saito, T.; Moore, H. D.; Hickner, M. A. *Macromolecules* **2010**, *43*, 599–601.
64. Kim, B.; Kim, J.; Jung, B. *J. Membr. Sci.* **2005**, *250*, 175–182.
65. Park, M. J.; Downing, K. H.; Jackson, A.; Gomez, E. D.; Minor, A. M.; Cookson, D.; Weber, A. Z.; Balsara, N. P. *Nano Lett.* **2007**, *7*, 3547–3552.
66. Schneider, Y.; Modestino, M.A.; McCulloch, B.L.; Hoarfrost, M.L.; Hess, R.W.; Segalman, R.A. *Macromolecules***2013**, *46*, 1543-1548.
67. Park, M.J.; Balsara, N.P. *Macromolecules***2008**, *41*, 3678-3687.

68. Ye, Y. Sharick, S.; Eric M. Davis, E.M.; Winey, K.I.; Elabd, Y.A. *ACS Macro Lett.* **2013**, 2, 575–580.
69. Amundson, K.; Helfand, E.; Quan, X.; Hudson, S. D.; Smith, S. D. *Macromolecules* **1994**, 27, 6559-6570.
70. Horvat, A.; Sevink, G. J. A.; Zvelindovsky, A. V.; Krekhov, A.; Tsarkova, L. *ACS Nano* **2008**, 2, 1143-1152.
71. Disabb-Miller, M. L.; Johnson, Z. D.; Hickner, M. A. *Macromolecules* **2013**, 46, 949–956.

Chapter 3

Experimental Details of RAFT Polymerization, Membrane Fabrication and Characterization

3.1. Introduction

This chapter will introduce general procedures of the block copolymer synthesis by RAFT polymerization, block copolymer quaternization with trimethylamine, and membranes fabrication used in the dissertation and concisely introduces the characterization methods. The polymer sulfonimide synthesis for PEM fuel cells will be noted in the **Chapter 7**. The preparation procedures and characterization techniques presented in this chapter are applicable to all block copolymer-based AEMs used in this work for structure and property elucidation.

3.2. Materials

All chemicals and reagents were purchased from Sigma-Aldrich (St. Louis, MO) except as noted. Styrene (>99 %) was distilled under reduced pressure. Vinylbenzyl chloride (VBC) (>90 %) was deinhibited by 0.5wt. % NaOH solution, followed by DI water. Hexyl methacrylate (HMA) (98%) and lauryl methacrylate (LMA) (96%) were washed with 0.1M aqueous NaOH solution and dried over sodium sulfate before distillation under reduced pressure. Stearyl methacrylate (SMA) (technical grade) was deinhibited by 0.1M NaOH solution, followed by DI water and ultimately stearyl

methacrylate was purified by recrystallization from hexane at -20 °C. 2,2'-Azobis(2-methylpropionitrile) (AIBN) (98 %) was purified by recrystallization from methanol and dried under vacuum oven at 40 °C overnight.. Allylmagnesium bromide (allylMgBr, 1 M in ether), hydrobromic acid solution (33 wt. % in acetic acid), and S-dodecyl- S'-(α,α' -dimethyl- α'' -acetic acid)trithiocarbonate (DDMAT) (98 %), 4-Cyano-4-[(dodecylsulfanylthiocarbonyl)sulfanyl]pentanoic acid (CDP) (97%), 1-bromopropane (99%) and magnesium turnings (99.5%, purum, for Grignard reactions) were used as received. Poly(2,6-dimethyl-1,4-phenylene oxide) (PPO) with the average molecular weight of 20,000 g/mol (\sim PDI = 1.50) and poly(styrene) (PS) with the average molecular weight of 35,000 g/mol were obtained from Sigma Aldrich. Radel NT 5500 was donated from Solvay Advanced Polymer (Alpharetta, GA). Trifluoromethanesulfonamide was received from TCI and used as received.

3.3 Synthesis of Block Copolymers

This section will present the general synthesis and characterization of well-defined block copolymers, quaternization of thus-formed block copolymers. The techniques used in membranes characterization will be discussed in detail.

3.3.1 Synthesis of Block Copolymers

The detailed procedures for the block copolymer syntheses in this dissertation will be offered in each section. Monomers must be purified by appropriate methods to remove

the polymerization inhibitors and side product impurities before use. The chain transfer agents were selected to better control of RAFT polymerization in controlled/living manner according to the chemical nature of the monomers. The monomer, chain transfer agent and appropriate solvent when applicable were added to a round-bottom reaction flask. The vessel was purged with argon to remove oxygen from the reaction system and sealed with rubber septum. The polymerization system was placed in a pre-heated oil bath under the proper temperature to perform the reaction. After the appropriate reaction time, the reaction vessel was allowed to cool to room temperature under inert atmosphere. The reaction contents were diluted with tetrahydrofuran (THF). The polymer was precipitated into methanol (MeOH), washed, precipitated for three times to remove any trace monomers. The polymer was dried in a vacuum oven at 40 °C overnight before characterization. The first block acted as the macro-CTA and the synthesis of diblock copolymers was performed in a similar fashion as described above. Additional specific polymerization conditions will be offered in the following chapters pertaining to the preparation of the well-defined block copolymers.

3.4 Characterization of Block Copolymers

This section will discuss the typical characterization of block polymers. Gel permeation chromatography (GPC) was used to determine the molecular weight and polydispersity index (PDI) of the synthesized polymers based near monodisperse poly(styrene) calibration standards and to ensure the successful chain extension of the

macro-CTA. Nuclear magnetic resonance spectroscopy (NMR) was also used to ascertain the degree of polymerization by end group analysis and block copolymer composition.

3.4.1 Gel Permeation Chromatography

Gel permeation chromatography (GPC) was conducted to determine the molecular weight and polydispersity index and calibrated with poly(styrene) standards (Varian, Lake Forest, CA) in tetrahydrofuran (THF) with a flow rate of 1 mL min^{-1} at $35\text{ }^{\circ}\text{C}$ on a Waters (Milford, MA) GPC system with a Waters 2414 refractive index (RI) detector. The GPC is equipped with Waters Breeze software for analysis and a 1515 isocratic HPLC pump. The non-quaternized homopolymer and block copolymers were dissolved in HPLC grade THF for this characterization.

3.4.2 Quaternization of Block Copolymers

In a typical quaternization, to a stirring solution of block copolymer in dimethylformamide (DMF) was added 2 equivalent aqueous trimethylamine and stirred at $50\text{ }^{\circ}\text{C}$ for 24 h. The homogeneous solution was cooled to room temperature and concentrated under reduced pressure to give an orange viscous liquid. The quaternized form $\text{PS}_{100}\text{-}b\text{-PBBS}_{45}$ was dried *in vacuo* overnight at $50\text{ }^{\circ}\text{C}$ to give an orange solid before use.

3.4.3 Nuclear Magnetic Resonance Spectroscopy

^1H and ^{13}C nuclear magnetic resonance (NMR) spectroscopies were performed on a Bruker (Bruker Biospin, Billerica, MA) CDPX-300 FT-NMR using CDCl_3 as solvent and the residue peaks of CDCl_3 at 7.27 ppm as internal references. The dried polymer samples were dissolved in CDCl_3 for NMR characterization. This technique was also employed to calculate the M_n of macro-CTAs from end group analysis. The total molecular weight of diblock copolymers were calculated from the ratio of the second blocks to macro-CTAs on the basis of the degree of polymerization. To obtain the most accurate molecular weight information from NMR spectra, the degree of polymerization of the macro-CTAs was designed to be below 100. The characteristic end groups of the macro-CTAs were clearly visible in ^1H NMR spectra.

3.5 Membrane Fabrication and Characterization

This section will discuss the key parameters for the evaluation of membrane performance. Measuring conductivity and water uptake in relative humidity conditions and liquid water techniques and membrane morphology determination will be described.

3.5.1 Membrane Fabrication

The quaternized polymer powders were added to a flask with aqueous NaHCO_3 or NaCl (1 M) and the solutions were decanted after 8 h upon standing and refilled every 8 h for two times to ensure complete ion exchange. The removal of excess NaHCO_3 or NaCl was carried out by dialysis with 6-8 kDa molecular weight cut-off (MWCO) membranes (Spectra/Por® 1 Dialysis Membrane purchased from Spectrum Laboratories, Inc.,

Rancho Dominguez, CA) in de-ionized water with fresh water changes three times at 8 h intervals. The bicarbonate or chloride form polymers were dried *in vacuo* at 40 °C for 24 h. The anion exchange membranes were cast from bicarbonate or chloride form quaternized block copolymers in toluene and n-propanol (v/v 1:1) or DMF and n-propanol (v/v 3:1) on polytetrafluoroethylene (PTFE) molds at room temperature for 24 h in a slightly ventilated desiccator. The membranes were then dried at room temperature prior to use for other measurements.

3.5.2 Water Uptake

Relative water uptake from the vapor phase was measured using a TA Instruments (New Castle, DE, USA) Q5000SA dynamic vapor sorption analyzer at 30 °C. The relative humidity of the sample chamber was controlled by mass flow control of a fully hydrated gas stream and a dry gas stream. The total gas flow rate was 200 std. cm³ min⁻¹. The mass of the membrane samples was around 15 mg and the relative humidity ranged from 20 % to 95 %. The samples were dried under vacuum before measurements. Humidity and temperature were controlled by an Espec SH-241 humidity chamber for relative-humidity conductivity measurement.

Liquid water uptake was measured after drying the membrane at 50 °C under vacuum for 12 h. The dried membrane was fully immersed in deionized water to equilibrate for 24 h before use. The hydrated membrane was lightly blotted with a

Kimwipe[®] to remove surface water and periodically weighed on an analytical balance until a constant hydrated mass was obtained, giving the mass-based water uptake.

Mass uptake was calculated from $(M_{wet} - M_{dry})/M_{dry}$. Hydration number (λ) or water molecules per ammonium group was calculated from

$$\lambda = \left(\frac{M_{wet} - M_{dry}}{18} \right) \left(\frac{1000}{M_{dry} \times IEC} \right)$$

Where M_{wet} is the sample mass at a given RH and, M_{dry} is the dry sample mass.

3.5.3 Conductivity measurements

AC impedance spectroscopy was used to measure the membrane resistance using a Solartron SI 1260A Impedance/Gain-Phase Analyzer. The film resistance was measured in a two-point, in-plane geometry at frequencies between 1 MHz and 100 Hz at 30 °C under humidified conditions. Humidity and temperature were controlled by an Espec SH-241 humidity chamber. The free-standing film conductivity was measured in a two-point, in-plane geometry at frequencies between 1 MHz and 100 Hz in liquid water at room temperature (~20°C). In both cases, the impedance was extrapolated to an imaginary component of zero to approximate the DC film resistance.

The conductivity (σ) of the film was calculated from the resistance (R) using:

$$\sigma = L/(RA)$$

where L is the distance between electrodes, R is the resistance of the membrane, and A is the cross-sectional area of the membranes and calculated from the sample thickness, t , and width, w , respectively.

3.5.4 Calculation of Ion Exchange Capacity (IEC)

The IEC of the polymers was calculated based on the ratio of the hydrophobic block and the hydrophilic block in quaternized chloride form from ^1H NMR data assuming 100 % amination. The ratio of hydrophobic and hydrophilic blocks was calculated by correspondingly characteristic peaks assuming that the polymer compositions remained constant before and after quaternization with aqueous trimethylamine solution.

3.5.5 Small Angle X-ray Scattering

Small angle x-ray scattering, SAXS, patterns were obtained on a Rigaku (formerly Molecular Metrology) instrument with a pinhole camera with Osmic microfocus source and parallel beam optic. The instrument had a Cu target with a 1.452 Å wavelength and also a multiwire 2D area detector. Measurements were conducted on dried samples under vacuum at ambient temperature. The typical collection times ranged from 2-4h to achieve a minimum of 300,000 photon counts. Scattering intensities were normalized for background scattering and beam transmission. Interdomain spacings were calculated from equation below:

$$d = 2\pi/q$$

where d is the interdomain spacing and q is the scattering vector in inverse Angstrom. D-spacing values are reported in nm.

3.5.6 Transmission Electron Microscopy

Transmission electron images were collected on a JEOL JEM 1200 EXII microscope with a tungsten emitter operating at 80 kV. All images were captured with unstained samples and recorded on a CCD camera. Cast membrane samples were cross-sectioned at -120 °C using a Leica Ultracut UC6 ultramicrotome with an EMFC6 cryo attachment by Missy Hazen of the Huck Institutes of the Life Sciences at the Pennsylvania State University. The sections were collected on grids coated with 400hex carbon/formvar. All images were of unstained samples.

3.5.7 Thermogravimetric Analysis (TGA)

Thermogravimetric analysis, TGA, (TA instruments 2050) was carried out under a nitrogen atmosphere from room temperature to 800°C and a heating rate of 10 °C min⁻¹. All the samples were first vacuum dried before TGA characterization.

3.5.8 Differential Scanning Calorimetry (DSC)

A differential scanning calorimeter, DSC, (TA instrument Q100) was used to measure the crystallinity of the samples. Membrane samples of 5-10 mg sealed in aluminum pans were first heated from room temperature up to 180 °C at 10 °Cmin⁻¹, cooled -50 °C at 10 °C min⁻¹, and second heated to 180 °C at 10 °Cmin⁻¹ under pure nitrogen. Heat flow as watts (mW) was recorded during the heating and cooling cycles. The enthalpy change, ΔH_m were obtained by normalizing the heat change at the thermal transitions and the polymer mass (g). The melting point, T_m , was defined as the peak temperature of the melting endotherm.

Chapter 4

Synthesis of Side Chain Block Copolymers for Stable Anion Exchange Membranes

This chapter is adapted from the draft Wang, L.Z.; Hickner, M. A. submitted for publication.

4.1 Introduction

There have been just a few reports on AEMs with nanophase separated morphology, the strategy of employing a block copolymer structure is expected to be useful in AEMs to boost conductivity and maintain robust membrane mechanical properties. Generally, block copolymers that are prepared from controlled/living polymerization techniques provide a template for the formation of ionic domains, where phase separation occurs on a nanometer scale due to the thermodynamic incompatibility between chemically dissimilar blocks. As a result, these materials are capable of forming a variety of self-assembled morphologies including spheres arranged on a cubic lattice, hexagonally packed cylinders, interpenetrating gyroids, and alternating lamellae. The self-organization of these block copolymers offers the opportunity for control of membrane morphology by manipulation of the chemical compositions and relative volumes of the constituent blocks. In ion-containing block copolymers, phase separation is anticipated to be quite strong due to the large solubility parameter difference between the ionic and non-ionic blocks. However, ions introduce complications in predicting the

resulting phase structure of the material including difficulty in estimating the solubility parameters and kinetic trapping of non-equilibrium morphologies during solvent casting of membranes. Despite these drawbacks, pursuing the block copolymer strategy for AEMs may help to further elucidate structure-property relationships in this class of materials.

In some key work on block copolymer AEMs, a chloromethylated block copoly(arylene ether sulfone) sample had higher hydroxide conductivity (29 mS cm^{-1} , water uptake = 20%, ca. $\lambda = 7.0$) than the random copolymer analog (15 mS cm^{-1} , water uptake = 13%, ca. $\lambda = 4.6$) at 20°C at similar IEC ($\sim 1.60 \text{ meq g}^{-1}$).⁸ Tanaka et al. confirmed that quaternized multiblock copoly(arylene ether) based membranes had greater hydroxide conductivity (144 mS cm^{-1} , IEC = 1.93 meq g^{-1}) than that of the random sample (34 mS cm^{-1} , IEC = 1.88 meq g^{-1}) at 80°C .⁹

In other work on commercially available block copolymer substrates, the highest obtained IEC (0.3 meq g^{-1}) of chloromethylated poly(styrene-*b*-ethylene-*co*-butylene-*b*-styrene) (Q-SEBS) copolymers was limited due to the gelation of the polymer at high degrees of chloromethylation. The Q-SEBS membrane showed moderate hydroxide conductivity of 5 mS cm^{-1} (IEC = 0.3 meq g^{-1} , water uptake = 13%, hydration number = 24) at 30°C .¹⁰ More recently, Tsai et al. found that the AEMs cast from PS-*b*-P(VBTMA)(OH) block copolymers in DMF with lamellar or cylindrical microstructures confirmed by SAXS showed conductivity dependence on the morphology and the generation of long range ordered conductive channels which facilitated the ion transport

in the prepared AEMs.¹¹ At 80°C with 90% relative humidity the conductivity of a high ion content sample ($\text{IEC} = 1.36 \text{ meq g}^{-1}$, 12.5 mS cm^{-1}) was approximately increased 4-fold compared to that of the low ion content sample ($\text{IEC} = 0.58 \text{ meq g}^{-1}$, 0.36 mS cm^{-1}). Part of this difference in conductivity between the samples was attributed to the morphological change from spherical to cylindrical or lamellar along with the IEC increase and percolation of the ion-functionalized phase.

In addition to continuing to raise the ionic conductivity of these materials, another significant challenge for AEMs is their chemical instability under alkaline conditions due to well-known degradation pathways of quaternary ammonium cations.¹² Li, et al. have developed a series of cationic poly(phenylene oxide) AEMs with alkyl side chains attached to the benzyl-linked cationic center. These materials displayed improved alkaline stability in cast membranes, likely due to the steric hindrance of the side chain in the solid state.¹³ Meanwhile, Hibbs reported a similarly good stability result for a poly(phenylene) backbone with trimethylalkylammonium cations attached to the backbone through a hexamethylene spacer, reminiscent of Tomoi, et al.¹⁴ Based on previous interesting results with block copolymer and side chain tethered cations, the purpose of this chapter is to demonstrate how the side chains influence the degradation and properties of styrene-backbone block copolymer-based AEMs. Block copolymers with C4 side chains connecting the backbone and cationic groups were synthesized by 1) terminal alkene-bearing monomers that were first polymerized, brominated and then quaternized or 2) post-polymerization Grignard attachment of allylmagnesium bromide to PS-*b*-PVBC block copolymers and subsequent conversion to quaternary ammonium

groups. These two synthetic approaches to similar materials are reported in detail along with their morphology, conductivity and degradation characteristics.

4.2 Experimental Section

Materials. All chemicals and reagents were purchased from Sigma-Aldrich (St. Louis, MO) except as noted. Allylmagnesium bromide (allylMgBr, 1 M in ether), hydrobromic acid solution (33 wt. % in acetic acid), and S-dodecyl- S'-(α,α' -dimethyl- α'' -acetic acid)trithiocarbonate (DDMAT) (98 %) were used as received.

Synthesis of 4-(3-butenyl)styrene (BeS). This compound was prepared following the previous literature.¹⁵ To a stirring solution of allylMgBr (1.6 L, 1 M) at 0 °C, VBC (195.2 g, 1.278 mol) in anhydrous diethyl ether (320 mL) was added dropwise and stirred overnight at room temperature. The reaction mixture was quenched with dilute hydrochloric acid (800 mL, 1 M) at 0 °C and extracted with diethyl ether (600 mL x3). The combined organic layers were washed with saturated brine (500 mL x2), dried over Na₂SO₄ and concentrated under reduced pressure. The compound was isolated by distillation under reduced pressure (164 g, Yield: 81 %). ¹H NMR (300 MHz, CDCl₃) δ 7.36 (d, J = 8.1 Hz, 2H), 7.17 (d, J = 8.1 Hz, 2H), 6.72 (dd, J = 18.0, 11.1 Hz, 1H) 5.88 (m, 1H), 5.73 (d, J = 18.0 Hz, 1H), 5.22 (d, J = 11.1 Hz, 1H), 5.10-4.99 (m, 2H), 2.73 (t, J = 7.5 Hz, 2H), 2.39 (m, 2H); ¹³C NMR (75 MHz, CDCl₃) δ 141.6, 138.0, 136.8, 135.3, 128.6, 126.1, 115.0, 113.0, 35.5, 35.2. (¹H NMR spectroscopy, Figure A1.)

Synthesis of PS-*b*-PBeS. In a typical experiment, a stirring solution of Macro-PS₁₀₀ (3.254 g, 0.313 mmol, $M_n^{NMR} = 10.4 \text{ kg mol}^{-1}$), BeS (11.394g, 72 mmol), AIBN (10.7

mg, 0.065 mmol) and benzene (1.8 mL) was bubbled with argon for 30 min and immersed in an oil bath thermostatted at 70 °C for 9 h. The reaction mixture was quenched by liquid nitrogen and warmed to room temperature. The mixture was diluted with a minimal amount of THF and the polymer was precipitated three times in methanol. The final polymer was dried *in vacuo* at 40 °C to give as PS₁₀₀-*b*-PBeS₅₄ ($M_n = 16.1 \text{ kg mol}^{-1}$, $M_w/M_n = 1.25$) as a light yellow solid.

Bromination of PS-*b*-PBeS to PS-*b*-PBBS. The bromination was carried out in a similar manner to the bromination of PS₁₀₀-*b*-P(VBC₉-*r*-BeS₁₇₈) to give PS-*b*-PBBS₄₅ ($M_n = 16.6 \text{ kg mol}^{-1}$, $M_w/M_n = 1.40$) from PS₁₀₀-*b*-PBeS₅₆. The molar ratio of HBr to olefin groups was maintained at 2.0 and the bromination yield was quantitative based on the complete disappearance of olefinic protons ($\text{CH}_2=\text{CH}-$) (5.90 and 5.10 ppm) and the appearance of bromobutyl protons (BrCH_2-) (3.40 ppm) in the ¹H NMR spectrum of Figure 4.1.

General Synthesis Procedure of PS-*b*-PVBC Block Copolymers. All polymerizations were carried out in a similar fashion in one-neck round bottom flasks sealed with septa. A typical polymerization is as follows: a stirring mixture of styrene (14.060 g, 0.135 mol), DDMAT (342.0 mg, 0.938 mmol) and AIBN (51.3 mg, 0.312 mmol) was bubbled with argon for 30 min and immersed in a preheated oil bath at 60 °C for 24 h. The reaction solution was quenched by liquid nitrogen for 5 min and warmed to room temperature over 30 min. The reaction mixture was diluted with THF, precipitated three times in a large amount of methanol and then dried *in vacuo* at 40 °C to give the polystyrene macroinitiator (Macro-PS₁₀₀, $M_n = 10.5 \text{ kg mol}^{-1}$, $M_w/M_n = 1.15$, $M_n^{\text{NMR}} = 10.4 \text{ kg mol}^{-1}$) as a yellow solid.

A solution of Macro-PS₁₀₀ (4.578 g, 0.440 mmol), VBC (18.314 g, 120 mmol), and AIBN (32.6 mg, 0.200 mmol,) in benzene (10 mL) was degassed by argon for 30 min and placed in a preheated oil bath at 70 °C for 11 h. Purification of the resulting polymer was carried out in a similar fashion to Macro-PS₁₀₀ to give PS₁₀₀-*b*-PVBC₁₆₇ ($M_n = 32.0 \text{ kg mol}^{-1}$, $M_w/M_n = 1.28$) as a light yellow solid. The average degree of polymerization of the PVBC block was calculated from the ratio of PVBC to PS based on the aromatic protons ($-\text{C}_6\text{H}_4-$ and $-\text{C}_6\text{H}_5-$) (7.20 to 6.80 ppm) to chloromethyl protons (ClCH_2-) (4.50 ppm) in the ^1H NMR spectrum.

General Synthesis Procedure of PS-*b*-P(VBC-*r*-BeS) -Scheme 1. In a typical experiment, to a stirring solution of PS₁₀₀-*b*-PVBC₁₆₇ (3.0 g, fraction of $-\text{CH}_2\text{Cl}$ 62.8 mol%, 14 mmol total) in THF (30 mL) was added allylMgBr (30 mL, 30 mmol, 1 M in ether) at 0 °C dropwise and stirred overnight. The reaction mixture was quenched by diluted HCl (30 mL, 1 M) at 0 °C and concentrated to around one fourth of the initial volume. The combined organic and inorganic layers were poured onto a mixture of methanol and DI water (v/v 1:1). The polymer was recovered by filtration. The obtained polymer ($M_n = 34.0 \text{ kg mol}^{-1}$, $M_w/M_n = 1.39$) was dried *in vacuo* overnight at 40 °C.

General Procedure for the Synthesis of PS-*b*-P(BBS-*r*-VBC) - Scheme 1. In a typical experiment, HBr (1.6 g, 20 mmol, ~3.5 mL) in acetic acid was added dropwise to a solution of PS₁₀₀-*b*-P(VBC₉-*r*-BeS₁₇₈) (2.15 g, 10 mmol alkene group) in toluene (120 mL) at 0 °C and stirred overnight. The reaction mixture was concentrated under reduced

pressure, diluted with a minimal amount of THF and re-precipitated in methanol. The polymer ($M_n=36.0 \text{ kg mol}^{-1}$, $M_w/M_n=1.61$) was dried *in vacuo* overnight at 40 °C.

Block Copolymer Quaternization. In a typical quaternization, to a stirring solution of PS₁₀₀-*b*-PBBS₄₅ (2.25 g, ~ 5 mmol -CH₂Br) in dimethylformamide (DMF) (10 mL) was added aqueous trimethylamine (3 mL, 20 mmol, 45 wt. %) and stirred at 50 °C for 24 h. The homogeneous solution was cooled to room temperature and concentrated under reduced pressure to give an orange viscous liquid. The quaternized form PS₁₀₀-*b*-PBBS₄₅ was dried *in vacuo* overnight at 50 °C to give an orange solid before performing ion exchange.

Membrane Formation and Characterization. The quaternized polymer powders were added to a flask with aqueous NaHCO₃ or NaCl (1 M) and the solutions were decanted after 8 h upon standing and refilled every 8 h for two times to ensure complete ion exchange. The removal of excess NaHCO₃ or NaCl was carried out by dialysis with 6-8 kDa molecular weight cut-off (MWCO) membranes (Spectra/Por® 1 Dialysis Membrane purchased from Spectrum Laboratories, Inc., Rancho Dominguez, CA) in de-ionized water with fresh water changes three times at 8 h intervals. The bicarbonate or chloride form polymers were dried *in vacuo* at 40 °C for 24 h. The anion exchange membranes were cast from bicarbonate or chloride form quaternized block copolymers in toluene and n-propanol (v/v 1:1) or DMF and n-propanol (v/v 3:1) on polytetrafluoroethylene (PTFE) molds at room temperature for 24 h in a slightly ventilated desiccator. The membranes were then dried at room temperature prior to use for other measurements.

Ion Exchange Capacity (IEC). The IEC was calculated based on the ratio of the hydrophobic block and the hydrophilic block in quaternized chloride form from ^1H NMR data assuming 100 % amination. The ratio of hydrophobic and hydrophilic blocks was calculated by the ratio of aromatic protons ($-\text{C}_6\text{H}_5^-$ and $-\text{C}_6\text{H}_4^-$) (7.20 to 6.80 ppm) to the chloromethyl protons (ClCH_2^-) (4.50 ppm) and bromobutyl (BrCH_2^-) (3.40 ppm) protons.

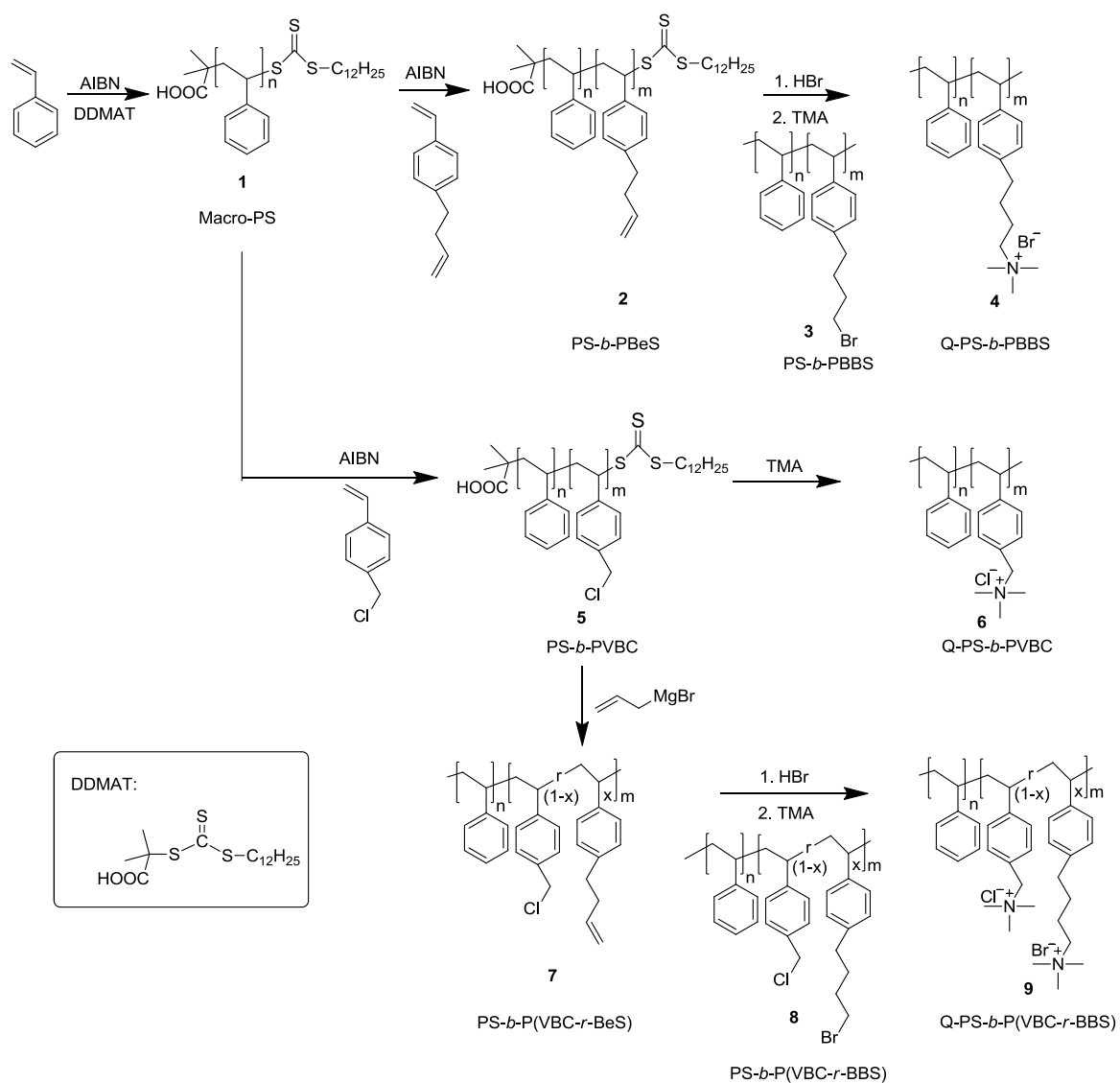
Stability Assessment. The block copolymer powders were immersed in excess 1M NaOH solution and the solution was decanted at 12, 18, 24 and 30 days and the samples were subject to ^1H NMR analysis with deuterated DMF/ CD_3OD or $\text{CF}_3\text{CD}_3\text{OD}$ (3:1, v:v). The homopolymers were added to 4M deuterated NaOD solution and the molar ratio of the quaternary ammonium group to the OD^- solution was maintained at 1:100. The mixture was then immersed in an 80 °C oil bath. The aliquots mixed with CD_3OD (~3:1 v/v) were subjected to ^1H NMR analysis after aging. Deuterated methanol, CD_3OD was used to distinguish the trimethylammonium protons of the side chain homopolymer in the ^1H NMR spectra. In the NaOD/ D_2O solution, the side chain protons were overlapped, making $\text{N}(\text{CH}_3)_3$ indistinguishable from the rest of protons in the C4 side chain.

4.3 Results and Discussion

Synthesis and Characterization of Side Chain Block Copolymers.

Three series of side chain block copolymers are presented in this work. First, side chain block copolymers of poly(styrene)-*b*-poly(bromobutylstyrene) (PS-*b*-PBBS, **3**) with narrow polydispersity indices (PDI) were synthesized by one-step HBr addition

from: poly(styrene)-*b*-poly(butenylstyrene) (PS-*b*-PBeS, **2**) prepared by reversible addition-fragmentation chain transfer (RAFT) polymerization as shown in **Scheme 4.1**, top line.



Scheme 4.1. Synthesis of quaternary ammonium-containing side chain block copolymers by RAFT polymerization.

For the preparation of well-defined block copolymers with controlled molecular weights and polydispersity indexes by living radical polymerization, atomic transfer radical polymerization (ATRP), nitroxide-mediated polymerization (NMP) and RAFT polymerization offer straightforward synthetic strategies. In our study, RAFT was chosen for the synthesis of the PS-*b*-PVBC block copolymers. ATRP was not feasible due to the benzylhalide monomer acting as an ATRP initiator. Normally NMP is conducted at temperatures above 110 °C to generate the radicals and longer reaction times are needed. The reactivity of VBC monomer is high under these conditions, rendering the polymerization less controlled than RAFT polymerization although successful synthesis of PS-*b*-PVBC materials has been reported, previously using NMP by Mahanthappa, et al.¹⁶In the poly(styrene) macroinitiator synthesis using DDMAT as the chain transfer agent and AIBN as the thermal initiator with the feed ratio [monomer]: [CTA]: [initiator] = 144:1:0.33 at 60 °C for 24 h in bulk, the polymerization showed high monomer conversion (~70%) and narrow polydispersity ($M_w/M_n = 1.15$) verified by GPC. The theoretical number average molecular weight ($M_n^{\text{theory}} = 10.7 \text{ kg mol}^{-1}$) based on the initiator concentration and monomer conversion was in good agreement with the values from ¹H NMR spectroscopy end group analysis ($M_n^{\text{NMR}} = 10.4 \text{ kg mol}^{-1}$), **Figure 4.1**, and GPC ($M_n^{\text{GPC}} = 10.5 \text{ kg mol}^{-1}$). The M_n^{NMR} from ¹H NMR was based on the intensity integration ratio of the resonances for the $-C_6H_5-$ protons (from 7.20 to 6.20 ppm) of the poly(styrene) repeat units to the resonance of the $-SCH_2-$ protons (3.27 ppm) on the terminal CTA end groups. These results confirmed the controlled characteristics of the RAFT polymerization for forming the desired macro-CTA.

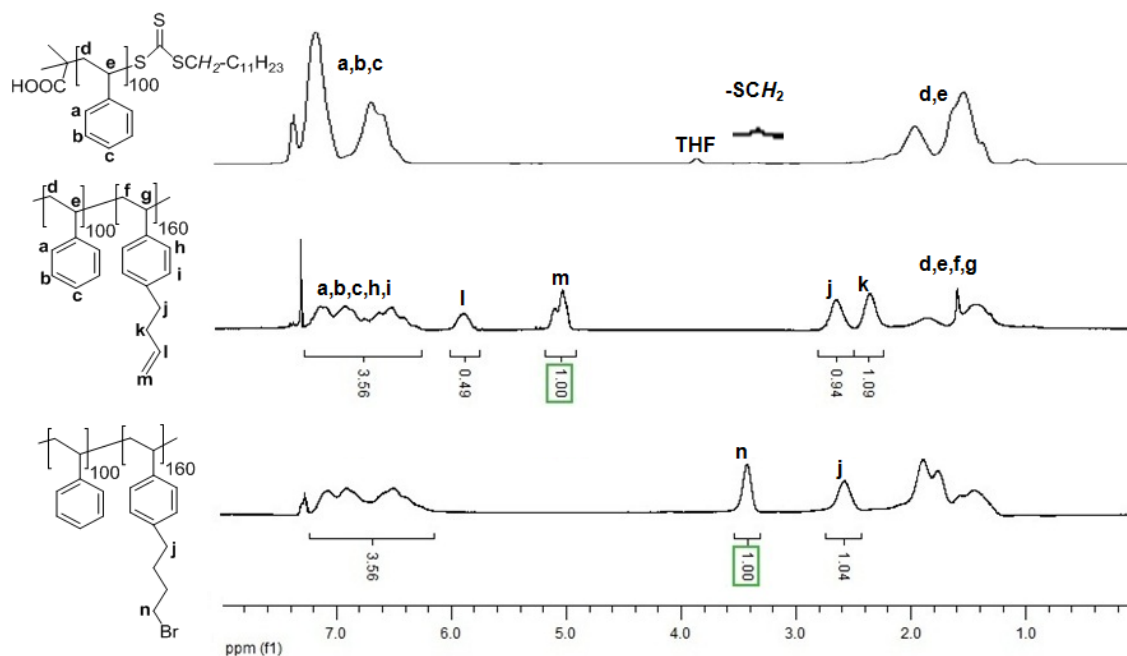


Figure 4.1. ¹H NMR spectra (300 MHz) of macro-PS₁₀₀, brominated PS₁₀₀-b-PBBS₁₆₀ and PS₁₀₀-b-PBeS₁₆₀.

The monomer 4-(3-butenyl) styrene was synthesized by the coupling reaction of vinylbenzyl chloride with allylMgBr solution in excellent yield following literature protocols.¹⁴ A styryl group capable of radical polymerization and a pendant alkene moiety coexist in the monomer. During the polymerization, the pendant alkene moieties were not involved in the radical reaction as tracked by ¹H NMR in either the homopolymer of poly(butenylstyrene) (PBeS) or block copolymers poly(styrene)-b-poly(butenylstyrene) (PS-b-PBeS). The terminal alkenes form short-lived secondary carbon radical species that do not participate in this type of polymerization at the reaction temperature used in this work. The prepared homopolymer (PBeS) using RAFT in bulk conditions showed narrow PDIs at short polymerization times with low monomer conversion. Extended

polymerization times resulted in the loss of controlled polymerization characteristics. Based on this result, in the block copolymer synthesis the conversion of the BeS monomer was maintained at a moderate percentage from 17% to 33%, typically.

The success of chain extension from poly(styrene) macro-CTA allowed the verification of exclusively selective polymerization of the styryl moieties generating block copolymers bearing alkene reactive moieties. The well-defined macro-PS₁₀₀ ($M_n^{\text{NMR}} = 10.4 \text{ kg mol}^{-1}$, $M_w/M_n^{\text{GPC}} = 1.15$) chain extension was performed by RAFT polymerization of BeS monomer ([BeS]:[macro-PS]:[AIBN] = 230:1:0.33) at 70 °C in bulk with moderate monomer conversion, producing the diblock copolymer PS₁₀₀-*b*-PBeS₅₄ ($M_n = 13.5 \text{ kg mol}^{-1}$, $M_w/M_n = 1.18$). The PDI of the obtained diblocks was in the typical range for controlled/living radical polymerizations while there were relatively narrow alkene peaks in the ¹H NMR spectrum. The ratio of benzyl protons (PhCH₂) (2.63 ppm) to olefinic protons (CH₂=CH) (2H, 5.10 and 1H, 5.90 ppm) and allyl protons (CH₂=CH-CH₂) (2.32 ppm) was maintained at 2:2:1:2 as shown in **Figure 4.1**. These observations supported the radical stability of the pendant alkene group and the living characteristics of RAFT chain extension polymerization. After polymerization and purification, the terminal alkenyl bonds were brominated by hydrobromic acid (HBr) radical addition without normal radical initiators as presented in **Scheme 4.1**, top line. The quantitative bromination of the diblocks in toluene with HBr generated well-controlled one-step post-modification diblock copolymer PS₁₀₀-*b*-PBBS₄₅ ($M_n = 16.6 \text{ kg mol}^{-1}$, $M_w/M_n = 1.40$), **Figure 4.2**. The ratio of PS block to PBBS block was altered slightly after HBr bromination within the limits of ¹H NMR detection.

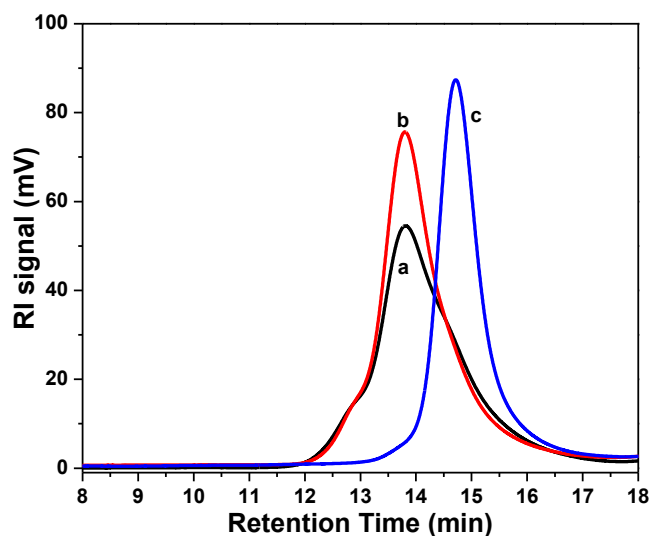


Figure 4.2. Gel permeation chromatograms of a) fully brominated PS₁₀₀-*b*-PBBS₄₅ from diblocks b) PS₁₀₀-*b*-PBeS₅₄ by chain extension and c) Macro-PS₁₀₀ initiator.

A series of poly(styrene)-*b*-poly(vinylbenzyl chloride) (PS-*b*-PVBC) block copolymers with different IECs was synthesized using similar methods as described above, **Figure 4.1** compounds **1**, **5** and **6**. The block copolymer PS-*b*-PVBC ($M_n^{\text{GPC}} = 32.0 \text{ kg mol}^{-1}$, $M_w/M_n = 1.28$) synthesized by chain extension of macro-PS₁₀₀ was confirmed by a molecular weight increase in the GPC analysis (see **Figure A1** Supporting Information). The low PDI and M_n increase indicated successful chain extension without apparent self-polymerization of the VBC monomers. Optimizing the ratio of monomers to CTA and the polymerization time, the PS-*b*-PVBC block copolymers with different PVBC block lengths were obtained.

Based on the preliminary encouraging results of the coupling of allylMgBr to the vinylbenzyl chloride and quantitative HBr bromination of the terminal alkene, the synthesis of diblocks of poly(styrene)-*b*-poly(vinylbenzyl chloride-*ran*-bromobutylstyrene) (PS-*b*-P(VBC-*r*-PBBS)) was devised using an alternate synthetic route to explore the effects of the coexistence of VBC and BBS on the side chain properties, **Figure 4.1**, bottom line. Using a post-polymerization modification strategy, side chains were appended to the PS-*b*-PVBC block copolymers with high yield Grignard attachment followed by quantitative HBr bromination at low temperature used to synthesize materials with a large fraction of trimethylbutylstyrene quaternary ammonium moieties. Appending the alkenyl chain could be achieved by Grignard, Negishi or Stille couplings to polymers bearing the chloromethyl pendant groups to produce the target side chain block copolymers with an olefin end group for further transformation.¹⁷ Given the high reactivity in the coupling reactions and commercial availability of allylMgBr as demonstrated in the (4-butenyl)styrene synthesis, Grignard coupling between allyl and benzyl chloride carbons was employed to construct the side chain block copolymer PS-*b*-P(VBC-*r*-BeS) in a similar fashion to the BeS monomer preparation.

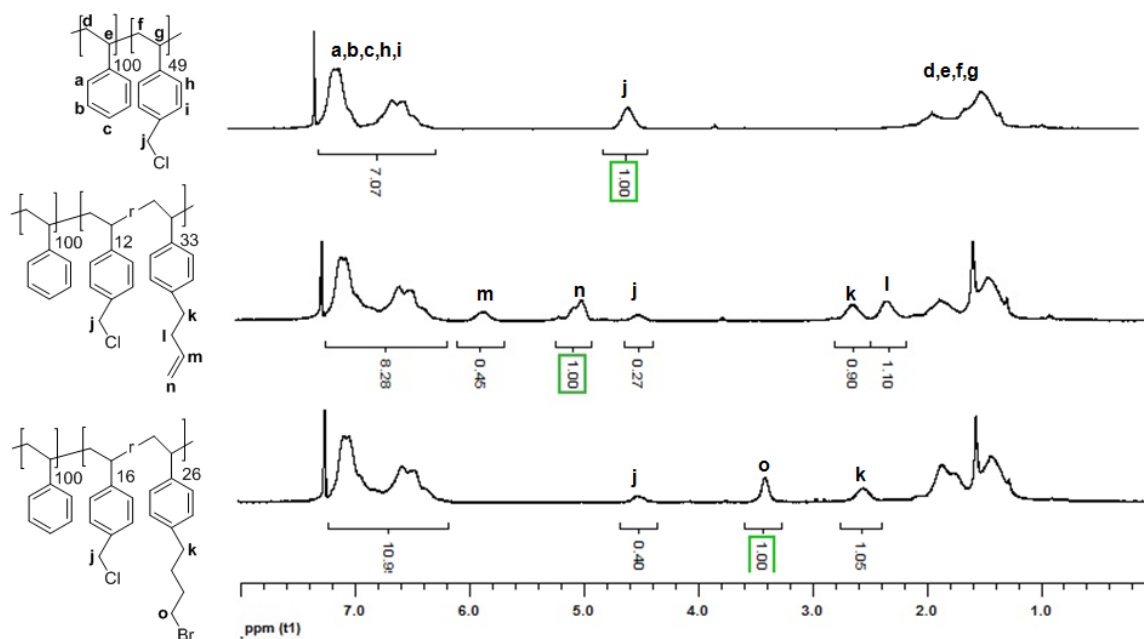


Figure 4.3. ^1H NMR spectra (300 MHz) of $\text{PS}_{100}\text{-}b\text{-PVBC}_{49}$, $\text{PS}_{100}\text{-}b\text{-P(VBC}_{12}\text{-}r\text{-BeS}_{33})$ and brominated $\text{PS}_{100}\text{-}b\text{-P(VBC}_{16}\text{-}r\text{-BBS}_{26})$.

A stirring THF solution of the block copolymer $\text{PS-}b\text{-PVBC}$ was treated with 1 M allylmgBr ether solution at 0 °C overnight, and the reaction mixture was purified by treatment with dilute HCl and then precipitated in methanol/water (v/v 1:1). The appearance of the resonances characteristic to benzyl protons ($-\text{PhCH}_2^-$) was observed at 2.63 ppm along with a substantial intensity decrease of the resonances of benzyl chloride protons ($-\text{PhCH}_2\text{Cl}$) at 4.50 ppm in the ^1H NMR spectra as shown in **Figure 4.3**. The yield of the attachment depended on the relative fractions of PS and PVBC blocks and varied approximately from 70% to 90% from the area ratio of the resonances of benzyl protons ($-\text{PhCH}_2^-$) at 2.63 ppm and benzyl chloride protons ($-\text{PhCH}_2\text{Cl}$) at 4.50 ppm from ^1H NMR. Furthermore, the chain coupling side reaction due to Grignard exchange was not identified by ^1H NMR spectroscopy, as validated by the absence of the characteristic

peak at 2.90 ppm, corresponding to bibenzyl protons ($-\text{PhCH}_2\text{CH}_2\text{Ph}-$) indicative of the high efficiency of the coupling between chloromethyl and allyl groups. However, the GPC traces indicated some crosslinking during polymer post-modification (**Figure A1** in Supporting Information).

Generally, thermal or photo radical initiators such as AIBN and 2,2-dimethoxy-2-phenylacetophenone (DMPA) are required in the terminal addition of HBr to olefin groups to initiate the radical pathway. However, in our case the terminal addition proceeded smoothly at room temperature without the addition of radical initiators. The bromo addition to the terminal double bond was performed by treatment of a dilute PS-*b*-P(VBC-*b*-BeS) solution in toluene with 33 wt. % HBr in acetic acid. The complete disappearance of the unique ^1H NMR resonances of benzyl protons at 2.50 ppm and olefinic protons at 5.90 and 5.10 ppm, respectively, and the appearance of the resonances of bromobutyl protons ($-\text{CH}_2\text{Br}$) at 3.40 ppm verified the quantitative bromination by HBr. In terms of the addition mechanism, the radical terminal addition to the double bonds was attributed to the trace amount of oxygen in the reaction system permitting the radical pathway and near exclusive anti-Markovnikov product.¹⁸ The overall composition ratio between hydrophobic block PS and pseudo-hydrophilic block (PVBC-*r*-PBBS) or its precursor PVBC slightly varied with the post-modification due to the polymer loss during recovery and purification, leading to IEC variation in the final product.

Side Chain Block Copolymer Quaternization and Membrane Formation

Exhaustive quaternization of PS-*b*-PVBC, PS-*b*-P(VBC-*r*-BBS) and PS-*b*-PBBS with excess 45% TMA aqueous solution or 30 wt% TMA in ethanol solution at 50 °C quantitatively resulted in quaternized block copolymers. PS₁₀₀-*b*-PVBC₁₀₄ and PS₁₀₀-*b*-BBS₁₆₀ copolymers in salt form were characterized by ¹H NMR as shown in **Figure 4.4**. In the quaternized sample, PS₁₀₀-*b*-PVBC₁₀₄, the disappearance of the chloromethyl (-CH₂Cl) moiety as a sharp peak at 4.50 ppm along with the appearance of the two benzylic protons, H₆, in the quaternized compound as a broad resonance at 4.90 ppm indicated quantitative conversion of benzyl halide to quaternary ammonium. The integral ratio of the benzylic protons, H₆, at 4.90 ppm to aromatic proton peaks, H_{1,2,3,4,5} from 6.20 to 7.80 ppm confirmed the quantitative conversion. The measured integral ratio value (0.21) was in agreement with the calculated value (0.22). In the C4 side chain sample, PS₁₀₀-*b*-BBS₁₆₀, the complete quaternization was confirmed by the integral ratio of methylene protons (-CH₂) adjacent to quaternary nitrogen to aromatic protons, H_{1,2,3,4,5} due to the overlap of methyl protons with the peak of the trace water. These figures showed 100% quaternization of chloromethyl and bromomethyl motifs by trimethylamine aqueous or ethanol solution.

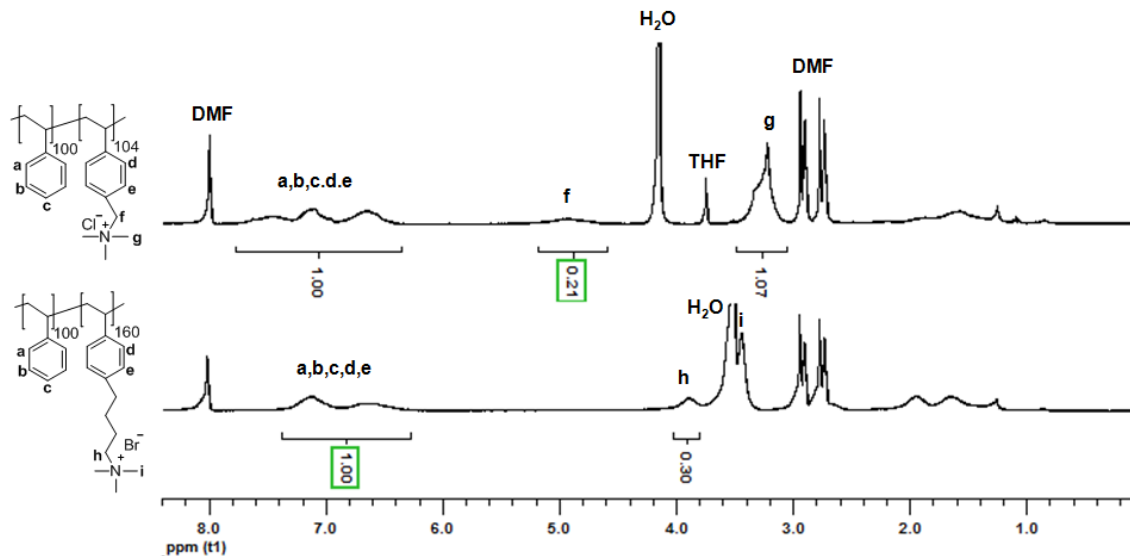


Figure 4.4. ¹H NMR spectra (300 MHz) of quaternized PS₁₀₀-b-PVBC₁₀₄ in d₇-DMF/CD₃OD (trace) and PS₁₀₀-b-BBS₁₆₀ in d₇-DMF.

The solubility of the styrene-based benzyltrimethylammonium containing copolymers in chloride form with high IECs was low in organic solvents. Efforts to dissolve PS-*b*-PVBC and PS-*b*-P(VBC-*r*-BBS) in single component solvents such as THF, CHCl₃, DMSO, DMF proved to be fruitless while PS-*b*-PBBS was soluble in DMF, aided by the increased miscibility of the C4 side chain with DMF. Attempts to dissolve PS-*b*-PVBC and PS-*b*-P(VBC-*r*-BBS) copolymers with toluene/1-propanol (v/v = 1:1) and DMF/1-propanol (v/v = 3:1) produced homogeneous solution while PS-*b*-PBBS copolymers were soluble in chloroform/1-propanol/methanol (v/v/v = 2:1:1) and DMF/1-propanol (v/v = 3:1). The presence of benzyltrimethylammonium groups in PS-*b*-PVBC or PS-*b*-P(VBC-*r*-BBS) copolymers required 1-propanol co-solvent to cast transparent membranes.

In previous styrene-based ionic liquid block copolymers,¹⁶ Weber, et al. found that solvent-cast membranes exhibited more ordered long-range structures than melt-pressed samples. Thus, the polymer membranes in our study were cast from solvent mixtures in PFTE molds. The cast membranes from this procedure showed long-range ordered morphologies as shown in the SAXS profiles. The properties of the prepared copolymer samples are summarized in **Table 4.1**.

Table 4.1. Properties of the prepared side chain block copolymers.

Sample	M_n^{GPC} (kg/mol)	PDI M_w/M_n	IEC (NMR)	d(SAXS) ^c (nm)	WU ^d (%)	Hydration number (λ) ^e
PS ₁₀₀ - <i>b</i> -PBBS ₄₅	16.6	1.40	1.97 ^a	24.5	26	7.3
PS ₁₀₀ - <i>b</i> -PBBS ₁₆₀	24.8	1.47	2.74 ^a	27.3	32	6.4
PS ₁₀₀ - <i>b</i> -PVBC ₄₉	17.1	1.45	2.34	26.0	31	7.3
PS ₁₀₀ - <i>b</i> -PVBC ₁₀₄	19.6	1.45	3.20	33.0	47	8.2
PS ₁₀₀ - <i>b</i> -PVBC ₁₆₇	32.0	1.28	3.66	39.2	59	9.0
PS ₁₀₀ - <i>b</i> -P(VBC ₁₆ - <i>r</i> -PBBS ₂₆)	21.5	1.55	2.06 ^b	18.0	25	6.8
PS ₁₀₀ - <i>b</i> -P(VBC ₃₂ - <i>r</i> -PBBS ₆₇)	25.4	1.48	2.96 ^b	20.1	34	6.3
PS ₁₀₀ - <i>b</i> -P(VBC ₁₂ - <i>r</i> -PBBS ₁₃₂)	37.5	1.76	3.18 ^b	23.8	42	7.3

^aIECs were determined in Br⁻ form; ^bIEC was calculated based on Cl⁻ after ion exchange with 1M NaCl aqueous solution; ^cdomain spacings were determined by $d = 2\pi/q$, where q is the location of the principal peak in SAXS patterns; ^{d, e} water uptake and hydration number calculated based on chloride (Cl⁻) form and PS-*b*-PVBC and PS-*b*-P(VBC-*r*-BBS) cast from toluene/1-propanol (v/v = 1:1) while PS-*b*-PBBS prepared from chloroform/1-propanol/methanol (v/v/v = 2:1:1).

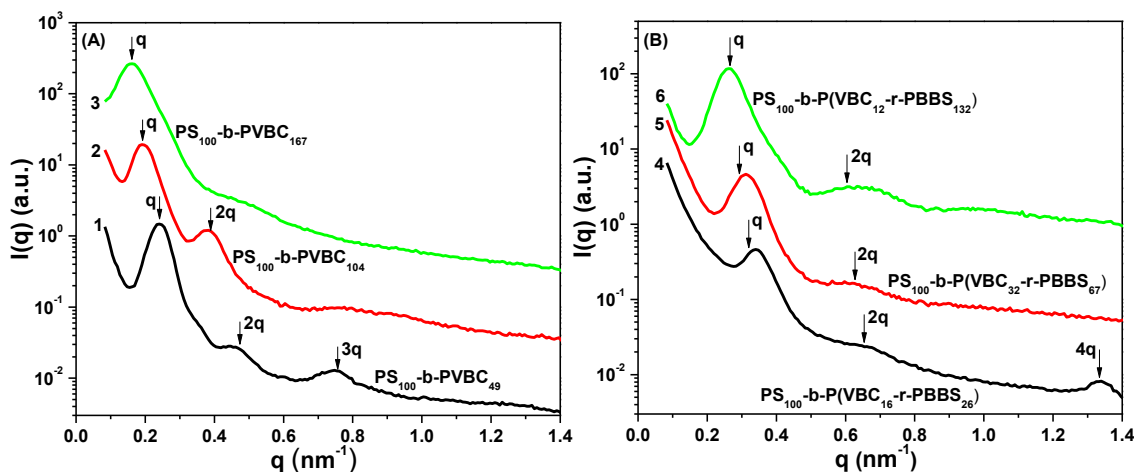


Figure 4.5. SAXS patterns of copolymer AEMs from (A) **1**: PS₁₀₀-*b*-PVBC₄₉, **2**: PS₁₀₀-*b*-PVBC₁₀₄, **3**: PS₁₀₀-*b*-PVBC₁₆₇, (B) **4**, **5**, **6** corresponding to the side chain samples made from PS₁₀₀-*b*-P(VBC₁₆-*r*-PBBS₂₆), PS₁₀₀-*b*-P(VBC₃₂-*r*-PBBS₆₇) and PS₁₀₀-*b*-P(VBC₁₂-*r*-PBBS₁₃₂).

Morphological Characterization of Side Chain AEMs

The increase in interdomain spacing of the PS₁₀₀-*b*-PVBC₄₉, PS₁₀₀-*b*-PVBC₁₀₄ and PS₁₀₀-*b*-PVBC₁₆₇ samples corresponded to an increase in the molecular weight of the ionic blocks, **Figure 4.5**. The principal peak positions shifted to smaller scattering vectors (q), corresponding to a larger interdomain spacing based on $d = 2\pi/q$, where d is the interdomain spacing and q is the scattering vector of the first-order reflection. PS₁₀₀-*b*-PVBC₄₉ in quaternary ammonium chloride form with an interdomain spacing 26.0 nm displayed an ordered morphology with SAXS reflections at ratios of 1:2:3, which is anticipated to be a lamellar morphology with long-range order. The order in the materials decreased when the hydrophilic block length was increased as indicated by the SAXS

patterns with only two strong peaks for $\text{PS}_{100}\text{-}b\text{-PVBC}_{104}$ with interdomain spacing of 33.0 nm and one peak for the $\text{PS}_{100}\text{-}b\text{-PVBC}_{167}$ sample with interdomain spacing 39.2 nm, **Figure 4.5A**. In **Figure 4.5B**, the AEM from $\text{PS}_{100}\text{-}b\text{-P(VBC}_{16}\text{-}r\text{-PBBS}_{26})$ showed SAXS reflections at ratios of 1:2:4 in which the peak at 3q was not visible, corresponding to a lamellar structure with interdomain spacing 18.0 nm. The AEMs from $\text{PS}_{100}\text{-}b\text{-P(VBC}_{32}\text{-}r\text{-PBBS}_{67})$ and $\text{PS}_{100}\text{-}b\text{-P(VBC}_{12}\text{-}r\text{-PBBS}_{132})$ showed only two scattering peaks at ratios of 1:2 with a sharp decrease in interdomain spacing (20.1 and 23.8 nm), compared to their quaternized precursors: $\text{PS}_{100}\text{-}b\text{-PVBC}_{104}$ and $\text{PS}_{100}\text{-}b\text{-PVBC}_{167}$ (33.0 and 39.2 nm). These data were consistent with a likely lamellar morphology in these materials. Furthermore, the quaternized side chain $\text{PS}_{100}\text{-}b\text{-PBBS}_{45}$ AEM with shorter hydrophobic block displayed strong segregated phase separation with 24.5 nm interdomain spacing while the AEM from $\text{PS}_{100}\text{-}b\text{-PBBS}_{160}$ lacked clearly defined higher scattering vector peaks and the interdomain spacing (27.3 nm) increase even slower compared to the length of the hydrophobic blocks in **Figure 4.6**.

Interestingly, the interdomain spacings of the benzyltrimethylammonium copolymers (26.0, 33.0 and 39.2 nm) from SAXS were similar to the estimated distance (22.8, 31.2 and 40.8 nm) of the poly(styrene) bond length (1.53 nm) multiplied by the degree of polymerization, N. These results implied that benzyltrimethyl ammonium copolymers showed the large extents of chain stretching compared to side chain block copolymers even in the presence of ionic groups.

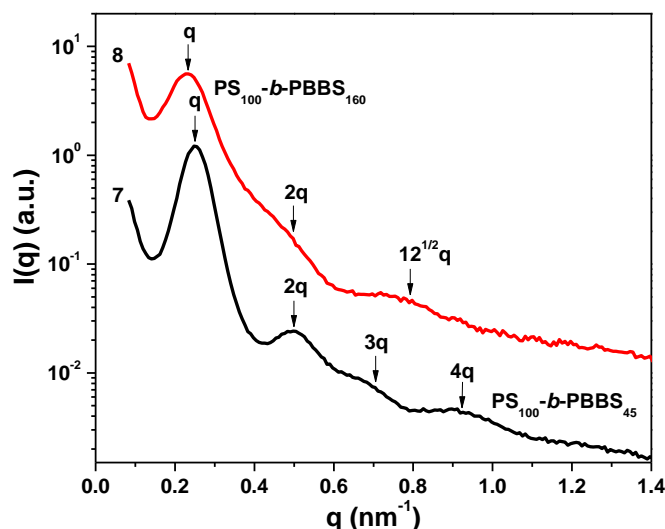


Figure 4.6. SAXS patterns of quaternary copolymer AEMs from $\text{PS}_{100}\text{-}b\text{-PBBS}_{45}$ (7), $\text{PS}_{100}\text{-}b\text{-PBBS}_{160}$ (8).

It appeared that increased hydrophobic block length disrupted the long-range ordered microstructures for $\text{PS-}b\text{-PVBC}$, $\text{PS-}b\text{-P(VBC-}r\text{-BBS)}$ and $\text{PS-}b\text{-PBBS}$ side chain copolymers, **Figure 4.4** and **Figure 4.5**. Presumably, the disruption was induced by kinetic trapping of the longer chains, indicated by the transition from relatively smaller interdomain sizes to larger ones. Moreover, the interdomain spacing of the $\text{PS}_{100}\text{-}b\text{-PBBS}_{160}$ block copolymer (27.3 nm) was smaller than that of benzyltrimethyl copolymer $\text{PS}_{100}\text{-}b\text{-PVBC}_{167}$ (39.2 nm). At the same hydrophobic and hydrophilic block lengths, the $\text{PS}_{100}\text{-}b\text{-PVBC}_{49}$ based AEM showed the largest interdomain spacing (26.0 nm), followed by $\text{PS}_{100}\text{-}b\text{-PBBS}_{45}$ (24.5 nm) and $\text{PS}_{100}\text{-}b\text{-P(VBC}_{16}\text{-}r\text{-PBBS}_{26})$ (18.0 nm), which displayed the smallest interdomain spacing among the AEMs as shown in **Figure 4.7**.

This trend also was demonstrated by the samples of $\text{PS}_{100}\text{-}b\text{-PVBC}_{104}$ (33.0 nm) and $\text{PS}_{100}\text{-}b\text{-P(VBC}_{32}\text{-}r\text{-PBBS}_{67})$ (20.1 nm). Based on the data for the PVBC and PBBS side chain samples, the presence of C4 side chains in block copolymers resulted in the reduction of the interdomain spacing. The coexistence of C4 side chains and benzyltrimethyl ammonium groups further decreased the interdomain spacing.

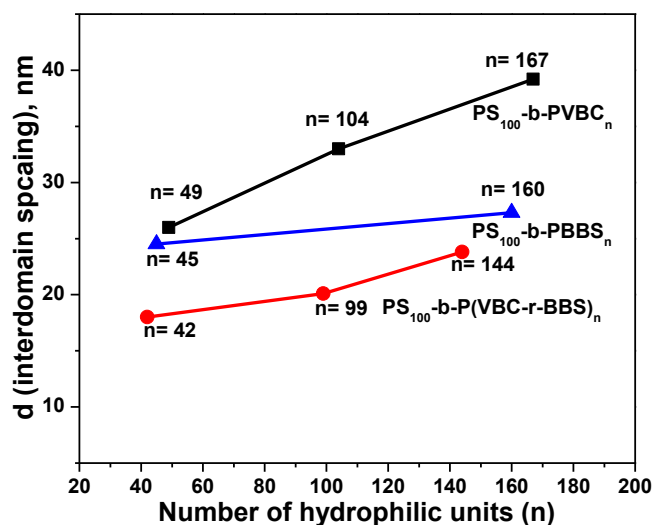


Figure 4.7. Interdomain spacing comparison of $\text{PS-}b\text{-PBBS}$, $\text{PS-}b\text{-PVBC}$ and $\text{PS-}b\text{-P(VBC-}r\text{-BBS)}$ block copolymers at the same hydrophobic block length.

As demonstrated by Elabd, et al.,⁴ the casting solvents for the membranes induced different interdomain spacings, depending upon a number of parameters such as solubility parameter and boiling point of the solvent used. However, in our case when $\text{PS-}b\text{-PVBC}$ and $\text{PS-}b\text{-P(VBC-}r\text{-PBBS)}$ were cast from the same solvent, the solvent factor was excluded. It is very likely that an entropic effect controlled the interdomain spacing.

At constant hydrophobic and hydrophilic block lengths, the interdomain spacing increasing was entropically unfavorable for the copolymers with soft side chain.¹⁹ In addition, the significant domain spacing reduction was probably due to the decrease of the segregation strength with longer side chains. Conventionally, the driving force of phase separation is the segregation strength, χN , where χ is the Flory-Huggins interaction parameter between two mismatched blocks and N is the total degree of polymerization. χ accounted for the segregation strength with the similar degree of polymerization. The soft C4 segments in the side chain block copolymers increased the miscibility of hydrophobic blocks (PS) and hydrophilic blocks, thus reducing the interaction parameter and ultimately leading to the decrease of the interdomain spacing.²⁰

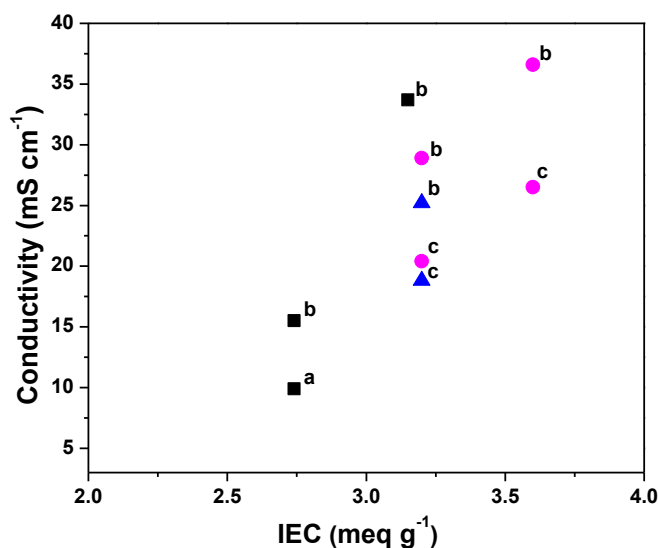


Figure 4.8. Solvent and ion effects on conductivity of (■) PS₁₀₀-b-PVBC₁₆₇, (▲) PS₁₀₀-b-P(VBC₁₂-r-BBS₁₃₂) and (●) PS₁₀₀-b-PBBS₁₆₀ at 30 °C as a function of ion exchange

capacity, a: cast from CHCl_3 /1-propanol/methanol ($v/v/v = 2:1:1$), b: cast from DMF/1-propanol ($v/v = 3:1$), c: cast from toluene/1-propanol ($v/v = 1:1$).

Water Uptake and Ion Transport of Side Chain AEMs

Water uptake of side chain membranes was measured at 30 °C at 95% relative humidity in chloride (Cl^-) form. Under humidified conditions, the styrene based membranes exhibited sufficient dimensional stability, but swelled excessively in liquid water. As shown in **Table 4.1**, the membranes showed similarly low water uptake ($\sim 8 \pm 1$ water per ammonium cation) irrespective of counterion type, casting solvent and microstructure.

Due to the brittleness of the block copolymer AEMs under high relative humidity conditions, the conductivity data was obtained for the samples listed in **Table A1** (Appendix A). At 30 °C and 95% RH, the chloride conductivity of benzyltrimethylammonium-based AEMs increased with increasing IEC facilitated by their increased water uptake. This increase was aided by the local dynamics of water and produced continuous conductive ion channels, as reported by previous research.²¹ The highest chloride conductivity (26.5 mS cm^{-1}) in **Figure 4.8** was obtained from the PS_{100} - b -PVBC₁₆₇ sample cast from toluene/1-propanol ($v/v = 1:1$) that had a lamellar structure as observed in SAXS, **Figure 4.5A**. It is believed that the immiscibility of hydrophobic and hydrophilic blocks drove phase separation of the block copolymers, thus leading to the formation of ionic domains for chloride transport.²² The effects of morphology on

ionic conductivity were not observed in this study, as most of materials displayed lamellar morphologies.

We hypothesize that the ionic conductivity of the membranes could be increased by the improvement of the micro-structures by enhancing ordering during solvent casting.²³ As discussed above, the samples from PS₁₀₀-*b*-PVBC₁₆₇ and PS₁₀₀-*b*-PBBS₁₆₀ generated clear solutions in DMF/1-propanol (v/v = 3:1). As seen in **Figure 4.9A**, PS₁₀₀-*b*-PVBC₁₆₇ sample cast from DMF/1-propanol showed a more ordered morphology than samples cast from toluene/1-propanol (v/v = 1:1), producing three clear SAXS peaks at the scattering vector positions and a reduction in domain spacing from 39.2 to 28.3 nm. The PS₁₀₀-*b*-PBBS₁₆₀ membrane showed slightly more ordered microstructures when cast from DMF/1-propanol (v/v = 3:1) versus chloroform/1-propanol/methanol (v/v/v = 2:1:1) and the domain spacing reduction from 27.3 to 18.8 nm, **Figure 4.9B**. The morphology improvement and domain spacing decrease appeared to be the result of better solubility of the polymers during casting. When comparing to the membranes cast from chloroform/1-propanol/methanol and toluene/1-propanol, the membranes cast from DMF/1-propanol showed greater conductivity under the same conditions. For example, PS₁₀₀-*b*-PBBS₁₆₀ cast from DMF/1-propanol with IEC = 2.74 meq g⁻¹ show higher bromide (Br⁻) conductivity (15.5 mS cm⁻¹), which was 57% higher than the membrane (9.9 mS cm⁻¹) cast from chloroform/1-propanol/methanol. PS₁₀₀-*b*-PVBC₁₆₇ membrane exhibited the highest chloride conductivity (36.6 mS cm⁻¹), increased by 38% from the membrane cast from toluene/1-propanol (26.5 mS cm⁻¹). However, PS₁₀₀-*b*-PBBS₁₆₀ and PS₁₀₀-*b*-PVBC₁₆₇ cast from DMF/1-propanol showed the similar water uptake as the

samples cast from toluene/1-propanol and chloroform/1-propanol/methanol, respectively. The similar trend of solvent effects on ionic conductivity increase was also observed for $\text{PS}_{100}\text{-}b\text{-PVBC}_{104}$, $\text{PS}_{100}\text{-}b\text{-P(VBC}_{12}\text{-}r\text{-BBS}_{132})$ samples as shown in **Figure 4.8**.

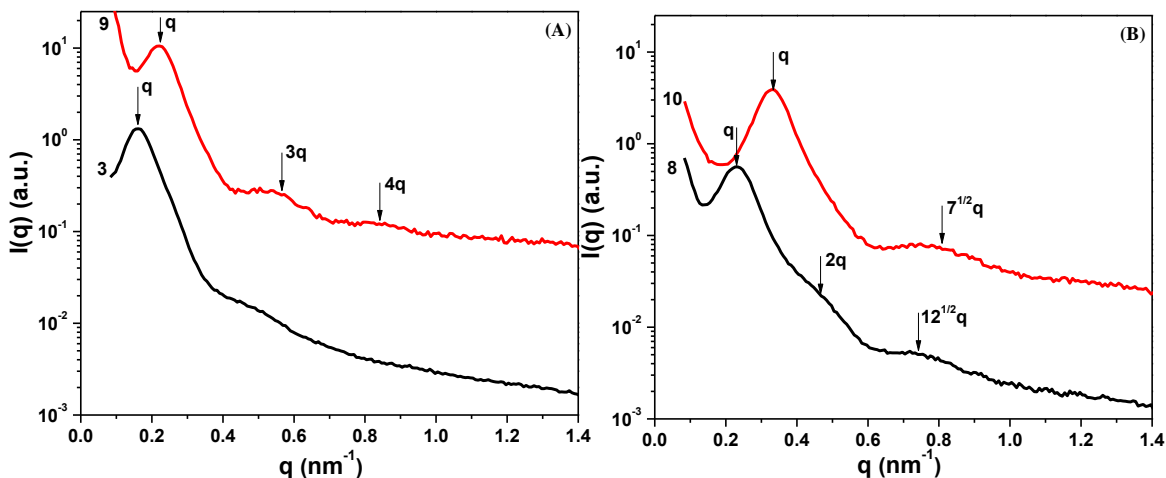


Figure 4.9. SAXS patterns of quaternary copolymer (A) $\text{PS}_{100}\text{-}b\text{-PVBC}_{167}$; (B) $\text{PS}_{100}\text{-}b\text{-PBBS}_{160}$, **3, 8**: cast from toluene/1-propanol ($v/v = 1:1$); **9, 10** cast from DMF/1-propanol ($v/v = 3:1$).

Surprisingly, when the samples of $\text{PS}_{100}\text{-}b\text{-PBBS}_{160}$ and $\text{PS}_{100}\text{-}b\text{-PVBC}_{104}$ were cast from DMF/1-propanol, $\text{PS}_{100}\text{-}b\text{-PBBS}_{160}$ sample in chloride form showed unexpectedly higher conductivity of 33.7 mS cm^{-1} compared to the $\text{PS}_{100}\text{-}b\text{-PVBC}_{104}$ sample with 28.9 mS cm^{-1} chloride conductivity at similar ion contents ($\text{IEC} = \sim 3.20 \text{ meq g}^{-1}$, $\lambda = \sim 7.0$). The ion transport of humidified AEMs was generally accepted to occur through water-assisted mechanism. However, the conductivity increase in $\text{PS}_{100}\text{-}b\text{-PBBS}_{160}$ sample was probably due to water transport aided with side chain motion as observed in ionic block

copolymers under anhydrous conditions wherein the ionic conductivity relies on side chain motion.²⁴

In contrast, PS₁₀₀-*b*-P(VBC₁₂-*r*-BBS₁₃₂) membrane showed slightly lower chloride conductivity of 18.8 and 25.2 mS cm⁻¹ than PS₁₀₀-*b*-PVBC₁₀₄ (20.4 and 28.9 mS cm⁻¹) at the same conditions (~3.20 meq g⁻¹, $\lambda = \sim 8.0$) cast from toluene/1-propanol (v/v = 1:1) and DMF/1-propanol (v/v = 3:1), respectively, **Figure 4.8**. It was believed the conductivity of PS₁₀₀-*b*-P(VBC₁₂-*r*-BBS₁₃₂) sample was supposed to be higher in the presence of trimethyl styrenylbutyl ammonium side chain as observed above. The conductivity decrease could be due to the increased energy barriers for chloride anion movement from benzyltrimethyl ammonium moieties to trimethyl styrenylbutyl ammonium cations. The side chain and benzyltrimethyl ammonium membranes exhibited high ionic conductivity in chloride (Cl⁻) but moderate water absorption in spite of their high IECs, which is conducive to high performance fuel cell membranes. These results provided an avenue to approach the increased conductivity by solvent induced long-range ordered microstructures and longer soft side chain introduction between ionic moieties and polymer backbone.

Alkaline Stability

The stability of AEMs in highly alkaline solution remains a critical issue.²⁵ The quaternary benzyl ammonium AEMs have been shown to degrade rapidly under fuel cell operation conditions. The alkaline stability of side chain and benzyl trimethylammonium block copolymers was evaluated by immersion of the quaternized powder in 1 M NaOH

in water at 80 °C with regular changes of the alkaline solutions every 144 h. The degradation of the samples was determined by the change of the ratios of the trimethylalkylammonium protons to those of benzene rings (partial degradation ^1H NMR in **Figure A4**, Appendix A) as shown in the following equation:

$$\text{Cations remaining} = (\text{ratio of } H_i/H_{\text{aromatic}})_t / (\text{ratio of } H_i/H_{\text{aromatic}})_0$$

Where H_i is the integration of methyl protons on ammonium cations, H_{aromatic} is the sum of aromatic protons, ($H_a+H_b+H_c+H_d+H_e$) on the aromatic rings, t stands for a given time and 0 is the beginning of the experiment.

Based on ^1H NMR data, the quaternized $\text{PS}_{100}\text{-}b\text{-PBBS}_{45}$ block copolymer was relatively stable for the first 12 days but the benzyl trimethylammonium copolymer $\text{PS}_{100}\text{-}b\text{-PVBC}_{49}$ lost 25% of its initial IEC. The remaining fraction of side chain trimethylammonium protons was 79% and 59% on 18, 30 days, respectively, while the percentage of benzyl trimethylammonium protons was 67% and 53% as shown in **Figure 4.10**.

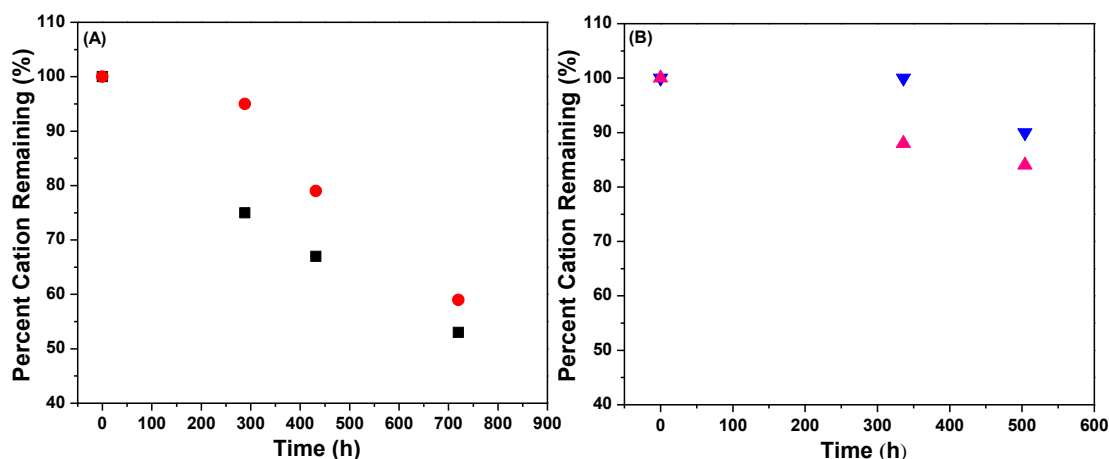


Figure 4.10.(A) Stability of (●) Q-PS₁₀₀-*b*-PBBS₄₅ and (■) Q-PS₁₀₀-*b*-PVBC₄₉; (B) (▼) Q-PBBS and (▲) Q-PVBC in NaOD/D₂O at 80 °C.

Based on the assessments of the long-term stability under alkaline conditions at 80 °C, the C4 side chain copolymer was slightly better than benzyltrimethyl copolymer, as we have observed with other side chain constructions. To confirm the degradation results, the aqueous soluble quaternized PBBS and PVBC polymers were degraded with 4M KOD in D₂O at 80 °C. The degradation in highly alkaline conditions of the pure quaternized samples was slower compared to previous tests in lower pH. The side chain sample showed no degradation after 14 days and the residue of butyltrimethylammonium remained at 90% after 21 days while the benzyltrimethylammonium showed significant degradation after 14 days with 88% quaternary ammonium remaining and 84% after 21 days. So based on the obtained data, the C4 side chain quaternized polymer was slightly more stable than the traditional benzyltrimethyl ammonium polymers.

The stability results were consistent with the previous poly(phenylene) side chains with hexamethylene spacer in 4M KOH at 90 °C.²⁶ After 14 days, the membrane showed 5% loss of conductivity without IEC loss. Compared to Yan's imidazolium side chain polyfluorene, stable in 1M KOH at 60 °C for 400h, the styrene based side chain copolymer showed comparable stability.²⁷

4.4 Conclusions

Block copolymer AEMs with C4 side chain tethered quaternary-ammonium groups were synthesized via RAFT polymerization through either a functional monomer approach or a post-polymerization side chain modification approach. The bifunctional monomer of 4-(3-butenyl) styrene underwent RAFT polymerization through the styrenyl moiety due to the inability of the olefinic groups to polymerize under radical conditions at moderate temperatures. The incorporation of 4-(3-butenyl)styrene and one-step post-polymerization bromination provided a direct synthetic approach to the pure side chain block copolymers and the quantitative HBr bromination of butenyl groups to bromobutyl groups was the key step for the synthesis of side chain block copolymers. This synthetic strategy is applicable to the extended side chain for functionalization. The quaternized side chain and benzyl trimethylammonium copolymers showed strong phase separation driven by the large segregation strength of radically different blocks. The introduction of C4 side chain in the block copolymers resulted in the reduction of the domain spacing in a great extent due to the increased miscibility between C4 side chain and hydrophobic block. The conductivity could be improved by solvent induced long-range ordered microstructures and longer soft side chain introduction between ionic moieties and polymer backbone. In the accelerated degradation experiments, the quaternized side chain copolymer and homopolymer showed better stability against alkaline conditions at 80°C compared to benzyltrimethyl ammonium counterparts. The copolymers stability suggested the C4 side chain block copolymers are a promising candidate for the AEM fuel cells. The concentration of the future work will on reducing water swelling to obtain excellent mechanical properties in liquid water. Furthermore, the phase separation

behavior of quaternized C4 side chain block copolymers is different from benzyltrimethylammonium copolymers and need to be further elucidated in both experiment and theory.

4.5 References

1. Ren, X.M.; Zelenay, P.; Thomas, S.; Davey, J.; Gottesfeld, S. *J. Power Source*, **2000**, *86*, 111-116.
2. Burke, A.F. *Proceedings. IEEE*, **2007**, *95*(4), 806-820.
3. Hickner, M.A.; Ghassemi, H.; Kim, Y.S.; Einsla, B.R.; McGrath, J.E. *Chem. Rev.* 2004, *104*, 4587-4612; Rubatat, L.; Shi, Z.Q.; Diat, O.; Holdcroft, S.; Frisken, B.J. *Macromolecules* **2006**, *39*, 720-730.
4. Elabd, Y.A.; Napadensky, E.; Walker, C.W.; Winey, K.I. *Macromolecules* **2006**, *39*, 399-407.
5. Ghassemi, H.; McGrath, J.E.; Zawodzinski, T.A. *Polymer* **2006**, *47*, 4132-4139; Harrison, W.L.; Hickner, M.A.; Kim, Y.S.; McGrath, J.E. *Fuel Cells* 2005, *5*, 201-212.
6. Kim, Y.S.; Dong, L.M.; Hickner, M.A.; Pivovar, B.S.; McGrath, J.E. *Polymer* 2003, *44*, 5729-5736.
7. Park, M.J.; Balsara, N.P. *Macromolecules* **2008**, *41*, 3678-3687; Knychala, P.; Dziecielski, M.; Balsara, N.P. *Macromolecules* **2013**, *46*, 5724-5730.
8. Zhao, Z.; Wang, J.H.; Li, S.H.; Zhang, S.B. *J. Power Sources* **2011**, *196*, 4445-4450.
9. Tanaka, M.; Fukasawa, K.; Nishino, E.; Yamaguchi, S.; Yamada, K.; Tanaka, H.; Bae, B.; Miyatake, K.; Watanabe, M. *J. Am. Chem. Soc.* **2011**, *133*, 10646-10654.
10. Zeng, Q.H.; Liu, Q.L.; Broadwell, I.; Zhu, A.M.; Xiong, Y.; Tu, X.P. *J. Membr. Sci.* **2010**, *349*, 237-243.
11. Tsai, T.H.; Versek, C.; Thorn, M.; Tuominen, M.; Coughlin, E.B. Chpt 15, ACS Symposium Series; Washington, DC, 2012.

12. Chempath, S.; Boncella, J.M.; Pratt, L.R.; Henson, N.; Pivovar, B.S. *J. Phys. Chem. C* **2010**, *114*, 11977-11983; Chempath, S.; Einsla, B.R.; Pratt, L.R.; Macomber, C.S.; Boncella, J.M.; Rau, J.A.; Pivovar, B.S. *J. Phys. Chem. C* **2008**, *112*, 3179-3182.
13. Li, N.W.; Leng, Y.; Hickner, M.A.; Wang, C.Y. *J. Am. Chem. Soc.* **2013**, *135*, 10124-10133.
14. Tomoi, M.; Yamaguchi, K.; Ando, R.; Kantake, Y.; Aosaki, Y.; Kubota, H. *J. Appl. Polym. Sci.* **1997**, *64*, 1161-1167; Hibbs, M.R.; *J. Polym. Sci.; B: Polym. Phys.* **2012**, in press
15. Zhang, H.M.; Ruckenstein, E. *Macromolecules* **1999**, *32*, 5495-5500.
16. Weber, R.L.; Ye, Y.S.; Schmitt, A.L.; Banik, S.M.; Elabd, Y.A.; Mahanthappa, M.K. *Macromolecules* **2001**, *44*, 5727-5735; Weber, R.L.; Ye, Y.S.; Schmitt, A.L.; Banik, S.M.; Elabd, Hickner, M.A.; Y.A.; Mahanthappa, M.K. *J. Polym. Sci. Part B: Polym. Phys.* **2011**, *49(18)*, 1287-1296.
17. Negishi, E.I. *Acc. Chem. Res.* 1982, **15**, 340; Labadie, J.W.; Stille, J.K. *J. Am. Chem. Soc.* **1983**, *105*, 669-670.
18. Kharasch, M.S.; Mayo, F.; *J. Am. Chem. Soc.* **1933**, *55*, 2468-2496; Farmer, E.H.; *Trans. Faraday Soc.* **1946**, *42*, 228-236.
19. Nakamura, I.; Wang, Z.G. *Soft Matter* **2012**, *8*, 9356-9367.
20. Kumar, R.; Muthukumar, M. *J. Chem. Phys.* **2007**, *126*, 214902-214913.
21. Yan, J.; Hickner, M.A. *Macromolecules* **2010**, *43*, 2349-2356.
22. Elabd, Y.A.; Hickner, M.A. *Macromolecules* **2011**, *44*, 1-11.
23. Kreuer, K.D. *J. Membr. Sci.* **2001**, *185*, 29-39.
24. Schneider, Y.; Modestino, M.A.; McCulloch, B.L.; Hoarfrost, M.L.; Hess, R.W.; Segalman, R.A. *Macromolecules* **2013**, *46*, 1543-1548.
25. Sean, S.; Hickner, M.A. *ACS Macro Lett.* **2013**, *2*, 49-52.
26. Fujimoto, C.; Kim, D.S.; Hibbs, M.; Wroblewski, D.; Kim, Y.S. *J. Membr. Sci.* **2012**, *423-424*, 438-449.
27. Lin, B.C.; Qiu, L.H.; Qiu, B.; Peng, Y.; Yan, F.; *Macromolecules* **2011**, *44*, 9642-9649.

Chapter 5

Low-Temperature Crosslinked Anion Exchange Membranes

This chapter is adapted from the draft Wang, L.Z.; Hickner, M. A. Polymer Chemistry 2014, DOI: 10.1039/C3PY01490H.

5.1 Introduction

AEMs based on block copolymers draw great interest due to the ability to tune their phase composition and phase separation properties. Segregating the ion-conducting phase and the hydrophobic phase in a block copolymer format enables independent tuning the ion conductive, water swelling and mechanical properties of the membrane.⁸ By coupling hydrophobic and hydrophilic blocks, poly(arylene ether) type multiblock aromatic AEMs have been reported. The aromatic copolymers exhibited higher hydroxide ion conductivity at 25 °C in liquid water (21 mS cm⁻¹ at IEC 1.50 meq g⁻¹ with water uptake 26%) than their random counterparts (15 mS cm⁻¹ at IEC = 1.58 meq g⁻¹ with water uptake 13%) in liquid water while maintaining good mechanical traits.⁹ Segmental ionene block copolymers have been prepared with reasonable conductivity of 50 mS/cm (liquid water, 25 °C) with a water uptake 180 wt% and an IEC 2.34 meq g⁻¹.¹⁰ Quaternary ammonium-functionalized styrene-ethylene/butylene-styrene (SEBS) block copolymers had excellent dimensional stability during hydration. Continuous hydrophobic domains were observed in this material by atomic force microscopy (AFM), which promoted an OH⁻ conductivity of 9.6 mS cm⁻¹ (liquid water, room temperature)

under IEC 1.54 meq g^{-1} but a high water uptake of 265 wt%.¹¹ The presence of soft segments facilitates membrane formation, but in some cases may lead to excessive swelling. High T_g hydrophobic blocks designed to greatly constrain the water swelling may also be employed if the membrane does not become too brittle.

The AEMs obtained from polystyrene based block copolymers are brittle yet highly swollen in liquid water, thus hampering their study in fuel cell devices. The synthesized crosslinked copolymer AEMs based on poly(vinylbenzyl chloride) and poly(butenylstyrene) copolymers in this work were self-supporting membranes and were robust in handling during characterization. Compared to non-crosslinked block copolymers, the crosslinked copolymers have been used to fabricate robust anionic membranes while the conductivity was only slightly reduced due to the crosslinking. In addition, crosslinked copolymers render AEMs with acceptable water uptake and reasonable conductivity in liquid water.

Previous results indicated crosslinking of block copolymers was a promising approach for the construction of high performance AEMs. One of the goals of the current work is to continue to increase the ion content of cationic polymers to promote higher conductivities in AEMs. Quaternized block copolymers with high ion exchange capacity (IEC) can show high water swelling or even be soluble in water but this disadvantage of high IEC materials can be overcome by crosslinking. The purpose of this paper is to demonstrate how crosslinking influences the properties of a series of AEMs by controlling the crosslinking length and sites in hydrophobic and hydrophilic blocks. The

crosslinking region was tuned by the block lengths and the crosslinking sites can be varied with the incorporation of BeS. In this report, the crosslinking effects on water uptake, conductivity and morphology will be discussed in detail.

5.2 Experimental

Materials. All chemicals and reagents were purchased from Sigma-Aldrich (St. Louis, MO) and used as received except as noted. 4-Vinylbenzyl chloride (VBC) (>90%) was deinhibited by 0.1M NaOH solution, followed by washing with DI water. 2,2'-Azobis(2-methylpropionitrile) (AIBN), (98%) was purified by recrystallization from methanol and dried under vacuum oven at 40 °C overnight.

Analyses. ^1H nuclear magnetic resonance (NMR) spectroscopy was performed on Bruker (Bruker Biospin, Billerica, MA) CDPX-300 FT-NMRs using CDCl_3 as solvent and the residue peak at 7.27 ppm as an internal reference. Gel permeation chromatography (GPC) was conducted to determine the molecular weight and polydispersity indexes and calibrated with poly(styrene) standards (Varian, Lake Forest, CA) in tetrahydrofuran (THF) with a flow rate of 1 mL min^{-1} at 35 °C on a Waters (Milford, MA) GPC system with a refractive index (RI) detector.

Synthesis of butenyl styrene (BeS). To a stirring solution of allylmagnesium bromide (1.6 L, 1 M) at 0 °C was added vinylbenzyl chloride (195.2 g, 1.278mol) in dry diethyl ether (320 mL) dropwise and stirred overnight at room temperature. The reaction mixture was quenched with diluted hydrochloric acid (800 mL, 1 M) at 0 °C, extracted with

diethyl ether (600 mL x3). The combined organic layers were washed with brine (500 mL x2), dried over (Na_2SO_4) and concentrated under reduced pressure. The product was isolated by distillation under reduced pressure (164g, Yield: 81%). The ^1H NMR spectrum of the final compound is shown in **Figure B1**.⁶

General Procedure for the Synthesis of Styrene-based Copolymers. Poly(vinylbenzyl chloride) (PVBC) was synthesized as the macroinitiator. The stirring solution of VBC (38.155 g, 250 mmol), S-dodecyl-S'-(α,α' -dimethyl- α'' -acetic acid)trithiocarbonate (DDMAT) (381.2 mg, 1.04 mmol), and AIBN (17.2 mg, 0.104 mmol) was bubbled with argon and immersed into a preheated oil bath at 70 °C for 24 h. The reaction mixture was quenched by liquid nitrogen and warmed to room temperature. The reaction mixture was diluted with THF, precipitated in a large amount of methanol three times and then dried in vacuo at 40 °C to give the PVBC macroinitiator (Macro-PVBC₁₀₀, $M_n = 13.6 \text{ k g mol}^{-1}$, $M_w/M_n = 1.14$, $M_n^{\text{NMR}} = 15.3 \text{ k g mol}^{-1}$) as a yellow solid.

The block copolymer PVBC₁₀₀-*b*-PBeS₁₀₇ was synthesized from Macro-PVBC₁₀₀ (1.526 g, 0.1 mmol), BeS (15.82 g, 100 mmol) and AIBN (3.3 mg, 0.02 mmol) at 70 °C for 12 h following the general procedure above. The number average degree of polymerization of the BeS was calculated based on the ratio of the PVBC ($-\text{CH}_2-$ at 4.50 ppm) to the BeS ($-\text{CH}=\text{CH}_2-$ at 5.30 ppm) in ^1H NMR spectroscopy. The number average degree of the polymerization of the random copolymer was calculated based on the mass conversion from monomer to polymer and the ratio of VBC ($-\text{CH}_2-$ at 4.50 ppm) units to BeS ($-\text{CH}=\text{CH}_2-$ at 5.30 ppm) units from the ^1H NMR spectrum of the

polymer. The ratio of the two repeat units was calculated from the integration of chloromethyl protons (CH_2Cl at 4.50 ppm) to two olefinic protons ($-\text{CH}=\text{CH}_2-$ at 5.30 ppm). All other block or random copolymers were synthesized in a similar fashion.

Crosslinking of PVBC-*b*-PBeS and Quaternized PVBC-*b*-PBeS to Form Membranes.

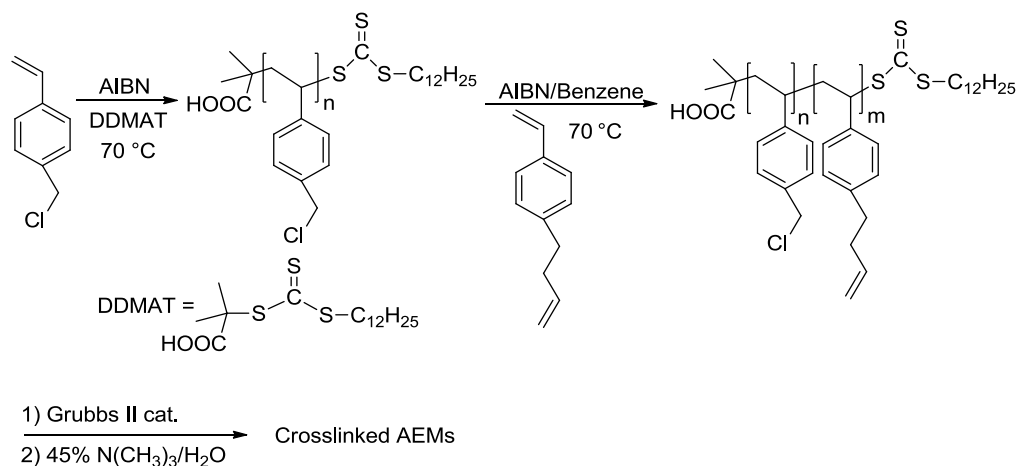
Crosslinked anion exchange membranes were formed by two approaches. In the first approach, termed heterogeneous quaternization, the 2nd generation Grubbs catalyst (2 mg) was added to the solution of the PVBC₄₄-*b*-PBeS₄₄ powder (100 mg) in the mixture of toluene (1.5 mL) and 1-propanol (0.5 mL) and stirred for 20 s. The solution was cast to a PTFE mould for 1 day in a slightly opened desiccator. Then the solid, dry membrane was immersed in ~45 wt% trimethylamine aqueous solution in a sealed container at room temperature for 48 h to convert the benzyl chloride groups in the crosslinked solid membrane sample to quaternary ammonium moieties. In the second approach, termed homogeneous quaternization, PVBC-*b*-PBeS block copolymer amination was performed by the addition of ~30 wt% trimethylamine in ethanol solution (4 molar equivalents to the benzyl chloride groups) to the 10% (w/v) solution of PVBC-*b*-PBeS in DMF and stirred at 50 °C for 24 h. The solution was concentrated under reduced pressure and dried in a vacuum oven at 50 °C for 24 h. The ~7% (w/v) quaternized polymer solution with Grubbs 2nd generation catalyst (100 mg polymer to 2.3 mg catalyst) in toluene and 1-propanol (v/v, 1:1) solution was cast on PTFE mold and placed in a slightly ventilated desiccator at room temperature for 24 h. The crosslinked AEMs were soaked in 1M NaHCO_3 solution for 48 h and immersed in deionized water for 24 h to remove the residual NaHCO_3 and then kept in DI water before conductivity measurements. The non-

crosslinked AEMs were cast from either ~ 7 wt% quaternized copolymers in toluene and 1-propanol (volume ratio 1:1, v/v) or non-quaternized copolymers in toluene and 1-propanol (volume ratio 3:1, v/v) followed by immersion in ~ 30 wt% trimethylamine in ethanol solution for 48 h.

5.3. Results and Discussion

Synthesis of Block Copolymers and Crosslinked Membrane Preparation

The block copolymer synthesis and crosslinked AEMs were prepared according to Scheme 1. Reaction of 4-vinylbenzyl chloride with allylmagnesium bromide in anhydrous diethyl ether gave the 4-(3-butenyl)styrene in excellent yield following previous literature. Block copolymers were synthesized by reversible addition-fragmentation chain transfer polymerization (RAFT) using S-dodecyl-S'-dodecyl- α,α' -dithiobis(methane) (DDMAT) as a chain transfer agent (CTA). First, vinylbenzyl chloride was polymerized with DDMAT to form poly(vinylbenzyl chloride) macroinitiators followed by polymerization of the poly(4-(3-butenyl)styrene) blocks.



Scheme 5.1. Synthesis of crosslinked AEMs strategy by RAFT polymerization and Grubbs 2nd generation catalyst.

The random copolymer was prepared under RAFT conditions using a 1.5:1 molar mixture of vinylbenzyl chloride and 4-(3-butenyl)styrene. The ratio of [monomer]:[CTA] was varied to obtain the target average degree of polymerization. The number-average degree of polymerization of the macroinitiators were calculated based on the ratio of the integration of ^1H NMR resonances for the chloromethyl protons (ClCH_2- at 4.50 ppm) on the repeat units to the resonances for the methylene protons ($-\text{CH}_2\text{S}-$ at 3.23 ppm) of the terminal RAFT agent macroinitiators. The broadened molecular weight distribution of poly(4-(3-butenyl)styrene) with increased polymerization time necessitated synthesis of poly(vinylbenzyl chloride) (poly(VBC)) as the first block. The 4-(3-butenyl)styrene features a styryl group capable of undergoing radical polymerization and a pendant alkene moiety for crosslinking by olefin metathesis. During the RAFT polymerization the pendant alkene groups were not involved in the RAFT reaction as monitored by ^1H NMR due to the low radical reactivity through the formation of short-lived secondary carbon

radicals. Chain extension at 70 °C of poly(VBC) macro CTAs of was performed to prepare the well-defined diblocks using 4-(3-butenyl)styrene (BeS) as the second block. The formation of the diblocks was monitored by the molecular weight increase (M_n) in GPC and through ^1H NMR spectroscopy. The PDIs were typical for RAFT chain extensions, see **Table B1**.

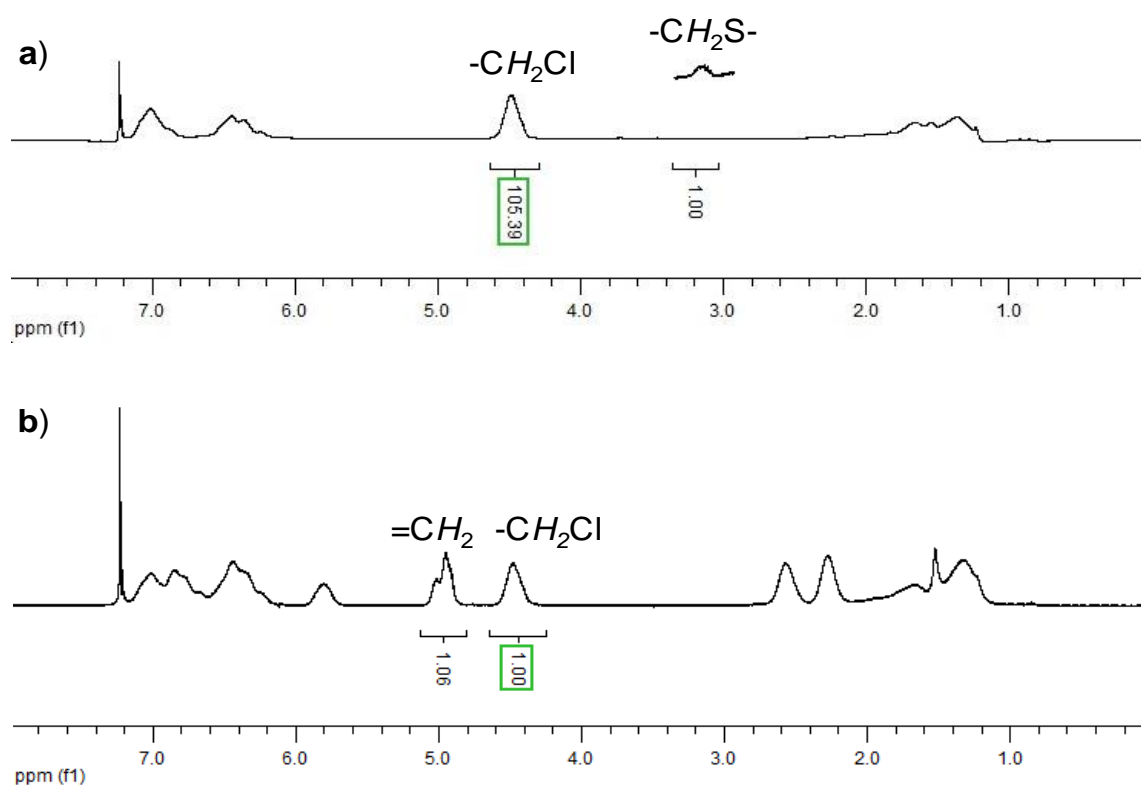


Figure 5.1. ^1H NMR spectra of a) macroinitiator PVBC₁₀₀ and b) block copolymer PVBC₁₀₀-*b*-PBeS₁₀₇.

The number average degrees of polymerization of the second blocks were calculated from the ratio of the integration of the ^1H NMR resonances of the olefinic protons ($=\text{CH}_2-$ at 5.30 ppm) in the side chain of butenylstyrene repeating units to the

integration of chloromethyl protons (ClCH_2^- at 4.50 ppm) adjacent the aromatic rings as shown in **Figure 5.1** and **Figure B2**. GPC data of the macroinitiator and block copolymers showed low polydispersity indices (PDIs) (<1.40) and narrow monomodal molecular weight distributions (**Figure 5.2** and **Figure B3**) against polystyrene GPC standards in THF solvent. Molecular weight characterization implied the RAFT conditions had controlled/living characteristics and the side reactions were minimized albeit the M_n s of all the block copolymers were not in good agreement with the GPC values due to the calibration based on poly(styrene) standards.

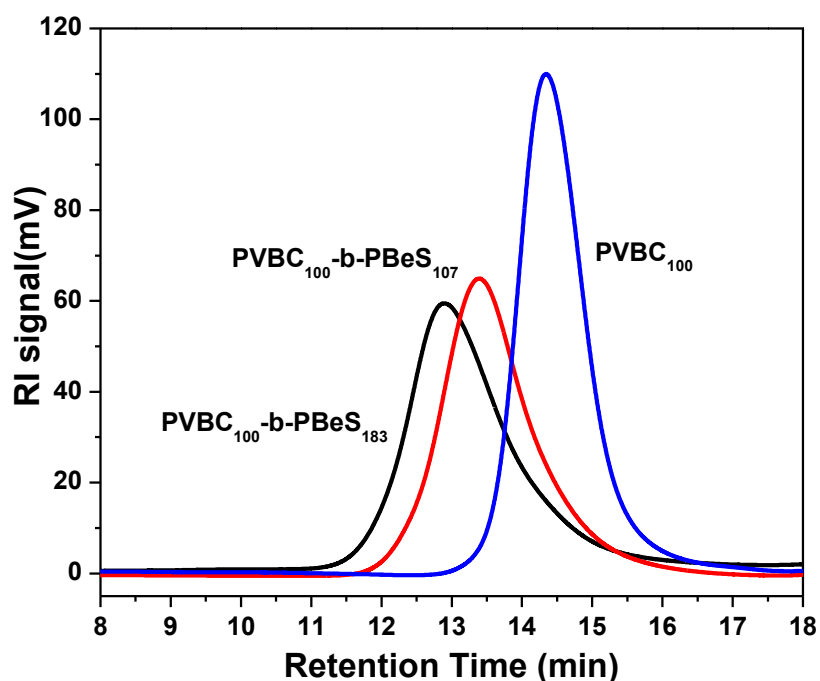


Figure 5.2. GPC profiles of macroinitiator PVBC_{100} and block copolymer $\text{PVBC}_{100}\text{-}b\text{-PBeS}_{107}$ and $\text{PVBC}_{100}\text{-}b\text{-PBeS}_{183}$.

The crosslinked AEMs were fabricated from the non-quaternized block copolymers during casting with a catalytic amount of 2nd generation Grubbs catalyst in a mixture of toluene and 1-propanol (volume ratio 1:1 v:v), followed by quaternization with 45% trimethylamine aqueous solution. The ratio of Grubbs 2nd generation catalyst to double bonds in the side chain was maintained at 0.75 mol% catalyst: double bonds for block and random copolymers. Grubbs 2nd generation catalyst was used for its high reactivity towards the metathesis reaction of the terminal olefinic double bonds and high stability to oxygen. After crosslinking, the membranes were insoluble in a mixture of toluene and 1-propanol (v/v 1:1) even at 60 °C, which is a good solvent for the quaternized block copolymers, indicating successful crosslinking. The crosslinked membranes maintained good dimensional stability in liquid water, thus reducing water uptake through the network of crosslinked sites. The un-crosslinked AEMs were prepared by solution casting from toluene and 1-propanol (volume ratio, 3:1, v/v) followed by immersion in 30% trimethylamine ethanol solution or directly cast from the quaternized block copolymers in toluene and 1-propanol (volume ratio, 1:1, v/v). The standard 45% aqueous trimethylamine solution was not used for quaternization of the cast film because the un-crosslinked AEMs had low dimensional stability in the aqueous solution. In this case, ~ 30 wt% trimethylamine in ethanol was used for quaternization to avoid excess swelling of the sample during conversion.

Properties of Crosslinked AEMs

The crosslinking effects on the AEM properties were evaluated for both block and random copolymers. Based on the water content data for crosslinked and non-crosslinked AEMs, **Table 5.1**, the water uptake (WU) of the crosslinked AEMs derived from block copolymers was lower than for their random crosslinked analogues in liquid water.

Table 5.1. Properties of crosslinked and un-crosslinked AEMs.

Sample	IEC (Cl) (meq/g)	Liquid WU (wt %)	95 % RH WU (Cl) (wt %)		σ_{Cl^-} (mS/cm)	$\sigma_{\text{HCO}_3^-}$ (mS/cm)	d-spacing (nm)	
			Xlink ^a	Un-Xlink ^a			Xlink ^a	Un-Xlink ^a
PVBC _{49-r} -PBeS ₅₀	2.65	80	41.2	33.7	16.9	13.6	NANA	
PVBC _{44-b} -PBeS ₄₄	2.70	70	42.3	40.0	18.4	14.6	10.0	20.4
PVBC _{100-b} -PBeS ₁₀₇	2.62	60	40.3	42.2	17.6	11.9	14.0	43.1
PVBC _{100-b} -PBeS ₁₈₃	2.00	45	30.4	33.3	11.6	8.2	15.3	54.1

a) Crosslinked and un-crosslinked block copolymers AEMs cast from the corresponding precursors with and without Grubbs II catalyst followed by amination.

It is likely that the crosslink density for the crosslinked block copolymer AEM was greater than that of the crosslinked random copolymer AEM due to the clustering of the crosslinking sites in the hydrophobic blocks. Additionally, the Grubbs catalyst had better crosslinking efficiency for the cross metathesis reaction between double bonds in block copolymers than in random copolymers due to the proximity of the quaternary ammonium groups to the double bonds in the random sample. The topology of the backbones in crosslinked AEMs did not alter the values of the relative humidity-water uptake (RH-WU) at 95%. The water uptake was mainly determined by the IECs values of the AEMs samples. However, in liquid water the crosslinking imparted mechanical

integrity against water swelling while the non-crosslinked AEMs were highly swollen to a gel in liquid water.

The conductivity of the crosslinked block copolymer AEMs, **Figure 5.3**, was higher than the crosslinked random copolymer AEMs due to the formation of ionic channels by microphase separation even in presence of the crosslinking moieties. From the morphology studies by SAXS there was no observed phase separation in the crosslinked random block copolymer PVBC₄₉-*r*-PBeS₅₀ AEM. For the crosslinked block copolymer PVBC₄₄-*b*-PBeS₄₄ AEM a single broad scattering maximum was observed corresponding to a 10.0 nm domain spacing, **Table 5.1** and **Figure B4**.

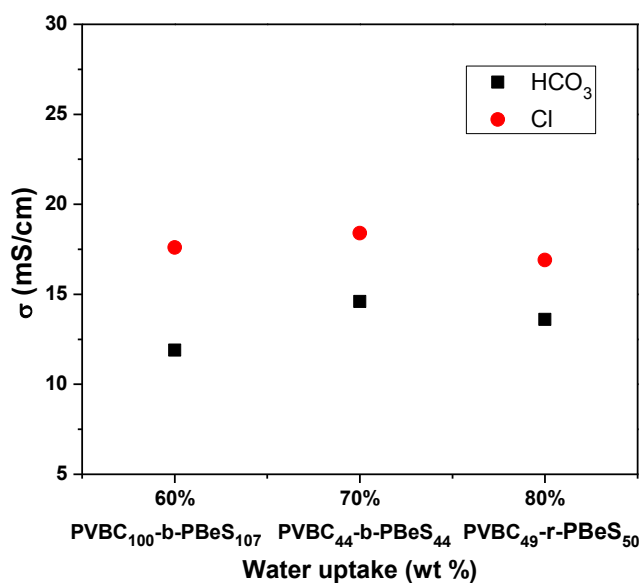


Figure 5.3. Conductivity versus water uptake for crosslinking AEMs: 60%, 70%, 80% corresponding to extended PVBC₁₀₀-*b*-PBeS₁₀₇, block PVBC₄₄-*b*-PBeS₄₄, random PVBC₄₉-*r*-PBeS₅₀ respectively.

For crosslinked block copolymer AEMs, an increase in the molecular weight of both blocks simultaneously reduced the water uptake and slightly decreased the conductivity in liquid water in both Cl^- and bicarbonate (HCO_3^-) forms in **Figure 5.3**, but there was no effect on the RH WU. The conductivity of the crosslinked AEMs increased with greater water uptake for a given IEC, highlighting the key role that water plays in ion transport in AEMs. At the same IEC, the crosslinked AEM based on the random copolymer had higher conductivity than the PVBC_{100} - b - PBeS_{107} block copolymer with lower water uptake. Additionally, the higher conductivity of AEMs in Cl^- form is attributed to the higher ion mobility of Cl^- (1.04 compared to $\text{K}^+ = 1.0$) than that of HCO_3^- (0.61 compared to $\text{K}^+ = 1.0$).¹² After crosslinking, the domain spacing of crosslinked samples was reduced compared to non-crosslinked samples due to the restriction of domain formation during casting.¹³

There was no obvious difference in water uptake among the crosslinked and non-crosslinked AEMs at 95% relative humidity (RH) in Cl^- form with similar IECs, **Table 5.1**. Compared to the non-crosslinked AEMs, crosslinking did not reduce the water uptake significantly on the basis of RH-WU data. The morphology of the crosslinked and non-crosslinked AEMs was elucidated by SAXS. The non-crosslinked AEMs displayed an ordered morphology with SAXS reflections at ratios of 1:2:3:4, which is anticipated to be a lamellar morphology with long-range order and was confirmed by TEM. Both heterogeneous and homogeneous quaternized AEMs showed long-range ordered morphology in SAXS, but in TEM images the heterogeneous AEM had better morphological order than the homogeneous AEM, **Figure 5.4** and **Figure B4**.¹⁴ The

heterogeneous quaternized and crosslinked AEM only gave a broad peak and the homogeneous quaternized and crosslinked AEM showed a narrow peak with higher order reflections. This difference of ordering in SAXS and TEM is due to the effect of quaternary nitrogen on the reduced reactivity of the Grubbs 2nd generation metathesis catalyst during the crosslinking.

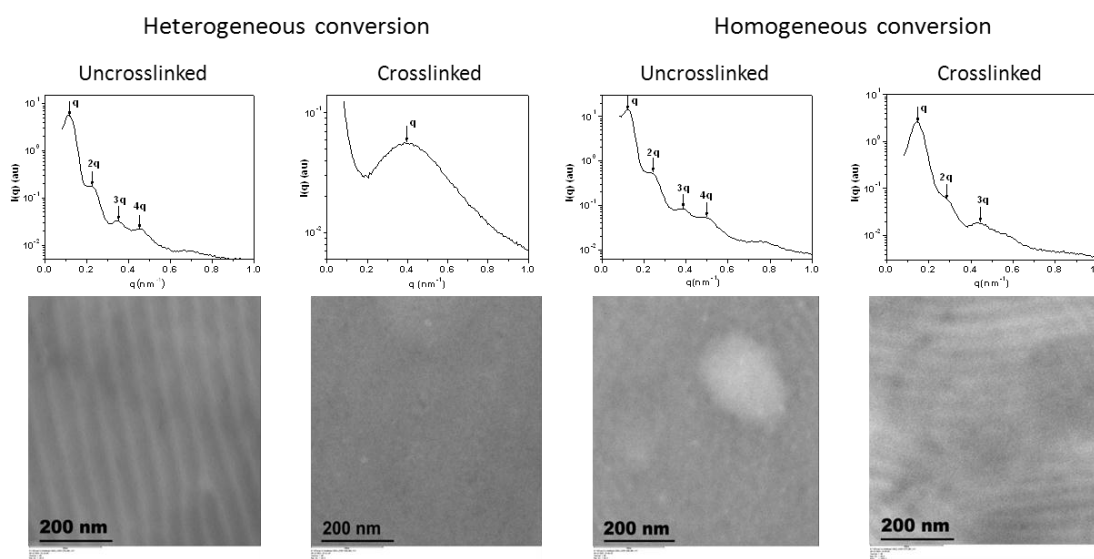


Figure 5.4. Small-angle X-ray scattering (SAXS) patterns and TEM micrographs of non-crosslinked and crosslinked AEMs in the dry state under vacuum from the precursor PVBC₁₀₀-*b*-PBeS₁₈₃.

The principal peaks of the heterogeneous and homogeneous samples from PVBC₁₀₀-*b*-PBeS₁₈₃ corresponded to 54.1 and 49.4 nm domain spacing, respectively, calculated from $d = 2\pi/q$. The morphology was formed before quaternization during the casting of the benzyl chloride form polymer and quaternization did not alter the morphology of the block copolymer membranes during the conversion from the benzyl

chloride to quaternary ammonium chloride. The SAXS profile of the crosslinked sample from the same precursor polymer PVBC₁₀₀-*b*-PBeS₁₈₃ exhibited only a single broad scattering maximum, indicative of a loss of the long-range ordered structure. The disappearance of the lamellar structure of the crosslinked sample is likely due to the limited amount of time allowed for polymer organization and restriction of the chains during casting and crosslinking. The domain spacing of the non-crosslinked AEMs was 54.1 nm, which was larger than that of the crosslinked AEM. The domain spacing of non-crosslinked AEMs is related to the length of hydrophobic and hydrophilic blocks but the addition of Grubbs 2nd generation catalyst reduced the domain spacing of the crosslinked AEMs due to less time for organization during solvent casting before gelation of the crosslinked phase. There was no ordering observed in either the crosslinked or un-crosslinked random copolymer AEM, **Figure B.5**. The conductivity of the crosslinked AEMs in Cl⁻ form was in the range of 11.6-18.4 mS/cm, depending upon IEC, water uptake and copolymer composition. The crosslinked AEMs in HCO₃⁻ form were obtained through ion exchange of the membranes in NaHCO₃ solution and the conductivity followed the same trend as the Cl⁻ counterparts but the conductivity in HCO₃⁻ was lower than that of AEMs in Cl⁻ form. The conductivity in liquid water of the crosslinked AEM from the PVBC₁₀₀-*b*-PBeS₁₈₃ copolymer (11.6 mS/cm) was greatly reduced compared to the conductivity of its un-crosslinked analogue in 100% RH which was 28.0 mS/cm. The lower conductivity of crosslinked sample was likely due to its poorer phase separation as elucidated by SAXS, **Figure 5.4**.

The homogeneously aminated crosslinked AEM prepared from quaternized block copolymer PVBC₁₀₀-*b*-PBeS₁₈₃ had higher water uptake (300 wt%) but lower conductivity (8.4 mS/cm) in liquid water in comparison to the heterogeneous crosslinked AEM from the same precursor block copolymer. Due to the high swelling of the homogeneously crosslinked sample, the concentration of conducting ions in the membrane was diluted and the conductivity was subsequently reduced. The excessive swelling, resulting in the low conductivity was partially due to the insufficient number of crosslinking sites due to the lower efficiency of the Grubbs catalyst in the presence of quaternary ammonium groups from homogeneous amination. When applying the same crosslinking strategy to quaternized PVBC₁₀₀-*b*-PBeS₁₀₇ sample, attempts to obtain a crosslinked AEM that was stable in liquid water were unsuccessful. This result was ascribed to the effect of the quaternary ammonium moiety on the reactivity of ruthenium based catalyst in the cross metathesis reaction. The quaternary ammonium group lowered the catalytic activity of Grubbs 2nd generation catalyst, which required more catalyst to obtain the same crosslinking density as the non-quaternized block copolymer. This reduction of the crosslinking efficiency of Grubbs 2nd generation catalyst in the quaternary ammonium functionalized copolymers was also validated by the domain spacing from SAXS.

The interdomain spacing in quaternized form of the AEM crosslinked from the non-quaternized copolymer PVBC₁₀₀-*b*-PBeS₁₈₃ sample was 15.3 nm while the interdomain spacing was 42.0 nm in the crosslinked sample prepared from the quaternized copolymer, which showed a well-ordered microstructure in SAXS as

displayed in **Figure 5.4**. We hypothesize that the rapid rate of crosslinking in the non-quaternized sample yielded a smaller domain spacing that was kinetically trapped. Because the rate of crosslinking was slower for the quaternized polymer, the domain spacing was larger due to more time for domain organization. The quaternization order had only a minor impact on the morphology of the non-crosslinked AEMs indicating that there was little kinetic trapping in these polymers. The domain spacing of heterogeneous quaternized AEM was 54.1 nm, perhaps due to the swelling of the domains upon conversion while it was 49.4 nm for homogeneous quaternized copolymer. Both samples showed a long-range ordered domain structure from the SAXS pattern.

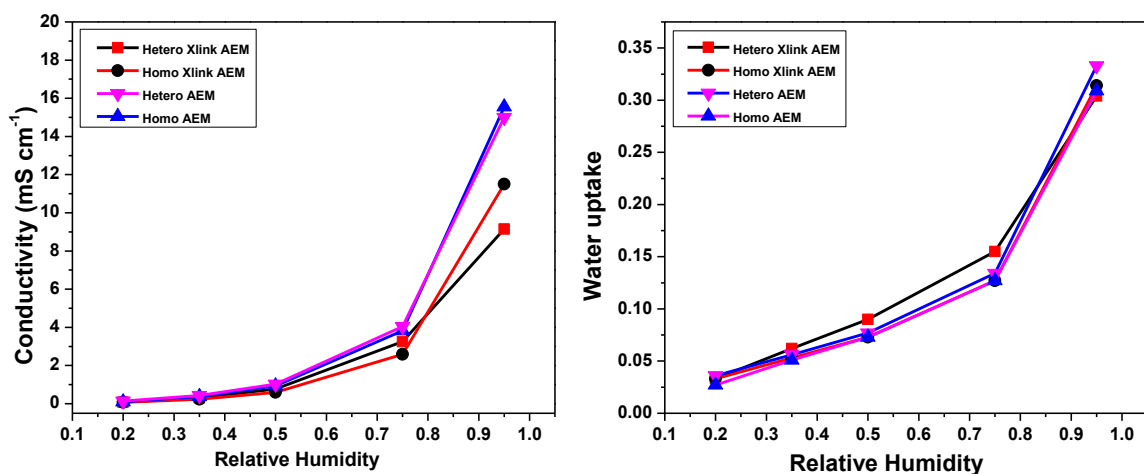


Figure 5.5. Humidity dependence of conductivity and water uptake in Cl^- form crosslinked and non-crosslinked AEMs from $\text{PVBC}_{100}\text{-}b\text{-PBeS}_{183}$ at 30 °C, Homo = homogeneous quaternization, Hetero = heterogeneous quaternization.

The morphology and crosslinking characteristics of the $\text{PVBC}_{100}\text{-}b\text{-PBeS}_{183}$ sample were reflected in the RH-dependent conductivity. This sample was chosen for conductivity and water uptake measurements because of its reasonable mechanical

properties due to its high molecular weight. The conductivity of homogeneously quaternized, crosslinked samples of PVBC₁₀₀-*b*-PBeS₁₈₃ had lower conductivity at 95% RH compared to heterogeneous and homogeneous non-crosslinked samples, as shown in **Figure 5.5**. The homogeneous and heterogeneous un-crosslinked PVBC₁₀₀-*b*-PBeS₁₈₃ samples exhibited nearly the same conductivity over the range of 20-95% RH since these sample had similar domain sizes, **Figure 5.4**. The conductivity of crosslinked PVBC₁₀₀-*b*-PBeS₁₈₃ samples at 95% RH was lower in comparison to uncrosslinked samples. This reduction is probably due to the relatively smaller domain sizes for heterogeneously quaternized and crosslinked PVBC₁₀₀-*b*-PBeS₁₈₃ sample. Additionally, at RH values below 50%, the water uptake determined the materials' conductivity. The crosslinked AEMs did not show good anion conductivity at low RH compared to examples of crosslinked proton exchange membranes due to the difference in ion mobility for protons versus anions.¹⁵

5.4. Conclusions

In summary, we have compared the properties of non-crosslinked and crosslinked random and block copolymer AEMs. The metathesis route provides a feasible low-temperature crosslinking solution for AEMs that can be performed during typical solution casting procedures. The water uptake of the crosslinked samples was reduced by increasing the length of the hydrophobic blocks while the random crosslinked AEM had higher water uptake than the block copolymer samples. In our study, heterogeneous quaternization after crosslinking yielded lower water uptake materials where

quaternization in solution and casting ionic form polymers showed higher water uptake. Un-crosslinked AEMs revealed long-range lamellar order. For crosslinked polymers a well-defined microdomain structure was not present and domain sizes decreased significantly due to gelation of the crosslinks and locking in the morphology during casting. To obtain the highest conductivity (18.4 mS/cm in Cl⁻ form in liquid water at room temperature) in crosslinked AEMs, the AEMs should have high ion concentration after water absorption (70% liquid WU) and maintain good phase separation. The AEMs with long-range ordered domain structures had good conductivity for similar IEC samples.

5.5 References

1. G. Merle, S.S. Hosseiny, M. Wessling and K. Nijmeijer, *J.Membr. Sci.*, 2012, **409-410**, 191.
2. J.R. Varcoe, R.C.T. Slade and E.L.H. Yee, *Chem. Commun.*, 2006, 1428.
3. S. Gu, R. Cai and Y. Yan, *Chem. Commun.*, 2011, 2856; L. Wu and T.W. Xu, *J.Membr. Sci.*, 2008, **322**, 286.
4. Y.P. Zha, M.L. Disabb-Miller, Z.D. Johnson, M.A. Hickner and G.N. Tew, *J. Am. Chem. Soc.*, 2012, **134**, 4493; N.J. Robertson, H.A. Kostalik IV, T.J. Clark, P.F. Mutolo, H.D. Abruna and G.W. Coates, *J. Am. Chem. Soc.*, 2010, **132**, 3400.
5. H.M. Zhang and E. Ruckenstein, *Macromolecules*, 1999, **32**, 5495; J.B. Beil and S.C. Zimmerman, *Macromolecules*, 2004, **37**, 778.
6. W.T. Lin, Z. Shao, J.Y. Dong and T.C. Mike Chung, *Macromolecules*, 2009, **42**, 3750.
7. K. Huang and J. Rzaev, *J. Am. Chem. Soc.*, 2011, **133**, 16726; K. Huang, D.P. Canterbury and J. Rzaev, *Macromolecules*, 2010, **43**, 6632; K. Huang, A. Jacobs and J. Rzaev, *Biomacromolecules.*, 2011, **12**, 2327.

8. Y.A. Elab., M.A. Hickner, *Macromolecules*, 2011, **44**, 1.
9. Z. Zhao, J.H. Wang, S.H. Li and S.B. Zhang, *J. of Power Sources*, 2011, **196**, 4445; J.H. Wang, Z. Zhao, S.H. Li, F.X. Gong and S.B. Zhang, *Macromolecules*, 2009, **42**, 8711.
10. M. Tanaka, F. Fukasawa, E. Nishino, S. Yamagushi, K. Yamada, H. Tanaka, B. Bae, K. Miyatake and M. Watanabe, *J. Am. Chem. Soc.*, 2011, **133**, 10646; K.M. Lee, W. Wycisk, M. Litt and P.N. Pintauro, *J. Membr. Sci.*, 2011, **383**, 254.
11. L. Sun, J.S. Guo, J. Zhou, Q.M. Xu, D. Chu and R.R. Chen, *J. of Power Sources*, 2012, **202**, 70.
12. J. Yan and M.A. Hickner, *Macromolecules*, 2010, **43**, 2349.
13. S. Aida, S. Sakurai and S. Nomura, *Polymer*, 2002, **43**, 2881.
14. I.W. Hamley, V. Castelletto, *Prog. Polym. Sci.*, 2004, **29**, 909.
15. Nakabayashi. K, Higashihara. T and Ueda. M, *Macromolecules*, 2010, **43**, 5756.

Chapter 6

Properties of Highly Ordered Block Copolymer Anion Exchange Membranes

This chapter is adapted from the draft Wang, L.Z.; Hickner, M. A. to be submitted.

6.1 Introduction

Ion conducting polymers having sulfonic acid or quaternary ammonium moieties are of great interest for applications in energy conversion devices such as fuel cells and batteries. In particular, ion-containing block copolymers have attracted significant attention due to their strong phase separation where ionic domains provide an avenue for ion transfer through nonionic matrix phases. The size of the continuously ionic and nonionic microdomains can be tailored and optimized by varying hydrophilic and hydrophobic block lengths to obtain the desired mix of properties.¹⁻⁴

There have been a few reports on AEMs based on ion conducting block copolymers. Tanaka, et al. observed that quaternized multiblock copoly(arylene ether) membranes had higher hydroxide conductivity (144 mS cm^{-1}) than the random sample (34 mS cm^{-1}) at 80°C at the IEC of 1.90 meq g^{-1} .⁷ In Zhang's study, block poly(arylene ether sulfone) copolymer displayed greater conductivity (29 mS cm^{-1}) than that of the random copolymer (15 mS cm^{-1}) at 20°C at the similar IEC ($\sim 1.60 \text{ meq g}^{-1}$) in hydroxide form.⁸ Coughlin and coworkers showed the morphologies effect on the ionic conductivity of PS-*b*-P(VBTMA)(OH⁻ form) AEMs. At 80°C under 90% relative

humidity the hydroxide conductivity of 12.5 mS cm^{-1} at higher $\text{IEC} = 1.36 \text{ meq g}^{-1}$ was approximately increased to 35 times that of the sample with $\text{IEC} = 0.58 \text{ meq g}^{-1}$ and 0.36 mS cm^{-1} .⁹ The conductivity increase was due to the morphological change from sphere to cylinder or lamellae as the IEC increases. The unique ordered ionic morphologies can tailor the ionic transport of AEMs. In addition, quaternized block copolymers have improved the mechanical strength and reduce the swelling comparing randomly functionalized copolymers via the hydrophobic phase reinforcing as showed by Terada, et al.¹⁰ However, there is no detailed in-depth study regarding the relationships of the morphology, ion conductivity and water uptake with controllable hydrophobic block composition in AEMs.

This chapter will describe how the properties of block copolymer anion exchange membranes (AEMs) vary with hydrophobic block composition and ion content. We will demonstrate the morphology, ion conductivity and water uptake relationships of block copolymer based AEMs at the different ion contents. The morphology of the AEMs will be characterized by small angle X-ray scattering (SAXS) and visualized by transmission electron microscopy (TEM). The goal of this work is to demonstrate the optimal AEM performance by manipulating the character of the hydrophobic and hydrophilic blocks. We also will focus on the hydrophobic, semicrystalline block composition in the AEMs that restrict liquid water swelling as the matrix phase. In particular, the factors conducive to the conductivity will be discussed in detail. Fundamental understanding of the structure-property relationships of well-controlled block copolymer based AEMs is crucial for the development of high performance conducting membranes.

6.2 Experimental Section

Synthesis of 4-butylstyrene (BS). Vinylbenzyl chloride (250 g, 1.638 mol) in anhydrous diethyl ether (250 mL) was added dropwise to a stirring suspended solution of Mg turnings (45 g, 1.875 mol) in anhydrous diethyl ether (750 mL) activated with a small piece of iodine (~ 0.2 g) at 0 °C for more than 2 h. The mixture was subsequently stirred at 0 °C for another 1 h and warmed to room temperature for 30 min. The reaction mixture was stirred for another 1 h.

To a stirring solution of 1-bromopropane (330 g, 2.683 mol) in anhydrous THF (1.5 L) at 0 °C was added the freshly prepared 4-vinylbenzylmagnesium chloride (~ 1.2 L) dropwise, slowly warmed up to room temperature and stirred overnight. The reaction mixture was quenched by methanol (50 mL), filtered, and concentrated under reduced pressure. The residue was treated with HCl (1M, 500 mL) at 0 °C and ethyl acetate (~500 mL x3). The combined organic layers were washed by water (500 mL x2), followed by brine washing (500 mL) and dried over Na₂SO₄ and concentrated under reduced pressure. The isolated product was purified by distillation under reduced pressure followed by column chromatography (SiO₂, hexane) to give as a colourless oil (120 g, Yield : 45%). ¹H NMR (300 MHz, CDCl₃) δ 7.35 (d, *J* = 6.9 Hz, 2H), 7.16 (d, *J* = 6.9 Hz, 2H), 6.66 (dd, *J* = 18.3, 11.1 Hz, 1H) 5.72 (d, *J* = 18.3 Hz, 1H), 5.20 (d, *J* = 11.1 Hz, 1H), 2.62 (t, *J* = 6.9 Hz, 2H), 2.35 (m, 2H), 2.15 (m, 2H), 0.94 (t, *J* = 7.8 Hz, 3H); ¹³C NMR (75 MHz, CDCl₃) δ 142.7, 136.9, 135.2, 128.7, 126.3, 112.9, 35.5, 33.7, 22.5, 14.1.

General Procedure for Synthesis of Methacrylate Based Block Copolymers.

All polymerizations were carried out in a similar fashion in one-neck round bottom flasks sealed with septa. A typical polymerization is as follows: A stirring mixture of hexyl methacrylate (23 g, 0.135 mol), CDP (618 mg, 1.5 mmol) and AIBN (50.4 mg, 0.3 mmol) was bubbled with argon and immersed in a preheated oil bath at 60 °C until the mixture reached high viscosity. The reaction solution was quenched by liquid nitrogen, warmed up to room temperature, diluted with THF and precipitated three times in a large amount of methanol. The polymer was recovered by filtration and dried *in vacuo* to give the poly(hexyl methacrylate) macroinitiator (Macro-PHMA₆₀, $M_n^{\text{GPC}} = 10.9 \text{ kg mol}^{-1}$, $M_w/M_n = 1.14$, $M_n^{\text{NMR}} = 10.2 \text{ kg mol}^{-1}$) as a viscous light yellow solid.

The mixture of Macro-PHMA₆₀ (6.6 g, 0.65 mmol), VBC (14.52 g, 95.1 mmol), and AIBN (21.7 mg, 0.13 mmol,) and benzene (9 mL) was degassed by argon for 30 min and placed in a preheated oil bath at 60 °C for 24 h. The resulting polymer was purified by three times precipitation in excess methanol and dried *in vacuo* to give PHMA₆₀-*b*-PVBC₃₄ ($M_n^{\text{GPC}} = 19.5 \text{ k}$, $M_w/M_n = 1.12$) with a theoretical IEC of 2.04 mmol g⁻¹ as a light yellow solid. The number average molecular weight of the second block was calculated based on ¹H NMR of the block copolymer.

General Procedure for the Synthesis of Styrene-based Block Copolymers.

Poly(vinylbenzyl chloride) (PVBC) was synthesized as the first block because the conversion of 4-butylstyrene monomers to poly(butyl styrene) (PBS) was relatively low based on the mass of precipitated polymer in methanol. The stirring solution of VBC

(38.5 g, 0.252 mol), DDMAT (1.16 g, 3.18 mmol), and AIBN (52.2 mg, 0.318 mmol) was bubbled with argon and immersed in a preheated oil bath at 70 °C for 24 h. The reaction mixture was quenched by liquid nitrogen and warmed to room temperature. The reaction mixture was diluted with THF, precipitated in a large amount of methanol three times and then dried *in vacuo* at 40 °C to give the PVBC macroinitiator (Macro-PVBC₄₄, $M_n^{\text{GPC}} = 5.9 \text{ kg mol}^{-1}$, $M_w/M_n = 1.10$, $M_n^{\text{NMR}} = 6.7 \text{ kg mol}^{-1}$) as a yellow solid.

The block copolymer synthesis was carried out in a similar manner to the synthesis of PHMA-*b*-PVBC with Macro-PVBC₄₄ (1.952 g, 0.3 mmol), BS (6.410 g, 40 mmol) and AIBN (9.6 mg, 0.058 mmol) to give PVBC₄₄-*b*-PBS₈₄ with theoretical IEC 1.94 mmol g⁻¹ as a light yellow solid.

Synthesis of PVBC-*b*-PBeS. The block copolymer PVBC₄₄-*b*-PBeS₈₂ was synthesized from Macro-PVBC₄₄ (1.67 g, 0.25 mmol), BeS (11.077 g, 70 mmol) and AIBN (8.2 mg, 0.05 mmol) at 70 °C for 7 h following the general polymerization procedure above.

Block copolymer quaternization. In a typical experiment, to a stirring solution of PVBC₄₄-*b*-PBS₈₄ (1.34 g, 3mmol -CH₂Cl) in dimethylformamide (DMF) (8 mL) was added aqueous trimethylamine solution (1.8 mL, 12 mmol, 45 wt.%) and stirred at 40 °C for 24 h. The suspension solution was concentrated under reduced pressure to give an orange solid. The quaternized form Q PVBC₄₄-*b*-PBS₈₄ was dried *in vacuo* overnight at 50 °C.

Ion Exchange Capacity (IEC). The IEC was calculated based on the ratio of the hydrophobic block and the hydrophilic block in 100% quaternized precursor from ^1H NMR. For the methacrylate or styrene based block copolymers, the IECs were calculated by the ratio of ester methylene ($-\text{CH}_2\text{OCO}-$) at 3.90 ppm or benzyl protons ($-\text{C}_6\text{H}_4\text{CH}_2-$) at 2.50 ppm to the chloromethyl protons (ClCH_2-) at 4.50 ppm.

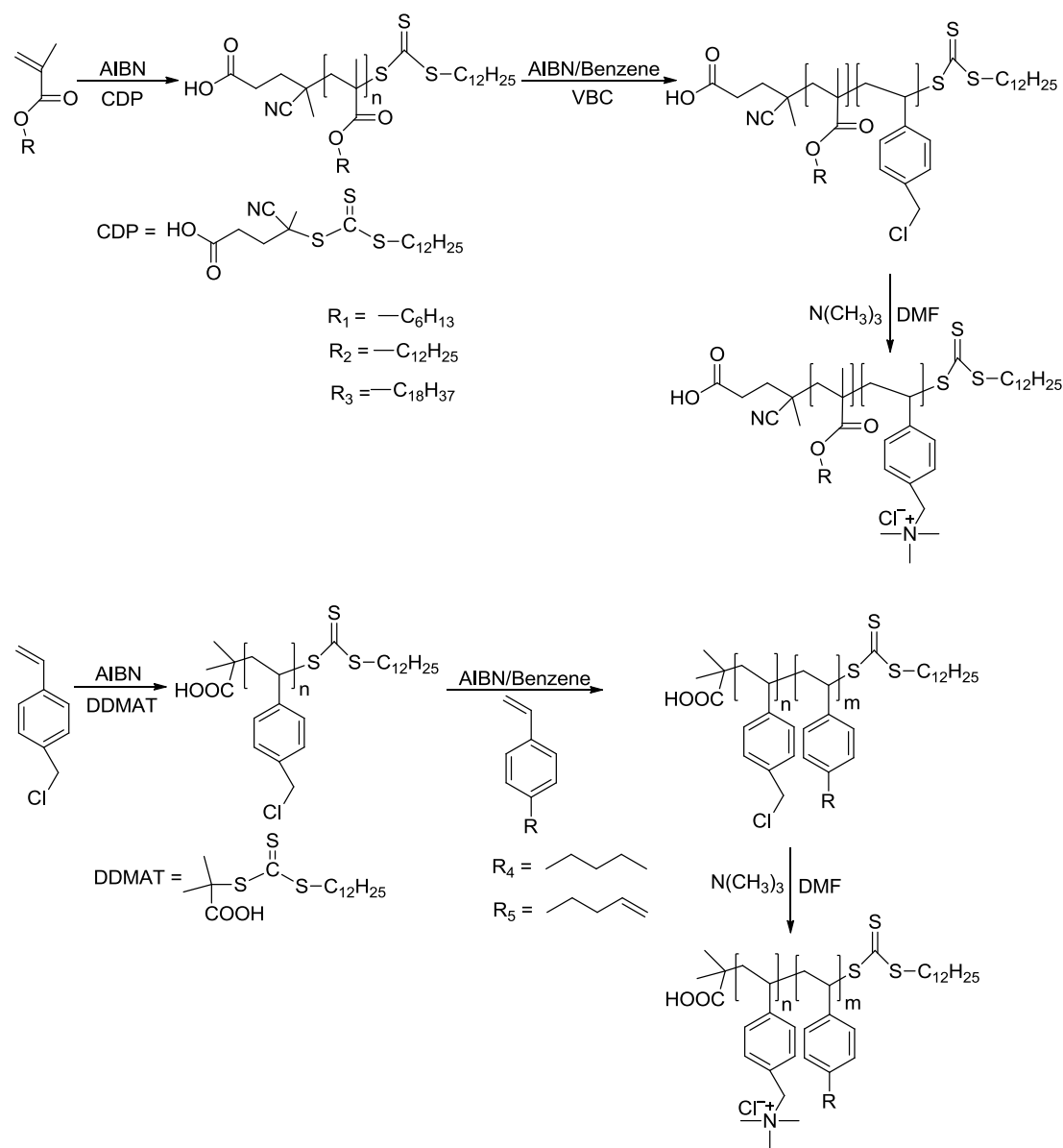
Thermal Behavior. A differential scanning calorimeter, DSC, (TA instrument Q100) was used to measure the crystallinity of the samples. Membrane samples of 5-10 mg sealed into the aluminum pans were first heated from room temperature up to 180°C at 10°Cmin^{-1} , cooled to -50°C at 10°Cmin^{-1} , and second heated to 180°C at 10°Cmin^{-1} under pure nitrogen. Heat flow as watts (mW) was recorded during the heating and cooling cycles. The enthalpy changes, ΔH_m were obtained by normalizing the heat change at the thermal transitions against the polymer mass (g). The melting point, T_m , was defined as the peak temperature of the melting endotherm. Thermogravimetric analysis, TGA, (TA instruments 2050) was carried out under a nitrogen atmosphere from room temperature to 800°C at a heating rate of $10^\circ\text{C min}^{-1}$.

6.3 Results and Discussion

Polymer Synthesis and Characterization

In this series of block copolymers, the hydrophobic block type was varied while maintaining a poly(vinylbenzyl chloride) (PVBC)-based ionic precursor block that was easily converted to benzyltrimethyl quaternary ammonium moieties. The hydrophobic

blocks incorporated hexyl (C_6H_{13}) methacrylate (HMA), lauryl ($C_{12}H_{25}$) methacrylate (LMA), and stearyl ($C_{18}H_{37}$) methacrylate (SMA) monomers. Diblock copolymers based on butenyl styrene and butyl styrene have also been synthesized according to the **Scheme 6.1**.



Scheme 1. Synthesis of quaternary methacrylate and styrene based block copolymers.

These polymers were synthesized using reversible addition-fragmentation chain transfer polymerization (RAFT) with more reactive monomers as the first blocks and quaternized with aqueous trimethylamine solution in the benzyl chloride blocks. The RAFT conditions for styrene-based diblocks and methacrylate-styrene-based systems were optimized to allow easy access to the target diblock structures. The benzyl chloride groups were introduced in one block during the polymerization and quaternization post-polymerization modification was required under mild conditions to minimize the side reactions on the methacrylate moieties.

The monomer 4-butylstyrene was synthesized by Grignard coupling of freshly prepared vinylbenzyl magnesium chloride with 3-bromopropane at 0 °C in moderate yield (45%) instead of Stille cross-coupling of 4-(n-butyl)chlorobenzene with a vinyltin reagent in presence of expensive organometallic catalysts.¹¹ The structural assignment of 4-butylstyrene was based on its NMR spectra as shown in **Figure 6.1**. The disappearance of chloromethyl ($-CH_2Cl$) protons at 4.50 ppm on starting synthon 4-vinylbenzyl chloride along with the appearance of quartet peak at 2.62 ppm ($-PhCH_2-$) are consistent with the formation of 4-butylstyrene while the signals at δ H_b, 6.66 (dd, $J = 18.3, 11.1$ Hz, 1H), H_a (trans), 5.72 (d, $J = 18.3$ Hz, 1H), and H_a(cis), 5.20 (d, $J = 10.5$ Hz, 1H), ppm in the olefinic region in the ¹H NMR correspond to three protons in the vinyl group. In a similar fashion, reaction of 4-vinylbenzyl chloride with allylmagnesium bromide in anhydrous ether gave the 4-(3-butenyl)styrene in 81% yield. The final product was readily purified by vacuum distillation and suitable for RAFT polymerization in our polymerization conditions. The structure of 4-(3-butenyl)styrene monomer was assigned on the basis of

the ^1H NMR spectra data and corresponded to the previous literature.¹² In particular, the signals at δ 2.73 (t, $J = 7.5$ Hz, 2H), 2.39(m, 2H) ppm in the ^1H NMR correspond to the benzyl(-PhCH₂-) and allyl protons (CH₂=CHCH₂-).

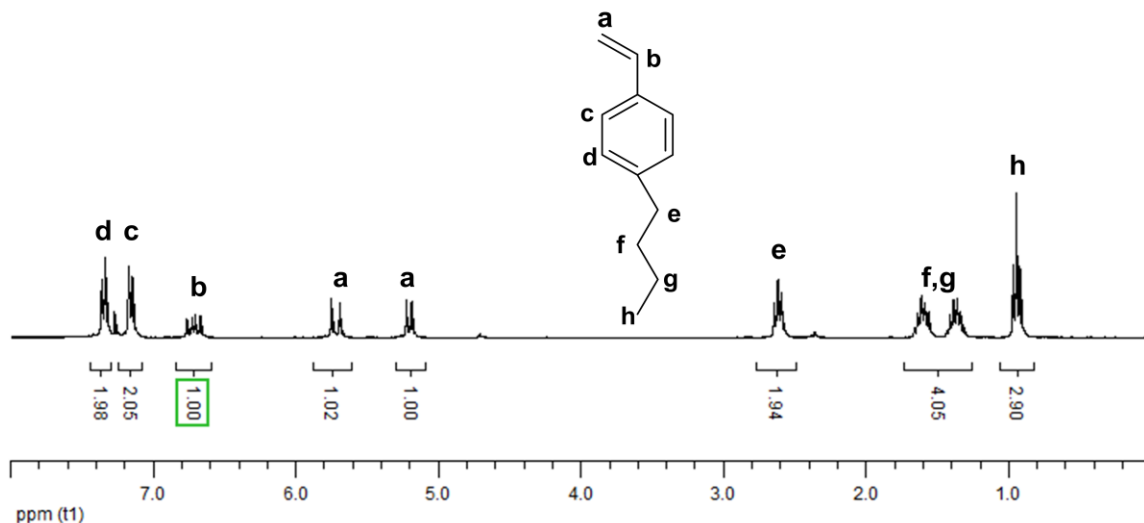


Figure 6.1. ^1H NMR spectra (300 MHz) of 4-butylstyrene.

The poly(methacrylate) based macroinitiators were prepared by RAFT polymerization of methacrylate monomers (HMA, LMA and SMA) using 4-cyano-4[(dodecylsulfanylthiocarbonyl)sulfanyl]pentanoic acid (CDP) as a chain transfer agent (CTA) and 2,2'-azobis(isobutyronitrile) (AIBN) as the thermal initiator at 60°C for 24 h with high conversion and high level control. The poly(vinylbenzyl chloride) macroinitiator was made by a similar strategy with the use of s-dodecyl-s'-(α,α' -dimethyl- α'' -acetic acid)trithiocarbonate(DDMAT) as chain transfer agent (CTA) in bulk. The feed ration of [monomer]:[CTA]:[AIBN] was varied with different monomers to obtain the target molecular weight block copolymers. The different chain transfer agents were

selected to facilitate block copolymers with low molecular weight distribution from various monomers used in this study. The partial polymerization results are summarized in **Table 6.1**.

Table 6.1. Parameters of block copolymers prepared by RAFT polymerization.

	1 st block			diblocks		
	M_n^{NMR}	M_n^{GPC}	M_w/M_n	M_n^{NMR}	M_n^{GPC}	M_w/M_n
PHMA ₆₀ - <i>b</i> -PVBC ₃₄	10.3	10.9	1.13	27.1	19.5	1.12
PLMA ₆₈ - <i>b</i> -PVBC ₆₅	17.3	16.0	1.16	24	21.0	1.19
PSMA ₇₅ - <i>b</i> -PVBC ₇₃	24.7	27.9	1.18	36.2	34.3	1.33
PVBC ₄₄ - <i>b</i> -PBS ₈₄	6.7	6.0	1.12	20.2	15.2	1.20
PVBC ₄₄ - <i>b</i> -PBeS ₈₂	6.7	6.0	1.12	19.7	14.6	1.26

* unit of M_n^{NMR} , M_n^{GPC} : kg mol⁻¹

The number-average molecular weights (M_n^{NMR}) of the macroinitiators were calculated based on the ratio of the integration of ¹H NMR resonances for the methylene protons (-CH₂O-) at 3.90 ppm or the chloromethyl protons (ClCH₂-) at 4.50 ppm on the repeat units to the resonances for the methylene protons (-CH₂S-) at 3.27 ppm on the terminal RAFT agent macroinitiators. GPC data showed low polydispersity indices (PDIs) (< 1.20) and narrow monomodal molecular weight distributions, based on polystyrene standards in THF. After chain extension of the macroinitiator the block copolymer shifted to the high molecular weight portion as depicted in **Figure 6.2**. The characterization implied the RAFT conditions had controlled/living characteristics and the side reactions were minimized albeit the M_n s of all the block copolymers were not in

good agreement with the GPC values due to the calibration based on polystyrene standards. However, the M_n s were close to the theoretical values calculated from the monomer conversions. The methacrylate-based monomers as the first building blocks had much more reactivity than styrene-based monomers, as expected. Oppositely, with poly(vinylbenzyl chloride) macroinitiator as the first block, two narrow monomodal homopolymers poly(hexyl methacrylate) and poly(vinylbenzyl chloride) were generated, as observed by GPC. The low conversion of butylstyrene to poly(butylstyrene) and the broadened molecular weight distribution of poly(4-(3-butenyl)styrene) with increased polymerization time necessitated poly(vinylbenzyl chloride) as the first block. Chain extension of macro CTAs poly(methacrylate) and poly(vinylbenzyl chloride) was performed to prepare the well-defined diblocks using vinylbenzyl chloride (VBC) for methacrylate based macroinitiators, 4-butylstyrene(BS) and 4-(3-butenyl)styrene (BeS) for VBC based macroinitiators as the second building blocks at 70 °C, respectively. The generation of the diblocks was confirmed by molecular weight increase (M_n) in GPC and characteristic peaks in ^1H NMR spectra. The PDIs of the block copolymers were in typical ranges for living/controlled polymerization, depending upon macroinitiators and sequential blocks. However, the molecular weight distribution of poly(vinylbenzyl chloride)-*b*-poly(butylstyrene) was broadened while making high molecular weight poly(butylstyrene) based block copolymers. The average degrees of polymerization of the second blocks were calculated from the ratios of the integration of the resonances of the ester methylene ($-\text{CH}_2\text{OCO}-$) in the side chain of methacrylates at 3.90 ppm or the benzyl protons (PhCH_2-) at 2.50 ppm in the side chain of styrene repeat units to the integration

of chloromethyl protons (ClCH_2 -) at 4.50 ppm attached to the aromatic rings, thus, the total M_n was obtained for the diblocks.

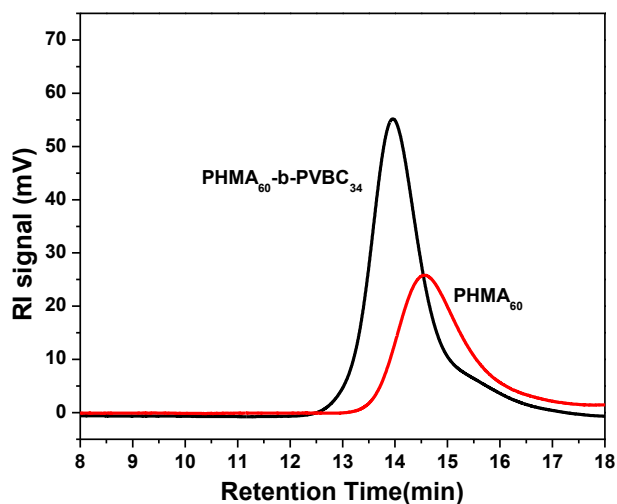


Figure 6.2. GPC chromatograms of a) PHMA₆₀ macroinitiator and b) PHMA₆₀-b-PVBC₃₄

Morphological Characterization

The diblocks were quaternized by 45% aqueous trimethylamine solution in dimethylformamide (DMF) at 50 °C for 24 h and the membranes was cast from toluene and n-propanol (v/v = 1:1) due to their low solubility in DMF. The quaternized copolymers were purified by reduced pressure evaporation, followed by vacuum oven treatment. There was no composition shift of the copolymers after quaternization since the ionic copolymers were not isolated by precipitation. PVBC₄₄-b- BS₈₄ copolymers in salt form was characterized by ¹H NMR as shown in **Figure C.2** in Appendix C. In the quaternized sample PVBC₄₄-b-PBS₈₄, the disappearance of the chloromethyl ($-\text{CH}_2\text{Cl}$)

moiety at 4.50 ppm and the appearance of the quaternized benzylic protons ($-\text{C}_6\text{H}_4\text{CH}_2-$) as a broad resonance at 4.90 ppm confirmed quantitative conversion to the quaternary ammonium group. The integration of the benzylic protons ($-\text{C}_6\text{H}_4\text{CH}_2-$) adjacent to quaternary ammonium group at 4.90 ppm to aromatic proton peaks ($-\text{C}_6\text{H}_4-$) from 6.20 to 7.80 ppm indicated 100% conversion. The measured integration ratio (0.17) was consistent with the theoretical value (0.18). These figures showed 100% quaternization of chloromethyl group by trimethylamine aqueous solution. Based on this information, the IEC was calculated by quaternary ammonium containing copolymer precursors. The quaternized block copolymers were used without further treatment.

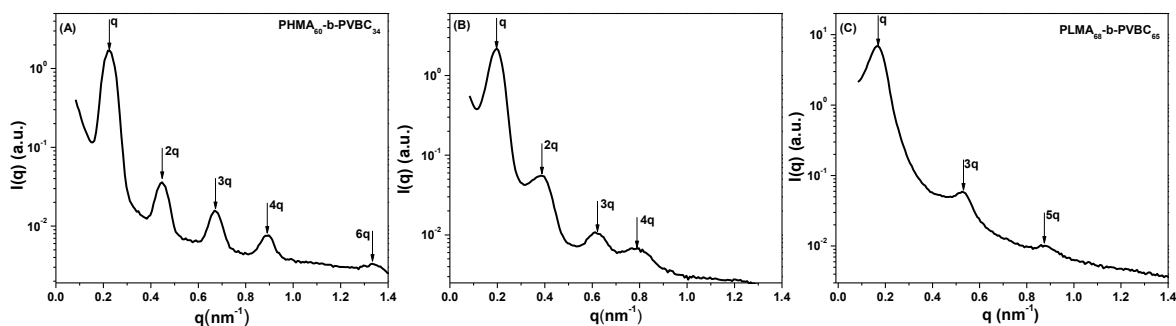


Figure 6.3. Small angle X-ray scattering (SAXS) patterns of (A) $\text{PHMA}_{60}\text{-}b\text{-PVBC}_{34}$; (B) $\text{PVBC}_{44}\text{-}b\text{-PBS}_{84}$; (C) $\text{PLMA}_{68}\text{-}b\text{-PVBC}_{65}$ of quaternized samples.

The membranes cast from quaternized block copolymers in the solvent mixture of toluene and 1-propanol ($v/v = 1:1$) were subjected to SAXS measurements at room temperature to elucidate their morphological features.¹³ The unstained samples were also imaged by transmission electron microscopy (TEM). The scattering pattern of the

PHMA₆₀-*b*-PVBC₃₄ AEM with SAXS reflections at ratios 1:2:3:4:6 in **Figure 6.3A** clearly indicated long-range ordered lamellar morphology from the spacing of the scattering peaks with an interdomain spacing of 27.3 nm, calculated with $d = 2\pi/q$, where q is the principal scattering vector. The predicted lamellar morphology from SAXS was confirmed with TEM studies of the PHMA₆₀-*b*-PVBC₃₄ in **Figure 6.4A**. The ionic block is represented by the darker region while the non-ionic block was the lighter-colored field. **Figure 6.4** showed ordered lamellar regions that are predominant in the sample. Some defects in terms of grain boundaries and micellar regions were visible in the microscopic analysis (**Figure C.4A and C.4B**, Appendix Part), but the SAXS pattern indicated highly long-range lamellar order in this sample. The average interdomain spacing of this sample in TEM was 35.0 nm. However, the scattering pattern of the PLMA₆₈-*b*-PVBC₆₅ AEM with SAXS reflections at ratios 1:3:5 showed the morphology with a low degree of long-range order with an average interdomain spacing of 40.1 nm, probably lamellar or cylindrical morphology. The morphology ultimately was revealed with TEM, showing less ordered cylindrical structure with interdomain spacing (the distance of cylinder center to center) at 42.5 nm. Additionally, PSMA₇₃-*b*-PVBC₇₅ exhibited less disordered morphology in SAXS with reflections at ratios 1:2 with the interdomain spacing of 32.5 nm, indicative of potential lamellar or cylindrical morphology without long-range order. However, the coexistence of lamellar and hexagonally packed cylindrical structures of PSMA₇₃-*b*-PVBC₇₅ sample was demonstrated by TEM image as shown in **Figure C.4C** (Supporting Information). Interdomain spacings of the cylinder and lamellae are 27.5 and 24.0 nm, respectively.

The coexistence of lamellar and cylindrical phases in quaternized PSMA₇₃-*b*-PVBC₇₅ sample was due to the strong segregation strength as observed by Simone et al. in PS-*b*-PEO block copolymers doped with ionic liquid.^{14a} Compared to mechanically robust membranes of PHMA₆₀-*b*-PVBC₃₄, the brittleness of PSMA₇₃-*b*-PVBC₇₅ was likely due to the partial crystallization of PSMA blocks at room temperature by alkyl (C18) side chain packing and orientation during casting as demonstrated below. Furthermore, the potentially crystallizable PSMA blocks in PSMA₇₃-*b*-PVBC₇₅ could have prevented the formation of the well-ordered microstructures.^{14b}

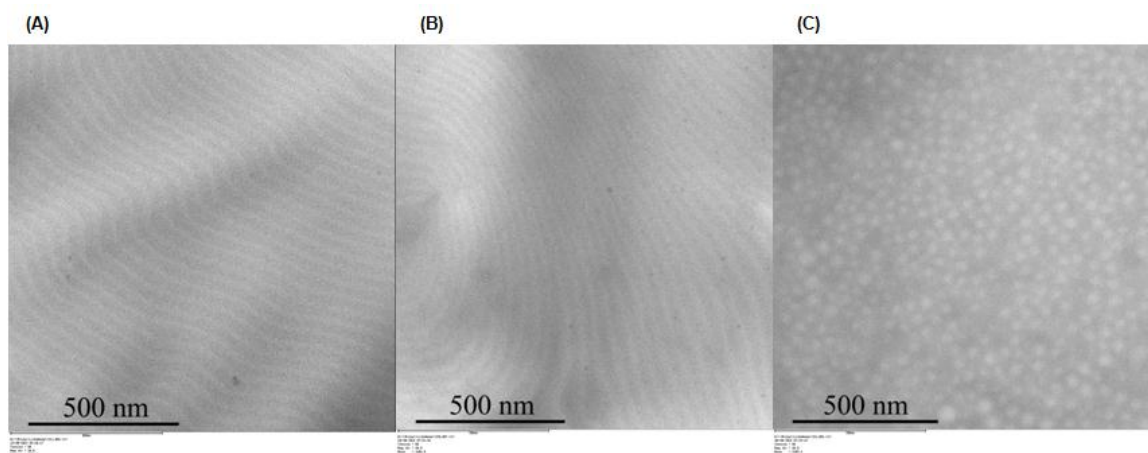


Figure 6.4. TEM micrographs of A) PHMA₆₀-*b*-PVBC₃₄ sample with lamellar morphology; B) PVBC₄₄-*b*-PBS₈₄ sample with lamellar morphology; C) PLMA₆₈-*b*-PVBC₆₅ sample with cylindrical morphology. All samples were unstained.

Both samples (PVBC₄₄-*b*-PBS₈₄ and PVBC₄₄-*b*-PBeS₈₂) of styrene-based diblocks composed of quaternized PVBC that was block with butyl styrene or butenyl styrene of showed long-range ordered lamellar microstructures in SAXS from the scattering peaks

ratios at 1:2:3:4. The domain spacings of the samples from PVBC₄₄-*b*-PBS₈₄ and PVBC₄₄-*b*-PBeS₈₂ were 32.5 and 31.9 nm, respectively. In TEM micrographs, **Figure 6.4B**, the microanalysis of PVBC₄₄-*b*-PBS₈₄ sample showed nearly perfect lamellar structures, which was consistent with the morphology based on SAXS analysis. Quaternized PVBC₄₄-*b*-PBS₈₄ and PVBC₄₄-*b*-PBeS₈₂ samples in TEM images exhibited average interdomain spacings at 31.4 and 34.4 nm, well in agreement with the interdomain spacings from SAXS. The nearly same hydrophobic and hydrophilic block length resulted in the similar interdomain spacings either in SAXS patterns or in TEM micrographs.

In addition to constant ion content, the effect of extending the length of hydrophobic and hydrophilic blocks on the block copolymer morphologies was also explored as listed in **Table C.1** (Supporting Information). The PDIs of the high molecular block copolymers were broader when increasing the second block length. From the GPC graph in **Figure C.3B**, the inactive end of the macroinitiator was also observed, leading to broader PDI. However, the domain spacing increase was not proportional to the increase of the hydrophobic block molecular weight at the same hydrophilic block length. For example, the interdomain spacing of PVBC₄₄-*b*-PBS₁₁₉ sample was 34.1 nm as evidenced by SAXS while the interdomain spacing of the PVBC₄₄-*b*-PBS₄₀₇ sample slightly increased to 35.9 nm as shown in **Figure C.5A** (Supporting Information). These samples exhibited lamellar microstructures as seen from **Figure C.5A**. As ion content of PVBC-*b*-PBS sample decreased to 0.59 meq g⁻¹, it appeared the long-range order was disrupted, which was indicated by the lack of the highly ordered scattering peaks at

higher scattering vectors compared to the sample of PVBC₄₄-*b*-PBS₁₁₉. This reduction in ordered microstructures could be attributed to the reduction of the interaction parameter between ionic and non-ionic domains. However, as the ion content of PLMA-*b*-PVBC increased, the long-range ordered microstructure was induced by the segregation strength of ionic and non-ionic blocks, as indicated by the SAXS data in **Figure C.5B**. The sample of PLMA₆₈-*b*-PVBC₆₅ with domain spacing 40.1 nm showed less ordered cylindrical morphology as described above while PLMA₆₈-*b*-PVBC₁₂₈ sample with domain spacing 49.4 nm exhibited a superiorly ordered nanophase separation with SAXS reflections at ratios 1:2:3:4:6 in **Figure 6.5B**. The change from less ordered to highly ordered microstructures corresponded to the hydrophilic block molecular weight increases. The domain spacing from 40.1 nm to 49.4 nm increased with the increase in ion contents from 2.09 to 2.88 meq g⁻¹. These results were consistent with the previous findings.¹⁵ The occurrence of domain spacing increase partially may be due to the increase in interaction parameter χ between the hydrophobic and hydrophilic blocks by the introduction of more ionic groups, leading to chain stretching. Interestingly, the sample of PLMA₆₈-*b*-PVBC₇₄ exhibited reflections at ratios of 1:3:5:7 with structure factor extinctions of 2q, 4q, 6q, suggesting a lamellar morphology with equal volume fraction of hydrophobic and hydrophilic blocks.

Water Uptake Behavior

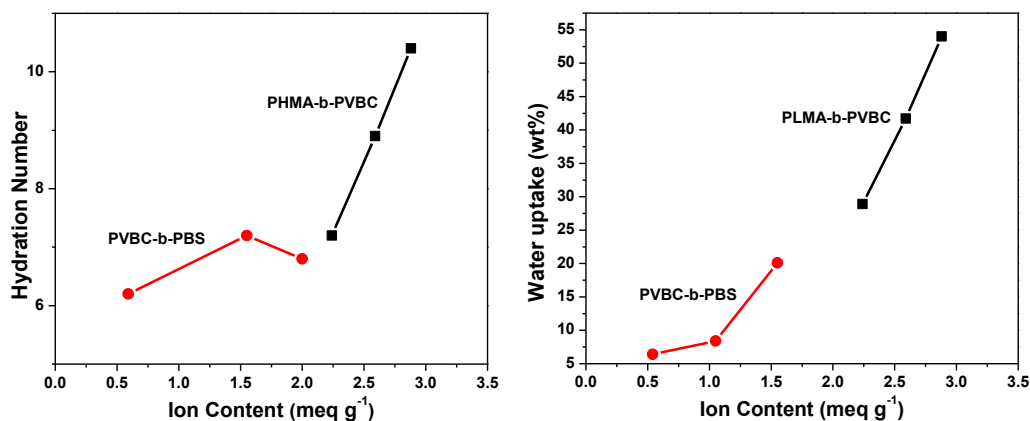


Figure 6.5. Hydration Number (λ) and water uptake (wt%) as a function of ion content at 30 °C under 95% relative humidity, PVBC-*b*-PBS (●) and PLMA-*b*-PVBC (■).

At similar quaternary ammonium content ($\text{IEC} = \sim 2.0 \pm 0.2$), the samples of PSMA, PLMA and PHMA absorbed ~ 7.0 water molecules per quaternary ammonium group regardless of lamellar or cylindrical microstructures. The difference of hydrophobic blocks in the membranes did not lead to enhanced water uptake. However, for PLMA-*b*-PVBC samples, when the IEC increased from 2.09 to 2.88 meq g^{-1} , the hydration number slightly increased from 7.2 to 10.4 water molecules per quaternary ammonium moiety. When the ion exchange capacity of PVBC-*b*-PBS samples decreased from 1.55 to 0.59 meq g^{-1} , the hydration number decreased slightly from 7.2 to 6.2 water molecules per quaternary ammonium group, but almost remained at ~ 7.0 water molecules per ammonium cation. The materials in this study showed low water absorption compared to quaternized chloromethylated multiblock poly(arylene ether sulfone) ($\text{IEC} = 1.44 \text{ meq g}^{-1}$, $\lambda = 32.2$). The low water absorption could be due to the hydrophobic blocks in these block copolymers compared to quaternized chloromethylated poly(arylene ether sulfone)^{16,17}

As expected, the hydration number in liquid water was higher than under 95% relative humidity. Both the PVBC₄₄-*b*-PBS₂₀₂ and PVBC₄₄-*b*-PBS₄₄₇ samples were mechanically robust in liquid water, which offered the opportunity for measuring the liquid water uptake. For example, the water absorption ($w_u = 20.0$ wt %, $\lambda = 10.5$) of PVBC₄₄-*b*-PBS₂₀₂ based AEM in liquid water was higher than in 95% relative humidity ($w_u = 8.4$ wt%, $\lambda = 4.4$). This result was in agreement with the previous literature reports.¹⁸ The low water absorption from the vapor phase could be due to the insufficient time to reach the equilibrium state for water uptake. Another possible explanation lied in the difference of water absorption kinetic from liquid water and vapor phase in which the water activity was low.

Thermal Behavior and Semicrystallinity of AEMs

We posit that the long-chain methacrylate hydrophobic block that contains some fraction of crystallinity in the block copolymer would constrain the swelling in liquid water. As demonstrated, the PSM₇₅-*b*-PVBC₇₃ membrane maintained its mechanical integrity in liquid water while the samples with shorter side chains such as PHMA₆₀-*b*-PVBC₃₄, PLMA₆₈-*b*-PVBC₆₅ and PVBC₄₄-*b*-PBS₈₄ were highly swollen under the same conditions. Quaternized PSM₇₅-*b*-PVBC₇₃ membrane with C18 side chains was high-modulus and wax-like in physical appearance, which indicated side chain crystallization. The hexyl (C6) and lauryl (C12) methacrylate side chains on the hydrophobic blocks were below the critical side chain length (>C12) for crystallization on methacrylate polymer backbones.¹¹

The quaternized PHMA₆₀-*b*-PVBC₃₄, PLMA₆₈-*b*-PVBC₆₅ and PVBC₄₄-*b*-PBS₈₄ were thermally stable to 220 °C while quaternized PSM₇₅-*b*-PVBC₇₃ began to degrade at 200 °C. The samples exhibited a two-step degradation process: ionic moiety degradation at 220 °C and second degradation event at 350 °C as shown by the TGA data in **Figure C.7** (see Supporting Information). The methacrylate samples decomposed in nitrogen quantitatively, but 5 wt% of char remained at 700 °C. The remaining char was formed due to the crosslinked structure by decarboxylation. However, PVBC₄₄-*b*-PBS₈₄ sample degraded completely above 800 °C in the absence of carboxyl groups. Based on the thermal degradation data, in the crystalline studies, the samples were heated to 180 °C to avoid degradation.

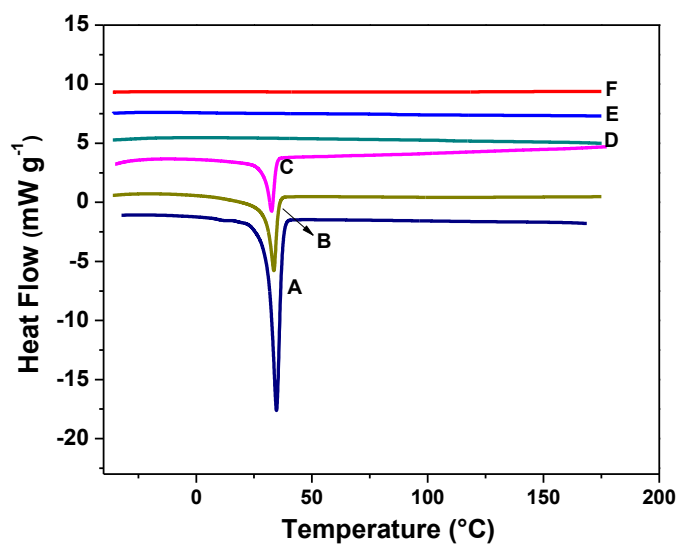


Figure 6.6. DSC thermograms of block copolymers with different side chains during the second heating scan. A: PSMA₇₅, B: PSMA₇₅-*b*-PVBC₇₃, C: quaternized PSMA₇₅-*b*-

PVBC₇₃, D: quaternized PLMA₆₈-*b*-PVBC₆₅, E: quaternized PHMA₆₀-*b*-PVBC₃₄, F: quaternized PVBC₄₄-*b*-PBS₈₄.

The quaternized PSM₇₅-*b*-PVBC₇₃ sample showed a single relatively sharp melting peak at $\sim 31^{\circ}\text{C}$ as displayed in **Figure 6.6**, sample b, indicative of the crystallinity of the block copolymer from crystallization of the C18 side chains. The melting temperature corresponded to the reported value for PSMA copolymer.¹¹ The crystallinity was calculated from the melting enthalpy of block copolymers relative to pure PSM₇₅ homopolymer synthesized by RAFT polymerization. The melting enthalpy of pure PSMA was 88.15 J g^{-1} , which is greater than the sample (62.8 J g^{-1}) prepared from conventional radical polymerization. The hydrophobic parts of quaternized and non-quaternized samples showed the enthalpy of 45.0 and 55.13 J g^{-1} , respectively. The semicrystallinity of quaternized and non-quaternized PSM₇₅-*b*-PVBC₇₃ samples was 51.0% and 62.5% , suggesting the quaternization did reduce the crystallization of the block copolymers. However, no detectable thermal transition was observed for PHMA₆₀-*b*-PVBC₃₄ sample due to the shorter side chain alkyl carbons (C6). The apparent melting peak was not found for PLMA₆₈-*b*-PVBC₆₅ in the second heating scan of DSC measurement in contrast to the crystalline ability as observed in previous report.¹² This semi crystalline behavior could be attributed to the lower molar fraction of PLMA block in the block copolymers. The semicrystalline PSM block with comb-like paraffinic side chains formed a double layer arrangement due to bulky methyl moiety on the methacrylate main chain as proposed in previous research. The membrane was stable in liquid water due to the crystallization of longer alkyl (C18) side chain. This result

provided an avenue to fabricate mechanically robust block copolymer based membranes against liquid water by crystallizable side chain introduction on the hydrophobic blocks of the block copolymers. Furthermore, delicate manipulation of semicrystalline blocks would afford to obtain highly conductive and low water uptake membranes, increasing chemical resistance and thermal stability.⁶

Ion Transport of AEMs

Controlling ion-containing membrane morphology can translate to tunable ion conductivity in these materials. So it is crucial to reveal the relationship between polymer microstructures and ionic conductivity in AEMs. The conductivity of all samples in chloride (Cl^-) form was measured at 30 °C as a function of relative humidity (RH) from 20% to 95% using AC impedance spectroscopy. The ionic conductivity increased with the increase in relative humidity, **Figure 6.7**. Below 50% RH, the ionic conductivity was substantially reduced due to in the absence of sufficient water in the hydrophilic domains for ion conduction above which the ion activity was increased, leading to increased ionic conductivity.

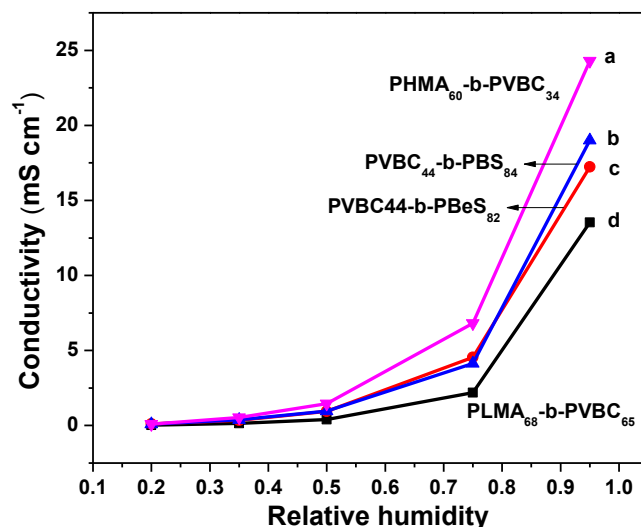


Figure 6.7. Conductivity dependence of relative humidity of a) PHMA₆₀-b-PVBC₃₄; b) PVBC₄₄-b-PBS₈₄; c) PVBC₄₄-b-PBeS₈₂; d) PLMA₆₈-b-PVBC₆₅ at 30 °C from 20 to 95% relative humidity in chloride (Cl⁻) form.

At 30 °C under 95% RH, the conductivity of PHMA₆₀-b-PVBC₃₄ sample had a conductivity of 24.30 mS cm⁻¹, which was the highest among the samples while PLMA₆₈-b-PVBC₆₅ sample had lower ionic conductivity (13.5 mS cm⁻¹). The lower conductivity of PLMA₆₈-b-PVBC₆₅ copolymers than PHMA₆₀-b-PVBC₃₄ was due to the microstructure differences and the lack of a long-range ordered morphology as shown in the SAXS data in **Figure 6.3** and TEM in **Figure 6.4**. Compared to the sample of PHMA₆₀-b-PVBC₃₄, the styrene-based block copolymers (PVBC₄₄-b-PBS₈₄ and PVBC₄₄-b-PBeS₈₂) exhibited slightly lower ionic conductivity (19.0 and 17.2 mS cm⁻¹) at 30 °C under 95% RH. The greater conductivity of PHMA₆₀-b-PVBC₃₄ sample can be attributed to the higher degree of self-assembly than styrene based samples as given in the SAXS profiles in **Figure 6.3**, which can increase the ionic conductivity of the membrane.

The effect of increased interdomain spacing on ionic conductivity was examined for samples with the same ionic content. The PVBC₁₀₀-*b*-PBeS₁₈₃ sample (with an interdomain spacing of 49.1 nm and a conductivity of 18.3 mS cm⁻¹ showed comparable conductivity to that of PVBC₄₄-*b*-PBeS₈₂ with a domain spacing of 31.9 nm and a conductivity of 20.2 mS cm⁻¹. Segalman and coworkers observed that the ionic conductivity was increased with an increasing size of the conducting domains in poly(styrene-block-histamine methacrylamide) diblock copolymers-based materials. The ionic conductivity mainly relied on chain motion of the ionic blocks instead of water – mediated conductivity.¹³ The reduction in the interdomain size lead to an increase in block copolymer interfaces and an increase in the interfacial width, resulting in a conductivity decrease. However, in the case of this study, the change of the interdomain size did not greatly influence the ionic conductivity since the water in the ionic blocks is responsible for the ionic transport due to the dominance of water-assisted mechanism.¹⁷ The slightly lower ion conductivity of PVBC₁₀₀-*b*-PBeS₁₈₃ (hydration number, $\lambda = 9.2$) could be due to ion dilution by higher water absorption than the sample PVBC₄₄-*b*-PBeS₈₂ (hydration number, $\lambda = 6.9$). But generally, the chloride conductivity increased with the increasing IEC with the aid of more water absorption. The sample of PVBC₁₀₀-*b*-PBeS₁₀₇ gave the higher ionic conductivity (IEC = 2.62 meq g⁻¹, 26.2 mS cm⁻¹) compared to PVBC₁₀₀-*b*-PBeS₁₈₃ based membrane (IEC = 2.00 meq g⁻¹, 18.3 mS cm⁻¹) due to the increase in IEC.

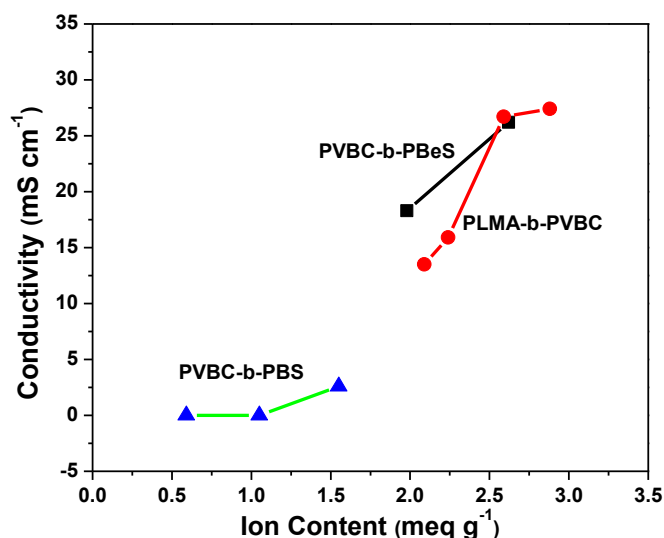


Figure 6.8. Conductivity dependence of ion contents, PVBC-*b*-PBS (▲), PLMA-*b*-PVBC (●) and PVBC-*b*-PBeS (■) in chloride (Cl⁻) form.

The percolation threshold is defined as the critical ion content to maintain the ion conductivity between conducting domains above which ions can fully permeate the membranes. The percolation threshold of the PVBC-*b*-PBS based AEMs was determined with low ion content samples. The PVBC-*b*-PBS samples have a percolation threshold based on quaternary ammonium fraction (~18 mol %), corresponding to IEC = 1.05 meq g⁻¹. The conductivity of PVBC-*b*-PBS non-linearly increased with increasing quaternary ammonium moieties, **Figure 6.8**. PVBC-*b*-PBS chloride conductivity increased from 0.3 to 2.6 mS cm⁻¹ over the range of 1.05 to 1.55 meq g⁻¹ at 30 °C under 95% RH. These results corresponded to the previous reports in the literature regarding the percolation threshold of the sulfonated poly(styrene)-*b*-poly(isobutylene)-*b*-poly(styrene) at similar

IECs where the percolation threshold was about 15 mol%.⁷ These data indicated the ion content fraction increase led to the sharp change in ionic conductivity. Interestingly, both of PVBC₄₄-*b*-PBS₂₀₂ and PVBC₄₄-*b*-PBS₄₄₇ samples were mechanically robust in liquid water due to low water absorption. Moreover, PVBC₄₄-*b*-PBS₂₀₂ sample (hydration number, $\lambda = 10.5$) in liquid water at 20 °C showed the same chloride conductivity (0.3 mS cm⁻¹) as the membrane under 95% relative humidity condition at 30 °C (hydration number, $\lambda = 4.4$). This trend also was demonstrated by the sample of PVBC₄₄-*b*-PBS₄₄₇, which displayed 0.2 mS cm⁻¹ in liquid water at 20 °C and under 95% relative humidity at 30 °C. In this case, the higher temperature (30 °C vs 20 °C) offset the lower water absorption (hydration number, $\lambda = 4.4$ vs 10.5) under humidified condition because the activity of the ions in the membranes is faster at higher temperature.

For PLMA-*b*-PVBC samples, the conductivity showed a significant increase from 15.9 to 27.4 mS cm⁻¹ (95 % RH, 30 °C) over an IEC range of 2.24 to 2.88 meq g⁻¹ due to their long-range ordered lamellar micro-structures, **Figure 6.6**. The increase in hydration number per quaternary ammonium group from 7.2 to 10.4 also facilitated the ion conductivity. However, both samples of PVBC₁₀₀-*b*-PBeS₁₀₇ and PLMA₆₈-*b*-PVBC₁₂₉ exhibited comparably high ion conductivity (26.2 and 27.4 mS cm⁻¹) due to their long-range ordered microstructures in **Figure C.5B**. The high conductivity was probably also due to the dimensional stability of the polymer membranes when exposed to 95% relative humidity, thus maintaining ordered microstructures under highly humidified conditions as reported in the study investigated by Ye, et al.^{18a,19,20} Sunder, et al. reported poly(styrene)-based block copolymer samples with tethered quaternary ammonium

cations. The sample of SAM (27-21) had a Cl^- conductivity of $\sim 4 \text{ mS cm}^{-1}$ at 25°C under an IEC of $\sim 2.50 \text{ meq g}^{-1}$.²¹ Ion clustered poly(arylene ether ketone) with benzyltrimethylammonium groups showed a bromide conductivity of $\sim 7 \text{ mS cm}^{-1}$ under an IEC of $\sim 2.55 \text{ meq g}^{-1}$ at 25°C .²² Compared to poly(arylene ether ketone) and poly(styrene) based AEMs, the PVBC_{100} -*b*- PBeS_{107} and PLMA_{68} -*b*- PVBC_{129} based AEMs with soft hydrophobic blocks are superior given the higher ionic conductivity (26.2 and 27.4 mS cm^{-1}) due to the long-range ordered microstructures under tunable high IECs.

6.4 Conclusions

This work elaborated block copolymer based AEMs with various hydrophobic blocks that showed high ionic conductivity (27.4 mS cm^{-1} , $\text{IEC} = 2.88 \text{ meq g}^{-1}$) in chloride form with highly ordered microstructures at low water absorption ($\lambda = \sim 6$ -10). The well-defined block copolymer based AEMs allowed the manipulation of morphological effects on ionic conductivity. High conductivity was attained by the increase in the ionic moieties of AEMs with long-range ordered microstructures as demonstrated in this study. An interdomain size increase did not significantly affect the ionic transport as the transport was through water assisted ionic phase and the phases were not small enough to influence the dynamics of water in these materials. This water-assisted effect was in contrast to ion transport dictated by polymer chain segmental motion which is dependent on the interdomain spacing. Below a critical ion exchange capacity of 1.05 meq g^{-1} , the ionic conductivity was remarkably reduced. The higher ion contents exponentially increased the ionic conductivity above the percolation threshold.

The styrene-based block copolymers showed comparable ionic conductivity to methacrylate based block copolymers with benzyltrimethylammonium moieties. The introduction of crystalline blocks restricted the liquid water swelling and maintained the mechanical integrity of AEMs. This concept is able to be used in preparation of mechanically robust block copolymer membranes through delicate manipulation of hydrophobic and hydrophilic blocks. The anion-containing block copolymer described herein provided guidelines for the design of water-transporting ion-conducting membranes.

6.5 References

1. Hickner, M.A. *Mater. Today***2010**, *13*, 34-41.
2. Elab, Y.A.; Hickner, M.A. *Macromolecules* **2011**, *44*, 1-11.
3. Varcoe, J.R.; Slade, R.C.T. *Fuel Cells***2005**, *5*, 187-200.
4. Pan, J.; Chen, C.; Zhuang, L.; Lu, J. *Acc. Chem. Res.***2012**, *45*, 473-481.
5. Elabd, Y.A.; Napadensky, E.; Walker, C.W.; Winey, K.I. *Macromolecules***2006**, *39*, 399-407.
6. a) Park, M.J.; Balsara, N.P. *Macromolecules***2008**, *41*, 3678-3687; Knychala, P.; Dziecielski, M.; Balsara, N.P. *Macromolecules***2013**, *46*, 5724-5730. b) Uehara, H.; Kakiage, M.; Sekiya, M.; Yamagishi, T.; Yamanobe, T.; Nakajima, K.; Watanabe, T.; Nomura, K.; Hase, K.; Matsuda, M. *Macromolecules***2009**, *42*, 7627-7630.
7. Tanaka, M.; Fukasawa, K.; Nishino, E.; Yamaguchi, S.; Yamada, K.; Tanaka, H.; Bae, B.; Miyatake, K.; Watanabe, M. *J. Am. Chem. Soc.***2011**, *133*, 10646-10654.
8. Zhao, Z.; Wang, J.H.; Li, S.H.; Zhang, S.B. *J. Power Sources***2011**, *196*, 4445-4450.
9. Tsai, T.H.; Versek, C.; Thorn, M.; Tuominen, M.; Coughlin, E.B. Chpt 15, ACS Symposium Series; Washington, DC, 2012.

10. Couture, G.; Alaaedine, A.; Boschet, F.; Ameduri, B. *Prog. Polym. Sci.***2011**, *36*, 1521-1557.
11. a) Wang, L.Z.; Hickner, M.A. *Polymer Chemistry*, 2014, DOI: 10.1039/C3PY01490H
b) Shang, S.R.; Huang, S.; Weiss, R.A. *Polymer*, **2009**, *50*, 3119-3127.
12. Xu, Y.; Becker, H.; Yuan, J.; Burkhardt, M.; Zhang, Y.; Walther, A.; Bolisetty, S.; Balauff, M.; Muller, H.E. *Macromol. Chem. Phys.***2007**, *208*, 1666–1675.
13. Littke, A.F.; Schwarz, L.; Fu, G.C. *J. Am. Chem. Soc.***2002**, *124*, 6343-6348.
14. Zhang, H.M.; Ruckenstein, E. *Macromolecules***1999**, *32*, 5495-5500.
15. Leibler, L. *Macromolecules***1980**, *16*, 1602-1617.
16. a) Simone, P.M.; Lodge, T.P. *ACS Appl. Mater. Interfaces***2009**, *1*, 2812-2820. b) Kariagata, K.; Toyama, R. *J. Appl. Polym. Sci.***1974**, *18*, 167-178.
17. Schneider, Y.; Modestino, M.A.; McCulloch, B.L.; Hoarfrost, M.L.; Hess, R.W.; Segalman, R.A. *Macromolecules***2013**, *46*, 1543-1548.
18. a) Ye, Y.; Sharick, S.; Eric M. Davis, E.M.; Winey, K.I.; Elabd, Y.A. *ACS Macro Lett.***2013**, *2*, 575–580; b) Zawodzinski, T.A.; Derouin, C.; Radzinski, S.; Sherman, R.J.; Smith, V.T.; Springer, T.E.; Gottesfeld, S. *J. Electrochem. Soc.*, **1993**, *140*(4), 1041-1047. c) K.D. Kreuer, *Solid State Ionics*, 2013, **252**, 93.
19. Moore, H.D.; Saito, T.; Hickner, M.A. *J. Mater. Chem.***2010**, *20*, 6316-6321.
20. Zawodzinski, T.A.; Derouin, C.; Radzinski, S.; Sherman, R.J.; Smith, V.T.; Springer, T.E.; Gottesfeld, S. *J. Electrochem. Soc.* **1993**, *140*, 1041-1047.
21. Sudre, G.; Inceoglu, S.; Cotanda, P.; Balsara, N. P. *Macromolecules***2013**, *46*, 1519–1527.
22. Chen, D.; Hickner, M.A. *Macromolecules***2013**, *46*, in press.

Chapter 7

Synthesis and Characterization of Polymeric Sulfonimides for Proton Exchange Membranes

7.1 Introduction

Proton exchange membranes (PEMs) have been attractive materials for decades in fuel cells as efficient portable, stationary and transportation power supplies. Herein, PEMs are the key component in electrochemical energy conversion devices in which the PEMs must have chemical, mechanical, thermal and good proton conductivity. Among the most extensively studied sulfonated PEMs, Nafion[®] serves the benchmark for the development of PEMs for fuel cells due to its commercial availability and advantageous merits in practical fuel cells. However, high cost, environmental concerns of fluoropolymers, and high methanol crossover of Nafion[®] has lead researchers to explore the alternative polymeric electrolyte membranes with sulfonic acid motifs. Aromatic hydrocarbon polymers such as sulfonated aromatic poly(arylene ether sulfone)s are one of the possible candidates for PEMs in fuel cells. The polymer backbone is thermally and mechanically stable, resistant to oxidation, not labile to acid hydrolysis while sulfonated aromatic poly(arylene ether sulfone)s maintain high ionic conductivity and low methanol crossover.^{1,2,3}

Sulfonimide containing PEMs were considered one of the promising alternatives to sulfonated PEMs due to their long-term high thermal stability and high proton conductivity. Moreover, the sulfonimide acid showed higher acid strength than

trifluorosulfonic acid as documented in previous research.⁴ In particular, the benzene sulfonimide was reported to generate a strong aqueous acid. The properties of sulfonimide group make it an excellent candidate in PEMs for fuel cells and other applications such as water treatment and gas separation. DesMarteau and co-workers prepared perfluorinated polymeric membranes with sulfonimide groups.⁵ They also reported the synthesis of perfluorocyclobutane aromatic polyethers by thermal [2+2] cyclopolymerization from trifluorovinyl aromatic ether monomers bearing sulfonimide groups. Feiring, et al. described the synthesis of poly(styrene) based copolymers with pendent sulfonimide groups for polymer electrolyte for lithium battery by sulfonimide styrene monomers.^{6,7} Sulfonimide containing phosphazene copolymers were prepared through multiple steps polymerization modification as reported by Hofmann, et al.⁸ Recently, McGrath and coworkers synthesized sulfonimide poly(arylene ether sulfone) via pre-polymerization modification.⁹ However, most of sulfonimide functionalization has been concentrated on the direct copolymerization of sulfonimide containing monomers. The sulfonimide containing monomers was highly expensive in terms of the cost during the synthesis, making sulfonimide based PEMs scaleup infeasible, particularly at industrial scales. For the preparation of sulfonimide containing copolymers, post-polymerization modification offers the inexpensive complementary synthetic route to direct polymerization.

This paper will describe the synthesis of sulfonimide containing copolymers with different polymer backbone via post-polymerization modification. The copolymers will

be characterized by various methods and the corresponding properties will be measured and compared with conventional sulfonated aromatic polymers.

7.2 Experimental Section

Materials All reagents and solvents were reagent-grade and used as received without purification. Poly(2,6-dimethyl-1,4-phenylene oxide) (PPO) with the average molecular weight of 20,000 g/mol and PDI of 1.50 and Poly(styrene) (PS) with the average molecular weight of 35,000 g/mol were obtained from Sigma Aldrich. Radel NT 5500 was donated from Solvay Advanced Polymer (Alphareta, GA). Trifluoromethanesulfonamide was received from TCI and used as received.

Synthesis of Radel, PPO and PS sulfonimides Sulfonated Radel PPO and PS (denoted as S-Radel, S-PPO and S-PS) with different ion exchange capacities were synthesized using a post-sulfonation **Scheme 7.1** according to previous report.^{10,11,12} A typical procedure for preparation of polymeric sulfonimide was described below with Radel sulfonimide as an example.

To a stirring mixture of S-Radel in anhydrous DMF (20 mL), was added dropwise thionyl chloride (4.4 mL, 0.060mol) at ambient temperature. The mixture was then heated to 60 °C and stirred for 24 h. Radel sulfonyl chloride was precipitated in ice water (150 mL). The product was collected by filtration, washed with ice-cooled water and dried in vacuum.

Radel sulfonyl chloride (1 g) and trifluoromethanesulfonamide (TFMS) (0.8 g) in DMF (10 mL) were added triethylamine (1.4 mL) was added dropwise at room temperature. The reaction mixture was stirred for 24 h at room temperature under an inert atmosphere. After completion of the reaction, DMF was evaporated under vacuum.

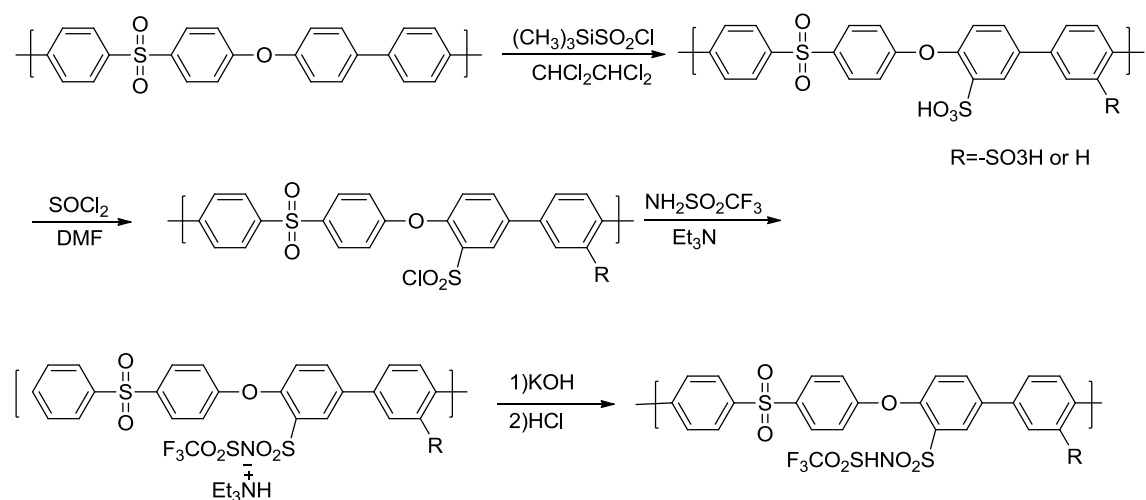
Radel sulfonimide triethylamine salt was thoroughly washed with water to remove unreacted trifluoromethanesulfonamide, dried *in vacuo* at 50 °C for 24 h. The triethylamine salt form copolymer was cast into thin membrane from a 7% (w/v) solution in DMF onto a clean glass plate and dried in a casting chamber. The triethylamine salt form membrane was then transformed into the sodium form by immersion in 1M NaOH for 24 h to convert the sulfonimide triethylamine salt to sodium form. The residual sodium hydroxide was removed by rinsing with water.

The sodium salt form membrane was converted into the acid form by the boiling of the films in 1M H₂SO₄ for 2 h to convert the pendant sulfonimide sodium salt into free acid. The residual sulfuric acid was removed by immersion in deionized water for 24 h. The membrane were then rinsed with deionized water and stored in deionized water.

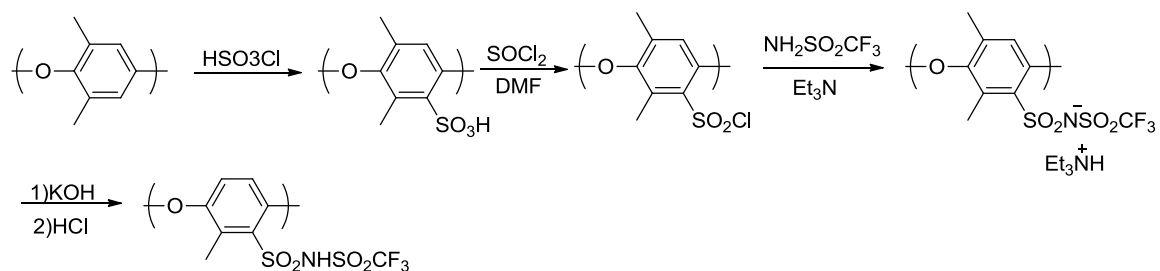
7.3. Results and Discussion

7.3.1 Synthesis of Sulfonimide Containing Polymers

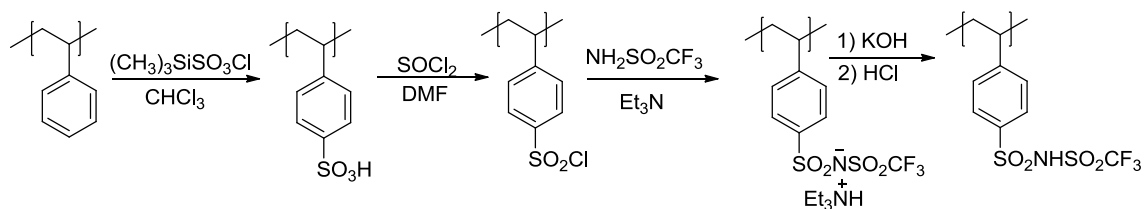
Synthesis of Radel Sulfonimide



Synthesis of PPO Sulfonimide



Synthesis of PS Sulfonimide



Scheme 7.1. Synthesis of Radel, PPO and PS based sulfonimides.

The synthesis of sulfonimide based poly(phosphazene) and poly(arylene ether sulfone) (PAES) has been examined from direct copolymerization of sulfonimide-containing comonomers as reported by Hofmann, et al. and Cho, et al., respectively.^{8,9} However, the synthetic strategies of sulfonimide-containing copolymers did not provide the universally synthetic routes and limit the taylorability for polymers with different backbone topologies. Synthetic routes for sulfonimide-containing copolymers were proposed in **Scheme 7.1** via controllable post-polymerization modification under mild conditions.

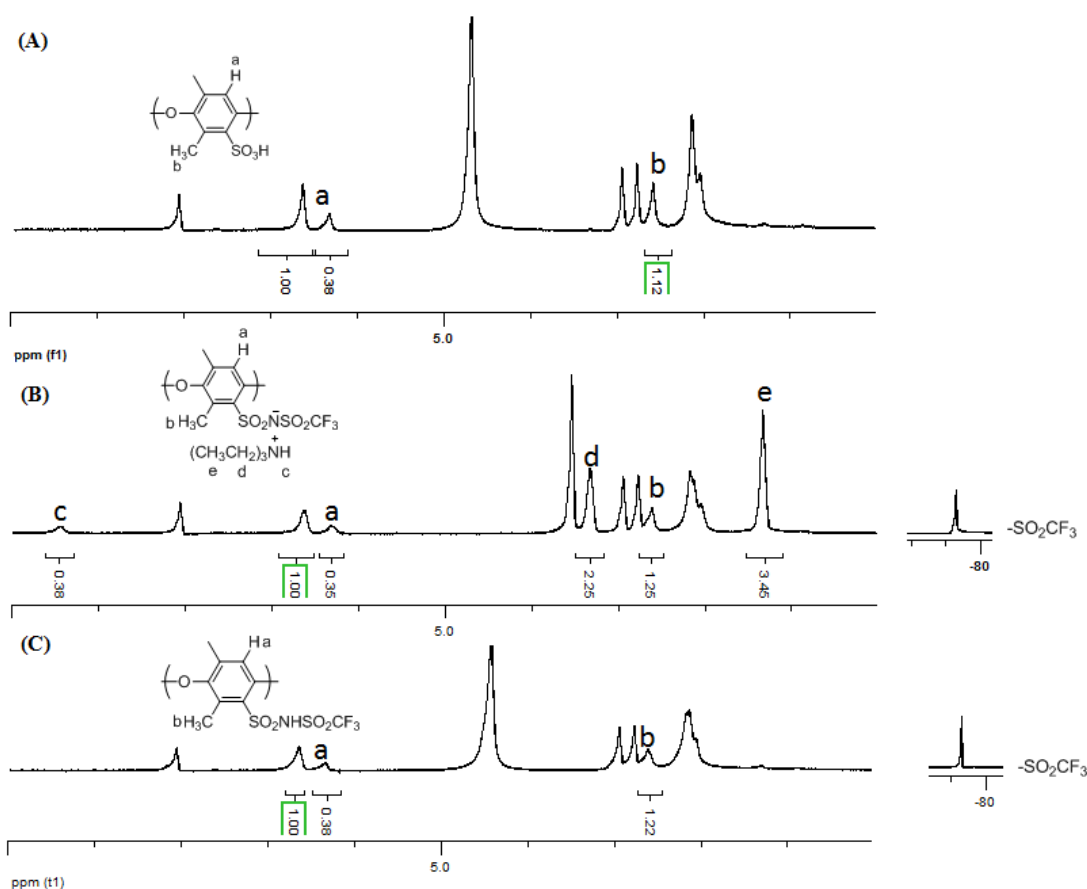


Figure 7.1. ¹H and ¹⁹F NMR of sulfonated PPO, functionalized PPO sulfonimide and PPO sulfonimide.

The incorporation of sulfonic acid moieties was performed using different sulfonic agents under mild conditions. Commercially available Radel[®] and poly(styrene) was sulfonated with trimethylsilylchlorosulfonate (TMCS) in tetrachloroethane and chloroform via mild sulfonation agents respectively while PPO with controllable sulfonation degree was subjected to sulfonation by chlorosulfonic acid. The sulfonation degree was controlled by the reaction temperature, reaction time and the ratio of sulfonation agents to polymer repeat units and limited by the low solubility of sulfonated polymers in chlorinated solvents. For example, the PPO sulfonation barely exceeded 40% in chloroform.¹³ S-PPO became soluble in dipolar aprotic solvents such as DMF after sulfonation.

The sulfonation degree of the generated polymers was determined by the characteristic peaks in ¹H NMR spectra and leveraged to calculate the ion exchange capacity (IEC) of the polymers. As seen in **Figure 7.1A**, the proton signals H_a and H_b in the sulfonated PPO (S-PPO) corresponded to the aromatic and methyl protons of the sulfonated moieties. Consequently, the intensity of signals H_a and H_b decreased with the IEC. The IEC values were calculated by sulfonated and un-sulfonated units in the generated polymers using the integral of signal H_a and aromatic protons in un-sulfonated units. The IEC of sulfonated Radel was also estimated in a similar fashion. The efficient conversion of sulfonate groups to chlorosulfonyl groups was carried out by thionyl chloride (SOCl₂) in DMF without affecting other functionalities in which DMF was used as catalyst and solvents at 60 °C. Reaction of SOCl₂ with DMF afforded the well-known Vilsmeier-Hacck reagent, resulting in quantitative formation of sulfonyl chloride motifs

from sulfonic acid attached on different polymer backbones. The polymers tethered with sulfonyl chloride were recovered from the crushed ice due to its stability at 0 °C. However, the sulfonyl chloride containing polymers were prone to be crosslinked upon heating depending on the electron density of un-sulfonated units.

The polymers containing sulfonyl chloride motifs were treated with excess trifluoromethanesulfonamide (TFMS) in the presence of triethylamine to generate the sulfonamide-containing polymers with triethylamine counterions. The formation of sulfonimide groups was quantitative compared to the sulfonation degree of the precursor polymers as determined on the basis of characteristic peaks from ^1H NMR spectroscopy in **Figure 7.1B**. The ratio of aromatic proton H_a at 6.27 ppm, to methyl protons H_b on the sulfonated units at 2.60 ppm, H_c at 9.44 ppm, H_d and H_e at 3.30 and 1.35 ppm, respectively, was approximately maintained at 1:3:1:6:9, indicating the 100% conversion to sulfonimide polymer with triethylamine moieties. The counter-cation of the sulfonimide anion on the polymers exchanged to sodium form from quaternary triethylammonium in excess 1M aqueous NaOH. The sulfonamide moieties with sodium counter-ions on the polymers were converted to acid form by boiling the polymers in 1M H_2SO_4 for 8 h. Further purification was accomplished by immersion of the cast membranes in DI water and drying *in vacuo*. The disappearance of the characteristic peaks H_d and H_e at 3.30 and 1.35 ppm along with the presence a broad single peak at -78.4 ppm in the ^{19}F NMR spectrum indicated the successful formation of the sulfonimides, **Figure 7.1C**. The in-depth analysis of Radel and PS sulfonimides was in

agreement with the results observed in the synthesis of PPO sulfonimides. The material parameters of the polymeric sulfonimides and key properties are presented in **Table 7.1**.

Table 7.1. Properties of sulfonated and sulfonimide samples.

Samples	IEC (meq g^{-1})	WU (wt %)	Conductivity (mS cm^{-1})	E_a (kJ mol^{-1})	Hydration Number (λ)
SI-Radel-1	1.14	20.9	12.4	10.80	10.1
SI-Radel-2	1.79	57.7	57.2	9.14	33.9
S-Radel-1	1.34	74.0	47.6	10.81	30.0
S-Radel-2	2.20	134.3	74.2	7.48	17.8
SI-PPO	2.00	34.0	7.9	14.13	9.4
S-PPO	2.79	111.1	11.5	10.74	22.1

7.3.2 Water Uptake and Proton Conductivity

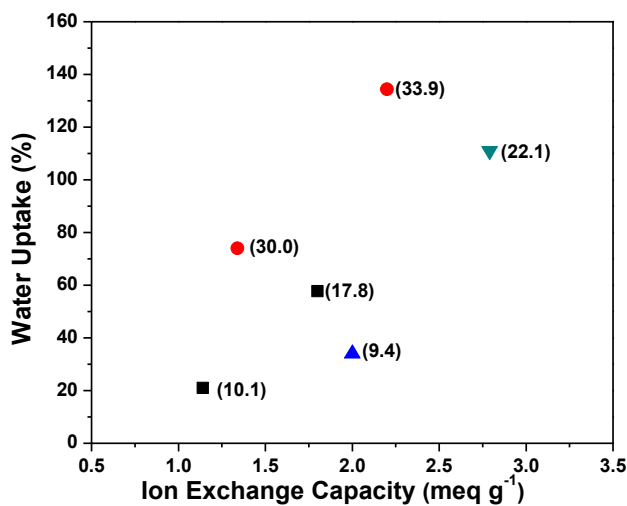


Figure 7.2. Water uptake as a function of ion exchange capacity at room temperature. SI-PPO (\blacktriangle), S-PPO (\blacktriangledown), S-Radel (\bullet) and SI-Radel (\blacksquare).

Water uptake is an important parameter that influences the ion conductivity and the mechanical integrity of PEMs. The water absorption of the membranes was measured in liquid water at room temperature. Generally, the water uptake of polymeric sulfonimides and sulfonic acid-containing materials increased with the increase in IEC as shown in **Figure 7.2** due to the increased hydrophilicity of ionic groups.¹⁵ However, the sulfonimide samples showed less water absorption and a lower hydration number, λ , than the sulfonic acid analogues. The Radel sulfonimide sample ($\text{IEC} = 1.80 \text{ meq g}^{-1}$) absorbed 17.8 water molecules per acid moiety ($\text{wu} = 59 \text{ wt } \%$) while the S-Radel ($\text{IEC} = 2.20 \text{ meq g}^{-1}$) showed hydration number of 33.9 water molecules per acid group ($\text{wu} = 110 \text{ wt } \%$). This trend of lower water absorption of the sulfonamide samples also was demonstrated in PPO and Radel sulfonimide materials. In addition to the acid moieties, the polymer with PPO backbone showed lower water uptake than the samples based on a Radel backbone.

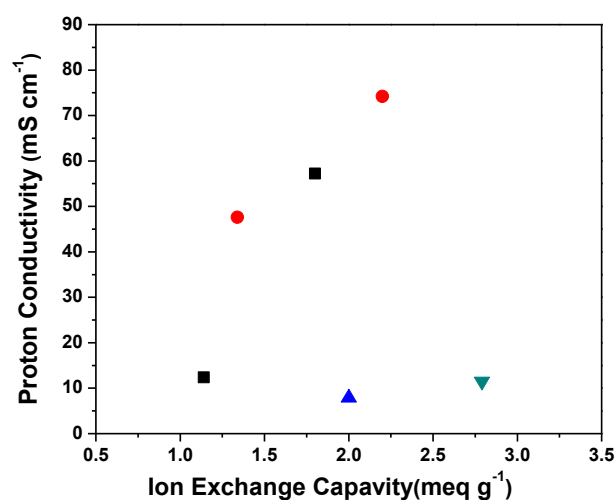


Figure 7.3. Conductivity of sulfonated and sulfonimides polymers. SI-PPO (▲), S-PPO (▼), S-Radel (●) and SI-Radel (■).

The proton conductivity increased with an increase in IEC for Radel and PPO sulfonated and sulfonimide samples at 20 °C, corresponding to an increase in water uptake. The S-Radel sample (IEC = 2.20 meq g⁻¹, water uptake = 134%) showed a higher proton conductivity of 74.2 mS cm⁻¹ compared to that of the sulfonated PPO membrane even at a higher IEC of 2.79 meq g⁻¹ (11.5 mS cm⁻¹, water uptake = 111%). The higher conductivity of the Radel sulfonimide sample compared to its PPO counterpart is shown in **Figure 7.3**. The Radel sulfonimide sample showed 7-fold proton conductivity of 57.2 mS cm⁻¹ compared to the PPO sulfonimide conductivity (7.9 mS cm⁻¹) under the similar IECs. The lower proton conductivity of the PPO sulfonimide sample versus its S-Radel analog was due to the electronic and miscibility properties of the polymer backbones, resulting in a possible difference of microstructures from backbone hydrophobicity and flexibility.^{15,16} However, the percolation threshold effect on the proton conductivity was observed in the Radel sulfonimide samples. Below the percolation threshold, the proton conductivity was significantly reduced due to the discontinuity of ionic conducting phase in the hydrophilic sequence. In this study, we found the proton conductivity transitioned at IEC of 1.14 meq g⁻¹ for Radel sulfonimide samples above which the proton conductivity increased exponentially.

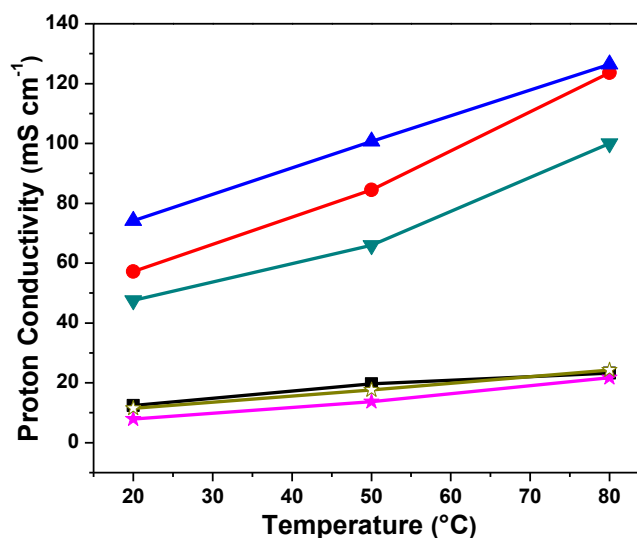


Figure 7.4. Proton Conductivity vs Temperature in liquid water. SI-PPO (★) (2.00 meq g⁻¹), S-PPO (☆) (2.79 meq g⁻¹), S-Radel (▲) (2.20 meq g⁻¹) and (▼) (1.34 meq g⁻¹), SI-Radel (●) (1.80 meq g⁻¹) and (■) (1.10 meq g⁻¹).

The in-plane proton conductivity of fully hydrated mechanically robust membranes was measured from 20 to 80 °C in liquid water. The proton conductivity linearly increased with temperature for all membranes in liquid water as presented in **Figure 7.4** due to the faster water dynamics at increased temperatures. At 80 °C, the proton conductivity of the Radel sulfonimide sample (IEC = 1.80 meq g⁻¹) approached the sulfonated Radel conductivity (IEC = 2.20 meq g⁻¹). Sulfonated and sulfonimide Radel samples exhibited a similar slope of conductivity with temperature which indicated that sulfonimide Radel had comparable activation energy of conductivity of sulfonated

Radel. The similar slope confirmed water-assisted transport mechanism following equation (2).

$$\sigma = A \exp\left(-\frac{E_a}{RT}\right) \quad (2)$$

where σ is the membrane conductivity (mS cm^{-1}); A is the pre-exponential factor ($\text{mS K}^{-1} \text{cm}^{-1}$), E_a is the proton conducting activation energy (kJ mol^{-1}), R and T are the ideal gas constant ($\text{J mol}^{-1} \text{K}^{-1}$) and the temperature (K), respectively. According to Eq. (2), the plot of $\ln(\sigma)$ versus $1/T$ allows for the calculation of the activation energy of the proton membranes. The sulfonimide Radel showed comparable activation energy (9.14 kJ mol^{-1}) to sulfonated counterparts (7.48 kJ mol^{-1}) considering the IEC difference. The activation energy decreased with the increase in IECs for all samples as shown in Table 7.1.

However, even at 80°C , the PPO samples in either ionic form showed lower conductivity than the Radel-based samples but the PPO values were comparable to that of Nafion[®] 112 membrane.¹⁷ The ion conductivity along with the water absorption provided an approach to obtain membranes with high proton conductivity and low water uptake by the conversion of sulfonic acid moieties to sulfonimide groups. The high conductivity and low water absorption of sulfonimide acid was probably due to the higher acidity than sulfonic acid as indicated in previous research. It was measured that the pK_a of aromatic sulfonimide samples was almost three orders of magnitude higher than that of aromatic sulfonic acid.¹⁸

7.3.3 Thermal Stability

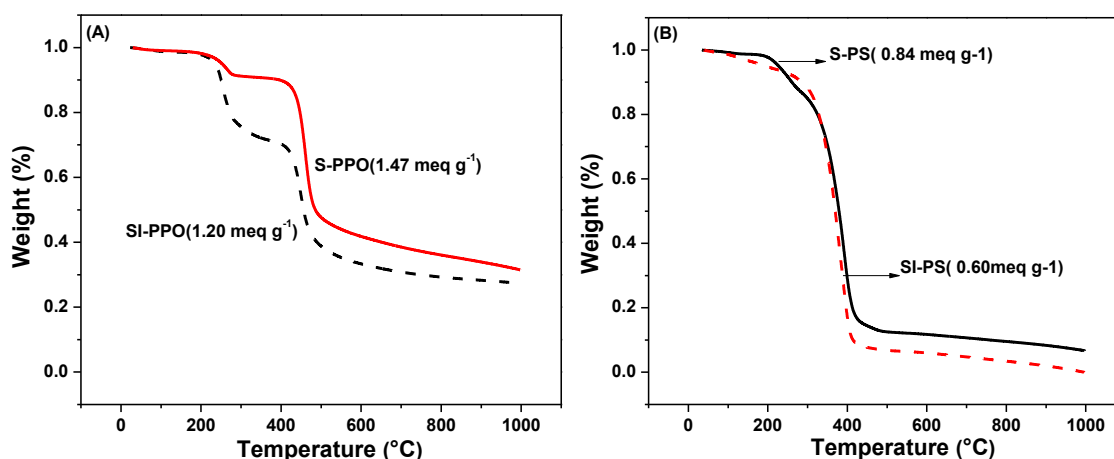


Figure 7.5. TGA curves of PPO and PS samples.

The thermal stability of the proton-containing side groups is one of the most important parameters in practical membranes because of the photogenic group's critical function in conductivity. Three weight loss events were observed in the TGA curves of PPO degradation as indicated in **Figure 7.5A**. The first weight loss at 100 °C was attributed to the loss of trace moisture from the air, less than 1 wt%. The second stage at 220 °C for sulfonated PPO was due to the splitting of $\text{-SO}_3\text{H}$ side moieties while the PPO superimides started to decomposed at 250 °C. The decomposition temperature of the main chain was at 440 °C for both PPO samples which is lower than pristine PPO at 470 °C.¹³ The lower thermal stability of PPO after functionalization is likely due to acid-labile main backbone. Sulfonated PS showed the same side chain degradation onset temperature as sulfonated PPO at 220 °C but a lower main chain decomposition temperature at about

330 °C. PS sulfonimide samples displayed the similar thermal degradation trend to sulfonated PS.

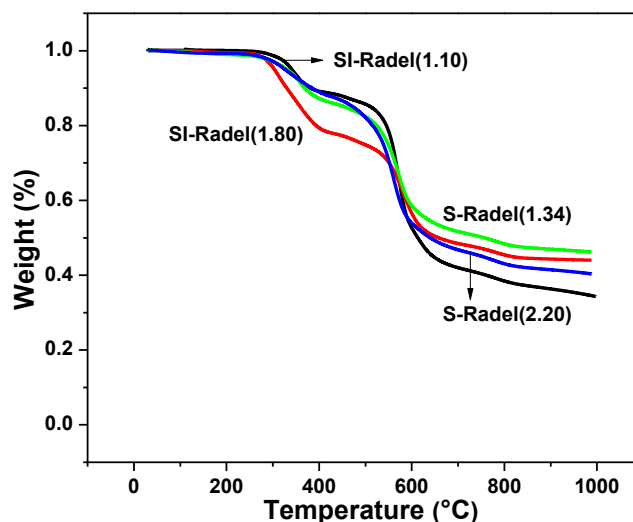


Figure 7.6. TGA curves of S-Radel and SI-Radel samples.

Sulfonated Radel showed similar thermal degradation behavior to PPO and PS samples on the TGA curves as shown in **Figure 7.6**. Sulfonated and sulfonimide Radel samples showed an onset $\text{-SO}_3\text{H}$ degradation temperature of 260 °C. In our study, Radel sulfonimide samples showed similar thermal degradation behavior to PPO and PS sulfonimide counterparts.

7.4 Conclusions

Sulfonimide-containing copolymers with different polymer backbones were successfully synthesized via low cost post-polymerization modification under mild

conditions. The proton conductivity of sulfonimide and sulfonated samples increased with the temperature. The Radel samples in either acid form displayed higher proton conductivity than PPO samples. These sulfonimide copolymers showed proton conductivity comparable to sulfonic analogs but lower water uptake. The thermal stability of sulfonimide copolymers was stable up to 250 °C under nitrogen atmosphere. The sulfonimide samples are applicable to long-term high temperature PEMs due to its higher ionic degradation temperature. These synthetic routes provided universal scale-up approaches for industry production due to the absence of expensive monomers purification.

7.5 References

1. Wang, F.; Hickner, M.A.; Kim, Y.S.; Zawodzinski, T.A.; McGrath, J.E. *J. Membr. Sci.***2002**, *197*, 231-242.
2. Hickner, M.A.; Ghassemi, H.; Kim, Y.S. ; Einsla, B.R.; McGrath, J.E. *Chem. Rev.***2004**, *104*, 4587-4612.
3. Kim, Y. S.; Wang, F.; Hickner, M.; Zawodzinski, T. A.; McGrath, J. E. *J. Membr. Sci.***2003**, *212*, 263-282.
4. Koppel, I. A.; Taft, R. W.; Anvia, F.; Zhu, S. Z.; Hu, L. Q.; Sung, K. S.; DesMarteau, D. D.; Yagupolskii, L. M.; Yagupolskii, Y. L.; Ignatev, N. V.; Kondratenko, N. V.; Volkonskii, A. Y.; Vlasov, V. M.; Notario, R.; Maria, P. C. *J. Am. Chem.Soc.* **1994**, *116*, 3047-3057.
5. DesMarteau, D. D. *J. Fluorine Chem.* **1995**, *72*, 203-208.
6. Feiring, A. E.; Choi, S. K.; Doyle, M.; Wonchoba, E. R. *Macromolecules* **2000**, *33*, 9262-9271.
7. Feiring, A. E.; Wonchoba, E. R. *J. Fluorine Chem.* **2000**, *105*, 129-135.

8. Hofmann, M. A.; Ambler, C. M.; Maher, A. E.; Chalkova, E.; Zhou, X. Y.; Lvov, S. N.; Allcock, H. R. *Macromolecules* **2002**, *35*, 6490-6493.
9. Cho, C.G.; Kim, Y.S.; Yu, X.; Hill, M.; McGrath, J. E. *J. Polym. Sci. Polymer Chemistry* **2006**, *44*, 6007-6014.
10. Huang, R.; Kim, J. *J. Appl. Polym. Sci.* **1984**, *29*: 4017-4027.
11. Kim, S.; Yan, J.; Schwenzer, B.; Zhang, J.; Li, L.; Liu, J.; Yang, Z.; Hickner, M. A. *Electrochem. Commun.* **2010**, *12*, 1650–1653.
12. Chakrabarti, A.; Filler, R.; Mandal, B. *ECS Transactions*, **2007**, *6(14)*, 77-88.
13. Fu, H.; Jia, L.; Xu, J. *J. Appl. Polym. Sci.* **1994**, *51*: 1399-1404.
14. Fujita, S. *J. Chem. Soc. Perkin Trans.* **1982**, *1*, 1519-1522.
15. Hickner, M.A.; Pivovar, B.S. *Fuel Cell*, **2005**, *5(2)*, 212-229.
16. Kreuer, K.D. *J. Membr. Sci.* **2001**, *185*, 29-39.
17. Yang, S.; Gong, C.; Guan, R.; Zou, H.; Dai, H.; *Polym. Adv. Technol.* **2006**, *17*, 360–365.
18. Leito, I.; Kaljurand, I.; Kpoel, I.A.; Yagupolskii, L.M.; Vlasov, V.M. *J. Org. Chem.* **1998**, *63*, 7868-7874.

Chapter 8

Summary and Future Research Direction

8.1. Summary and Conclusions

The research in this thesis has furthered our understanding of block copolymer-based ionic conducting membranes, the C4 side chain effects on the chemical stability of ionic moieties of poly(styrene) based anion exchange membranes, how the crosslinking of ionic block copolymers influences the properties of mechanically robust membranes in liquid water and how the semicrystalline block incorporation of ionic block copolymers affects the intrinsic properties of anion exchange membranes. This thesis has not only clarified the properties of ion conducting membranes, but has also used home-made novel AEM materials to obtain insight to provide pathways for next generation materials in ionic conducting materials.

8.1.1.Highly Conductive Side Chain Anion Exchange Membranes

The well-defined block copolymers with C4 side chain terminal alkenes were synthesized via RAFT polymerization through the bifunctional monomer of 4-(3-butenyl)styrene and styrene, providing a direct synthetic approach to the pure side chain block copolymers. The quantitative HBr bromination of butenyl groups to bromobutyl groups was the key step for the synthesis of halide containing side chain block copolymers. This synthetic strategy is applicable to the extended side chain for ionic block copolymers.

The introduction of C4 side chain in the block copolymers resulted in the reduction of the domain spacing due to the increased miscibility between C4 side chain and hydrophobic block. The conductivity was improved by solvent induced long-range ordered microstructures and longer soft side chain introduction between ionic moieties and polymer backbone. The quaternized side chain copolymer showed better stability against alkaline conditions at 80°C compared to benzyltrimethyl ammonium counterparts. The copolymers stability suggested the C4 side chain block copolymers are a promising candidate for the AEM fuel cells.

8.1.2 Low-Temperature Crosslinked Anion Exchange Membranes

The metathesis crosslinking route provides a solution of fabricating robust AEMs against liquid water. In my study, the crosslinking effects on the properties of AEMs were researched. For crosslinked polymers a well-defined microdomain structure was not present and domain sizes decreased significantly compared to uncrosslinked materials. To obtain the higher conductivity in crosslinked AEMs, the AEMs should have high ion concentration under optimal water uptake. The AEMs with long-range ordered domain structures are suitable candidates under low humidity conditions for ionic conducting membranes.

8.1.3 Highly Ordered Block Copolymer Anion Exchange Membranes

This work showed the ionic conductivity could be manipulated by controlling the morphologies of ionic block copolymers with different hydrophobic blocks. The ion

concentration had great effects on the ionic conductivity. The introduction of crystalline blocks remained the mechanical integrity of AEMs against liquid water. This concept is able to be used to make mechanically robust block copolymer membranes through the incorporation of crystalline composition as indicated by DSC thermograms. The anion-containing block copolymer offered guidelines for the design of block copolymer-based ion-conducting membranes used in liquid water.

8.1.4 Polymeric Sulfonimide Proton Exchange Membranes

Sulfonimide-containing copolymers were synthesized via low cost post-polymerization modification under mild conditions. These sulfonimide copolymers showed comparable proton conductivity to sulfonic analogs but lower water uptake and higher thermal stability. The sulfonimide samples are viable to long-term high temperature PEMs due to its higher ionic degradation temperature. These synthetic routes provided universal scale-up approaches for industry production.

8.2 Future Research Direction

The concentration of the future work will on increasing the chemical stability of ionic moieties for long-lasting purpose in electrochemical devices, reducing water swelling to obtain mechanically robust membranes in liquid water and maintaining high ionic conductivity. The interdomain spacing reduction of side chain block copolymers needs to be further elucidated in theory and may be applied to make lower interdomain spacing neutral block copolymer films with long-range ordered microstructures. The

block copolymer-based crosslinked AEMs potentially are leveraged to test its performance in water treatment and gas separation.

Furthermore, understanding the ionic block copolymer morphology its relation to polymer composition could allow for additional constructing novel membranes with desirable microstructures. The solvents influences on the nanophase separation should also be assessed in conjunction with the final properties of the as-cast membranes. It may be desirable to construct ionic block copolymer phase behavior in a similar fashion of non-ionic block copolymers. The interaction parameters also can be measured by SANS and compared with non-ionic copolymers. The ionic block copolymer studies on thin film are also ongoing. The comprehensive understanding of block copolymers based membranes is not established, and it is necessary to obtain the information to prepare the next generation ionic conducting membranes.

The sulfonimide containing copolymers are also being researched in organic solar cell doping to improve the power conversion efficiency. The superacid functionalized copolymers should be explored via C-H activation to reduce the cost of the widely developed coupling due to its high cost.

Appendix A

Synthesis of Side Chain Block Copolymers for Stable Anion Exchange Membranes

A.1 Determination of Molecular Weight and Composition of Block Copolymers

Typically, ^1H NMR spectroscopy and size exclusion chromatography (SEC) were used to measure the molecular weight of macroinitiators and diblock copolymers from the ratio of second block to the macroinitiators.

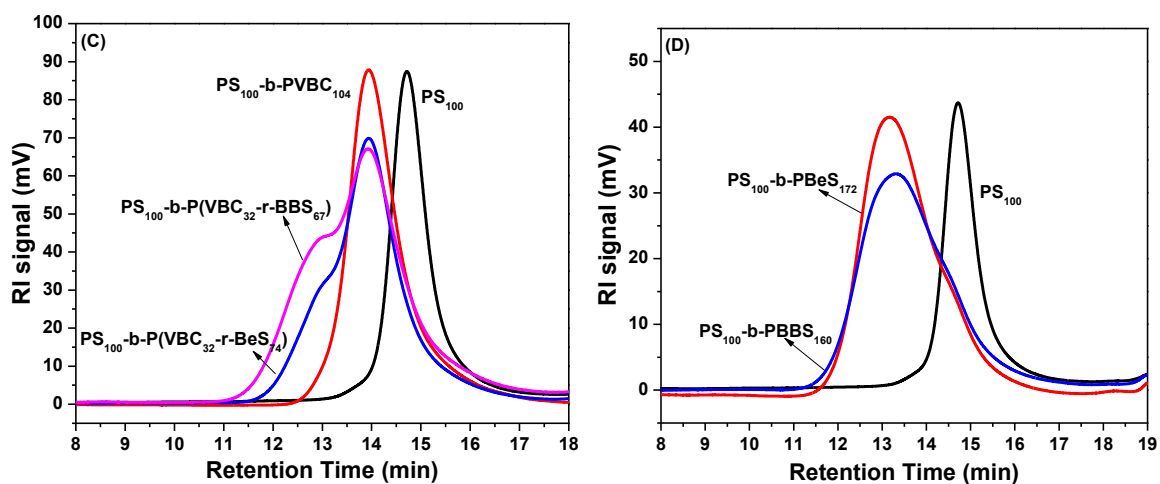


Figure A1. GPC graphs of macroinitiator PS_{100} , PS-b-PVBC , PS-b-P(VBC-r-BeS) , PS-b-P(VBC-r-BBS) , PS-b-PBeS and PS-b-PBBS .

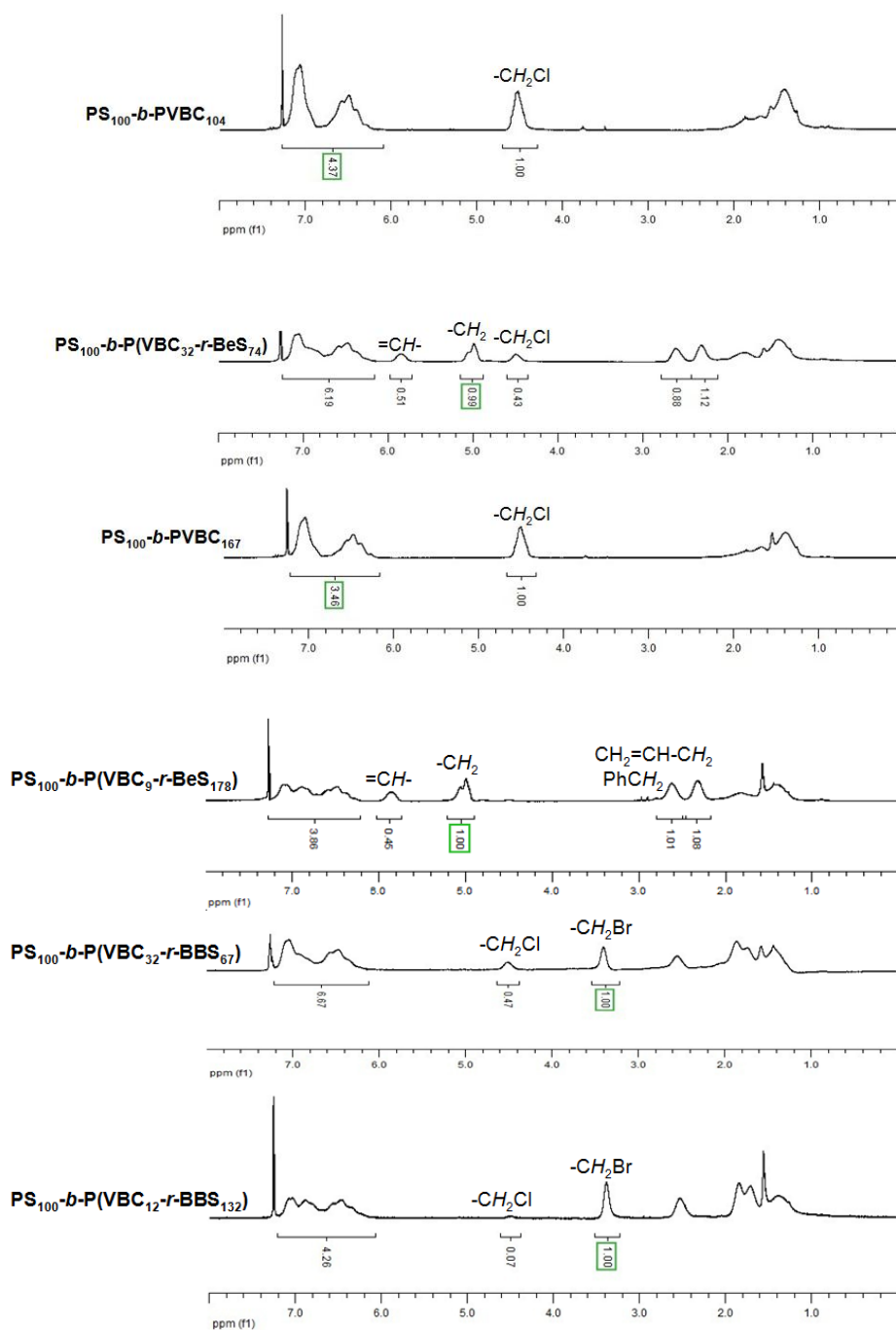


Figure A2. ^1H NMR spectra of $\text{PS-}b\text{-PVBC}$, $\text{PS-}b\text{-P(VBC-}r\text{-BeS)}$ and $\text{PS-}b\text{-P(VBC-}r\text{-BeS)}$ block copolymers.

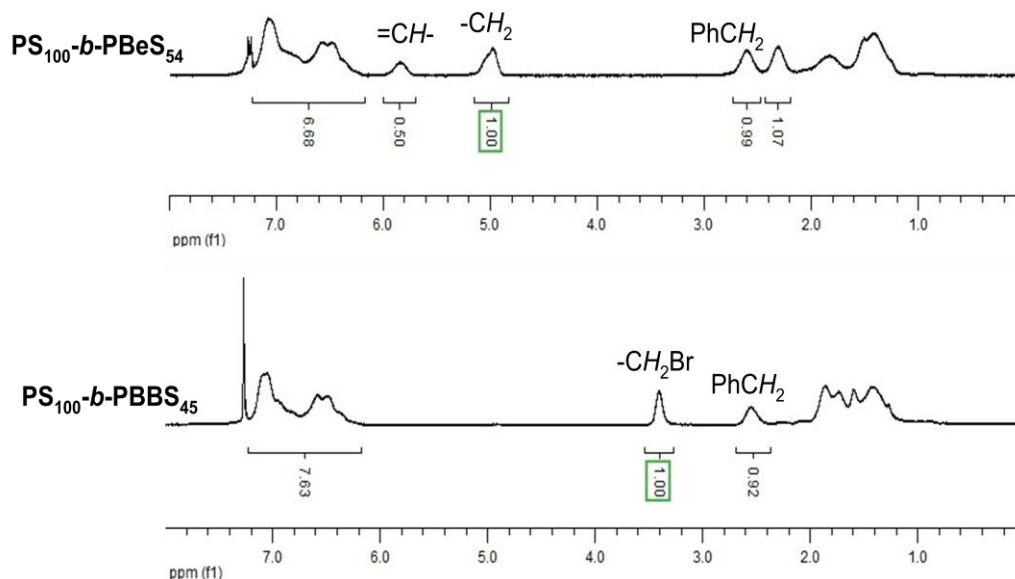


Figure A3. ^1H NMR spectra of PS-*b*-PBeS and PS-*b*-PBBS block copolymers in CDCl_3 at 25 °C.

Table A1. Properties of Synthesized Block Copolymer Anion Exchange Membranes

Sample	IEC (NMR)	d(SAXS) ^a (nm)	d(SAXS) ^b (nm)	Conductivity ^a (mS cm ⁻¹)	Conductivity ^b (mS cm ⁻¹)
PS ₁₀₀ - <i>b</i> -PBBS ₁₆₀	3.15	27.3	18.8	NA	33.7
PS ₁₀₀ - <i>b</i> -PVBC ₁₀₄	3.20	33.0	NA	20.4	28.9
PS ₁₀₀ - <i>b</i> -P(VBC ₁₂ - <i>r</i> -PBBS ₁₃₂)	3.18	23.8	NA	18.7	25.2
PS ₁₀₀ - <i>b</i> -PVBC ₁₆₇	3.66	39.2	28.3	26.5	36.6

The IEC of the PS₁₀₀-*b*-PBBS₁₆₀ sample was calculated from chloride form after ion exchange with 1M aqueous NaCl; conductivity was measured at 30 °C under 95% relative humidity in chloride form; a, the membranes were cast from toluene/1-propanol (v/v = 1:1) except PS₁₀₀-*b*-PBBS₁₆₀ in bromide form was cast from chloroform/1-propanol/methanol (v/v/v = 2:1:1); b, the samples were prepared from DMF/1-propanol (v/v = 3:1).

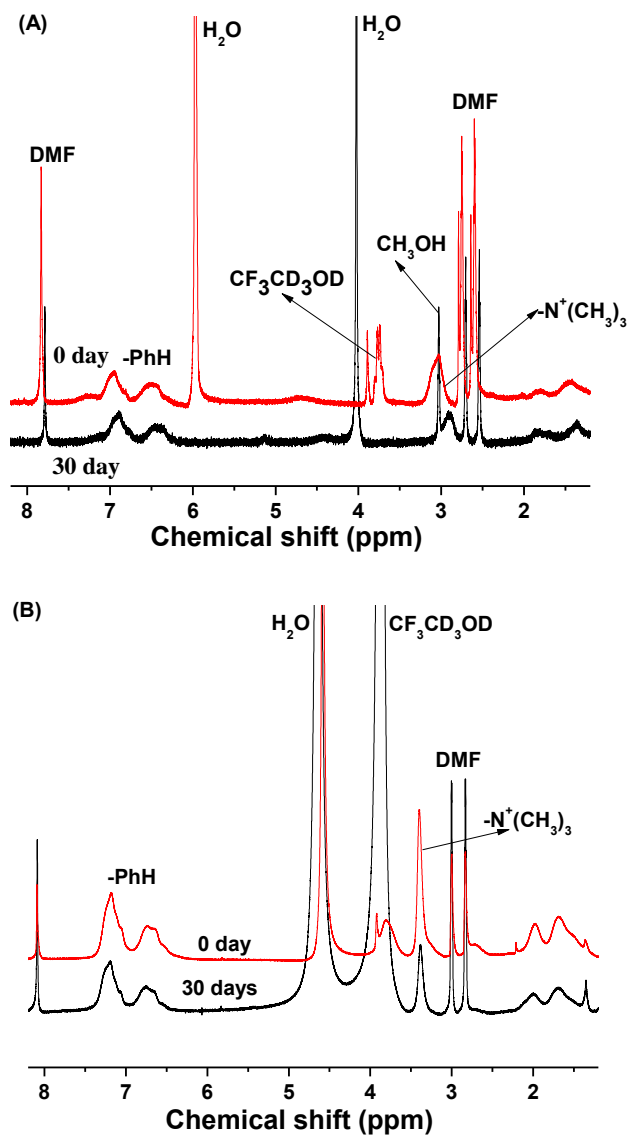
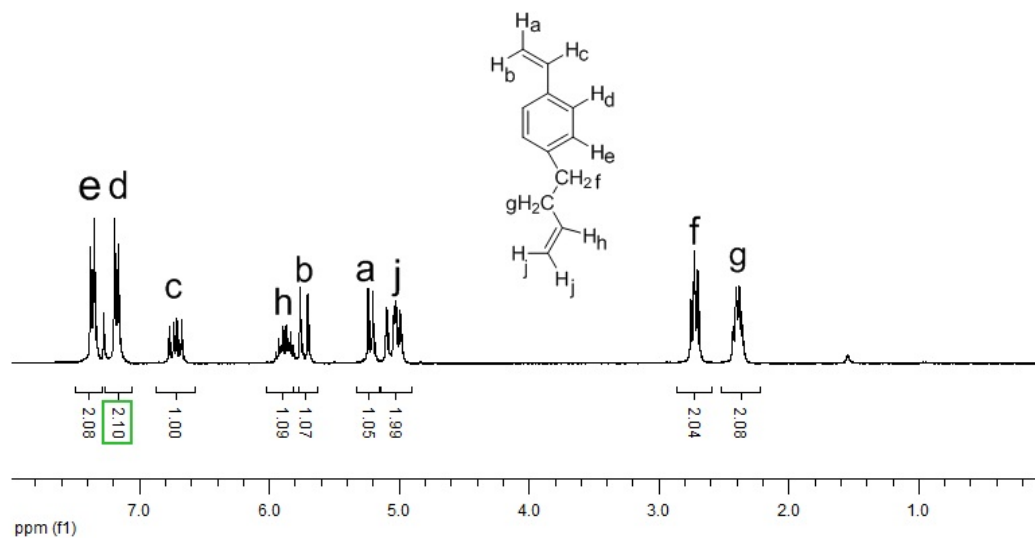


Figure A4. ^1H NMR spectra of (A) quaternized C4 side chain $\text{PS}_{100}\text{-}b\text{-PBBS}_{45}$ and (B) benzyltrimethyl ammonium copolymers powder from $\text{PS}_{100}\text{-}b\text{-PVBC}_{49}$ in 1M KOH at 80 °C for 30 days. -PhH denotes aromatic protons.

Appendix B

Low-Temperature Crosslinked Anion Exchange Membranes



FigureB1. ^1H NMR spectrum of 4-(3-butenyl)styrene.

Table B1. Block Copolymer Molecular Weights and Polydispersity Indices.

	M_n (kg mol^{-1})	M_w (kg mol^{-1})	M_w/M_n
PVBC ₄₉ - <i>r</i> -PBeS ₅₀	19.4	26.6	1.37
PVBC ₄₄ - <i>b</i> -PBeS ₄₄	12.3	16.1	1.31
PVBC ₁₀₀ - <i>b</i> -PBeS ₁₀₇	26.1	33.7	1.29
PVBC ₁₀₀ - <i>b</i> -PBeS ₁₈₃	33.4	45.8	1.37

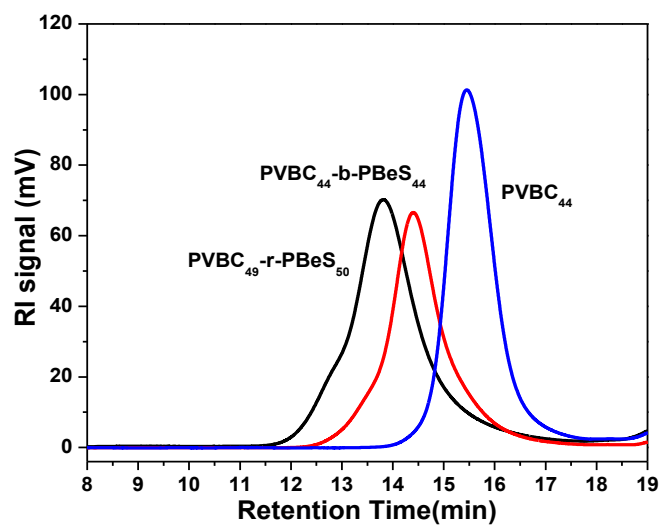


Figure B2. GPC graphs of macroinitiators and block and random copolymers.

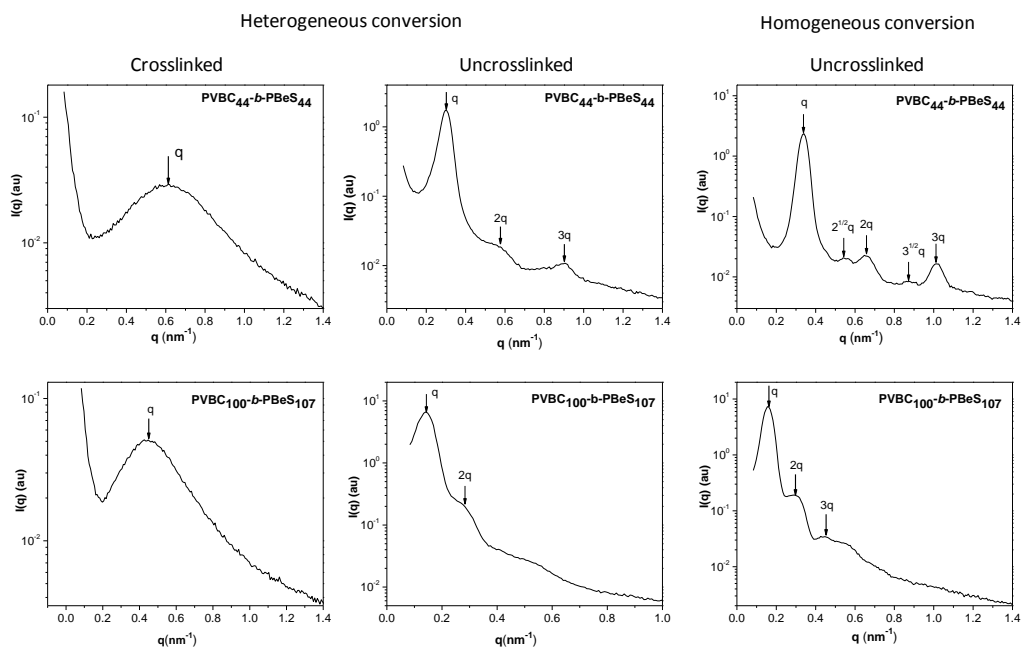


Figure B3. SAXS profiles of block AEMs formed under different conditions.

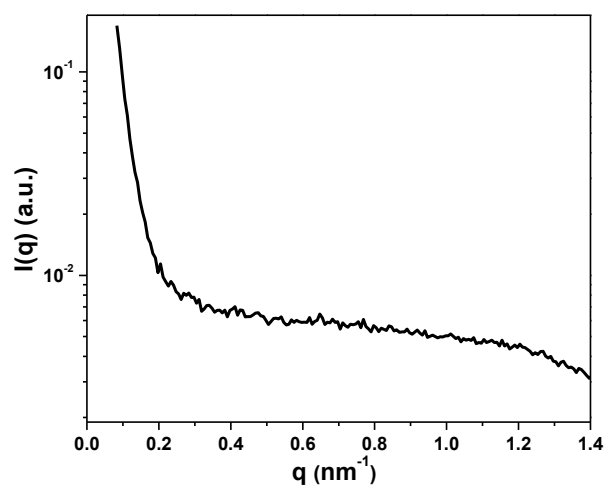


Figure B4. Random PVBC₄₉-*r*-PBeS₅₀ crosslinked AEM formed using heterogeneous amination.

Appendix C

Properties of Highly Ordered Block Copolymer Anion Exchange Membranes

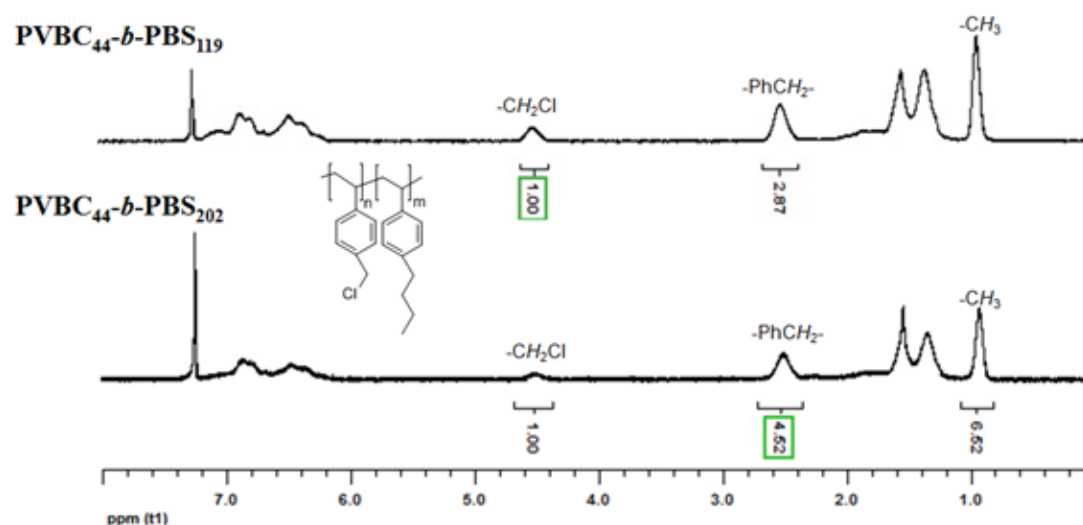


Figure C.1. ^1H NMR spectra of block copolymers.

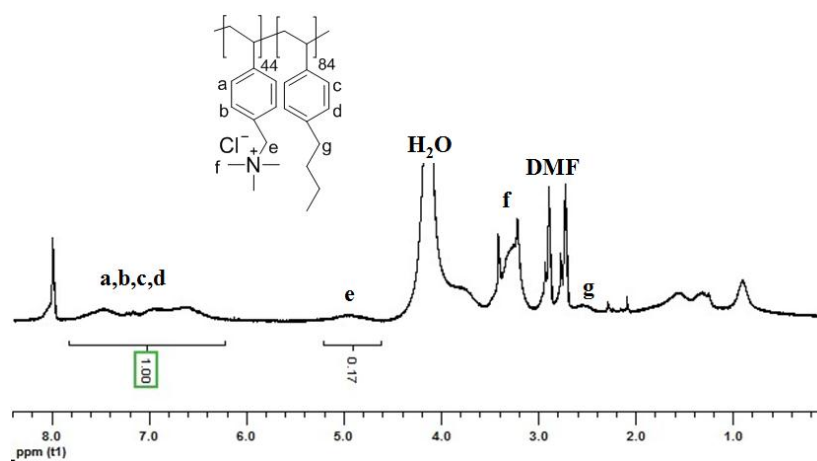


Figure C.2. ^1H NMR spectrum quaternized $\text{PVBC}_{44}\text{-}b\text{-PBS}_{84}$.

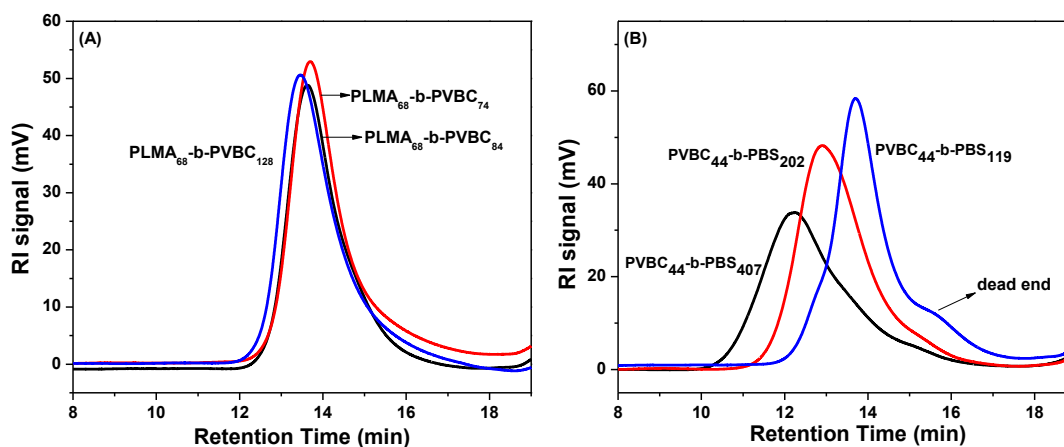


Figure C.3. GPC chromatograms of A) PLMA-*b*-PVBC and B) PVBC-*b*-PBS

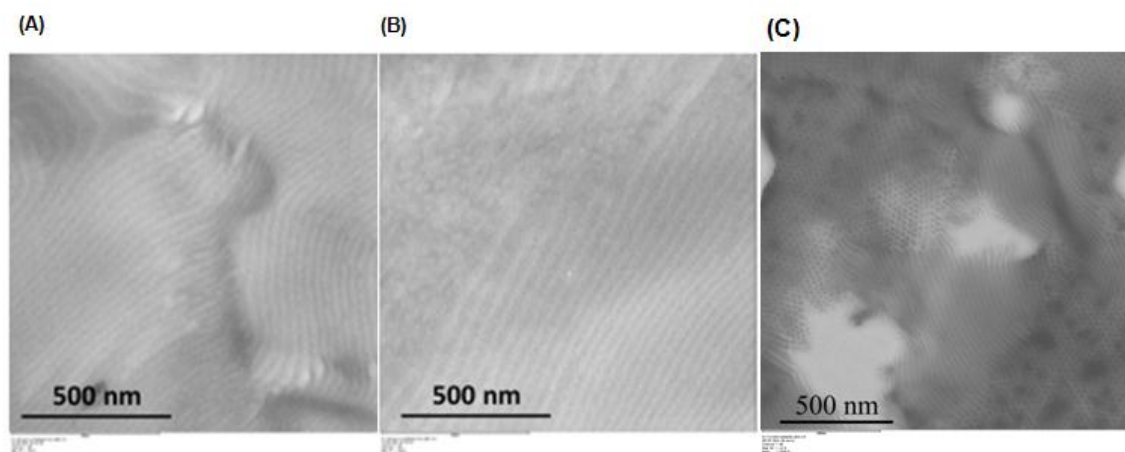


Figure C.4. TEM micrographs of A, B) PHMA₆₀-*b*-PVBC₃₄ sample with defects; C) PSMA₈₄-*b*-PVBC₈₄ sample with cylindrical morphology. All samples were unstained.

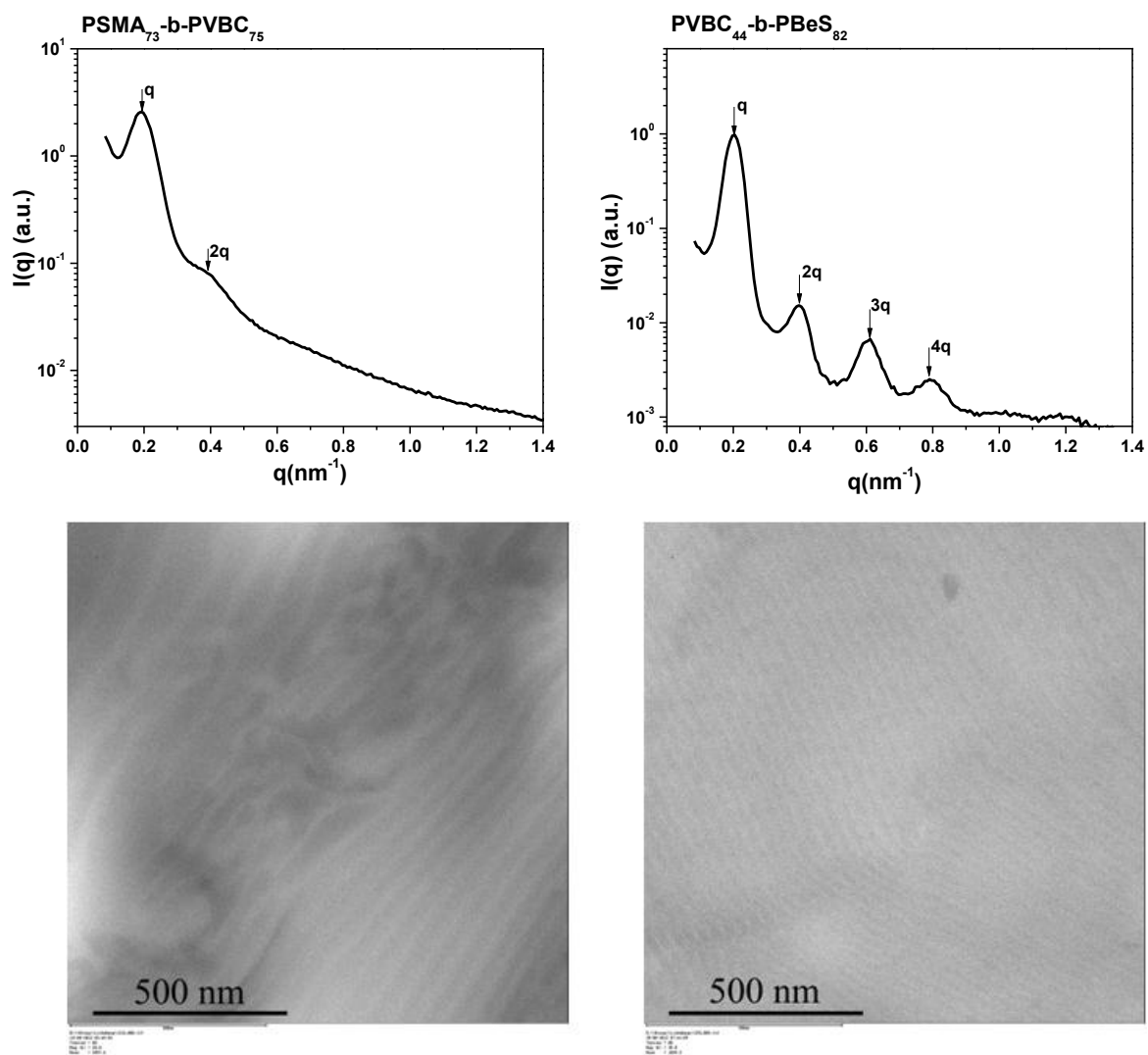


Figure C.5. SAXS profiles and TEM micrographs of PSMA₇₃-b-PVBC₇₅ sample (left) and PVBC₄₄-b-PBeS₈₂ sample (right) with lamellar morphologies. All samples were unstained.

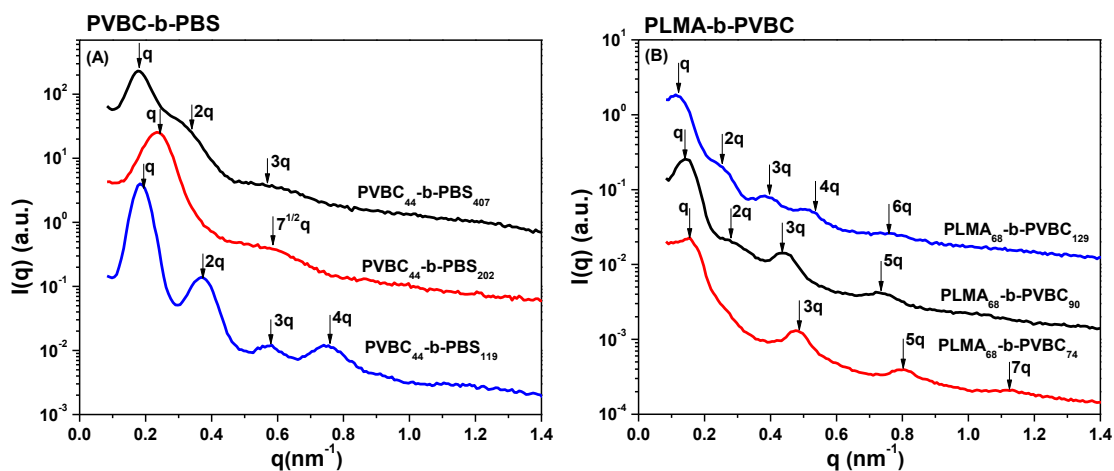


Figure C.6. SAXS profiles of PLMA-*b*-PVBC and PVBC-*b*-PBS samples. All samples were unstained.

Table C.1. Water uptake and ionic conductivity of the prepared samples with IEC of $\sim 2.0 \text{ meq g}^{-1}$.

sample	Theoretical IEC ^{NMR} (Cl)	WU @ 95% RH	Hydration Number(λ)	RH-Conductivity @95% (mS cm ⁻¹)
PHMA ₆₀ - <i>b</i> -PVBC ₃₄	2.04	32.4%	6.65	24.30
PLMA ₆₈ - <i>b</i> -PVBC ₆₅	2.09	34.4%	6.79	13.53
PSMA ₇₃ - <i>b</i> -PVBC ₇₅	1.79	26.6%	6.52	NA
PVBC ₄₄ - <i>b</i> -PBS ₈₄	1.94	30.3%	6.66	19.00
PVBC ₄₄ - <i>b</i> -PBeS ₈₂	1.98	32.9%	6.95	17.23

Table C.2. Properties of samples with low and high ion contents.

sample	M_n^{GPC} kg mol^{-1}	PDI M_w/M_n	IEC^{NMR} (Cl)	WU (%)	λ	Conductivity (mS cm^{-1})	d (SAXS) (nm)
PLMA ₆₈ - <i>b</i> -PVBC ₇₄	17.5	1.34	2.24	28.9	7.2	15.86	40.1
PLMA ₆₈ - <i>b</i> -PVBC ₉₀	18.7	1.32	2.59	41.7	8.9	21.25	43.1
PLMA ₆₈ - <i>b</i> -PVBC ₁₂₉	20.1	1.37	2.88	54.0	10.4	27.40	49.4
PVBC ₄₄ - <i>b</i> -PBS ₁₁₉	15.9	1.58	1.55	20.1	7.2	13.32	34.1
PVBC ₄₄ - <i>b</i> -PBS ₂₀₂	27.2	1.57	1.05	8.4	4.4	0.37	26.4
PVBC ₄₄ - <i>b</i> -PBS ₄₄₇	42.0	1.85	0.54	6.4	6.2	0.20	35.9

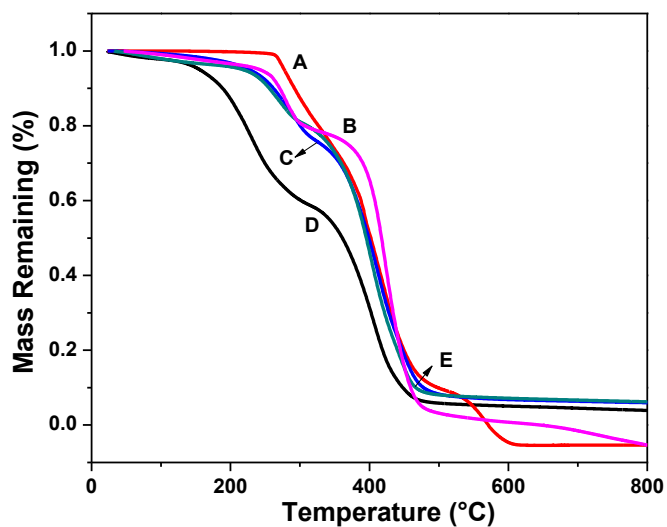


Figure C.7. TGA curves of block copolymers: A: PSMA₇₅-*b*-PVBC₇₃, B: quaternized PVBC₄₄-*b*-PBS₈₄, C: quaternized PLMA₆₈-*b*-PVBC₆₅, D: quaternized PSMA₇₅-*b*-PVBC₇₃, E: quaternized PHMA₆₀-*b*-PVBC₃₄.

VITA

Lizhu Wang

Lizhu Wang was born in Liaoning, China. He received his Bachelors of Science degree in Applied Chemistry from Jilin University, Changchun, China, 2003 and Master of Science in Organic Chemistry from Marquette University, Milwaukee, USA, 2009. He began his graduate studies at the Pennsylvania State University in February of 2011 under the guidance of Dr. Michael Hickner. His PhD dissertation was involved in the synthesis and characterization of block copolymer based solid polymer electrolytes for ion exchange membranes in fuel cells.